UiT
THE ARCTIC UNIVERSITY OF NORWAY

FACULTY OF SCIENCE AND TECHNOLOGY

Department of Geology

Structural and geochemical mapping of a Fe-mineralized quartz-mica rich unit in the Ringvassøya Greenstone Belt, West Troms Basement Complex

With focus on origin, mineralization and structural relations

—

Hallgeir Elvenes

GEO-3900 Master's Thesis in Geology

May 2015

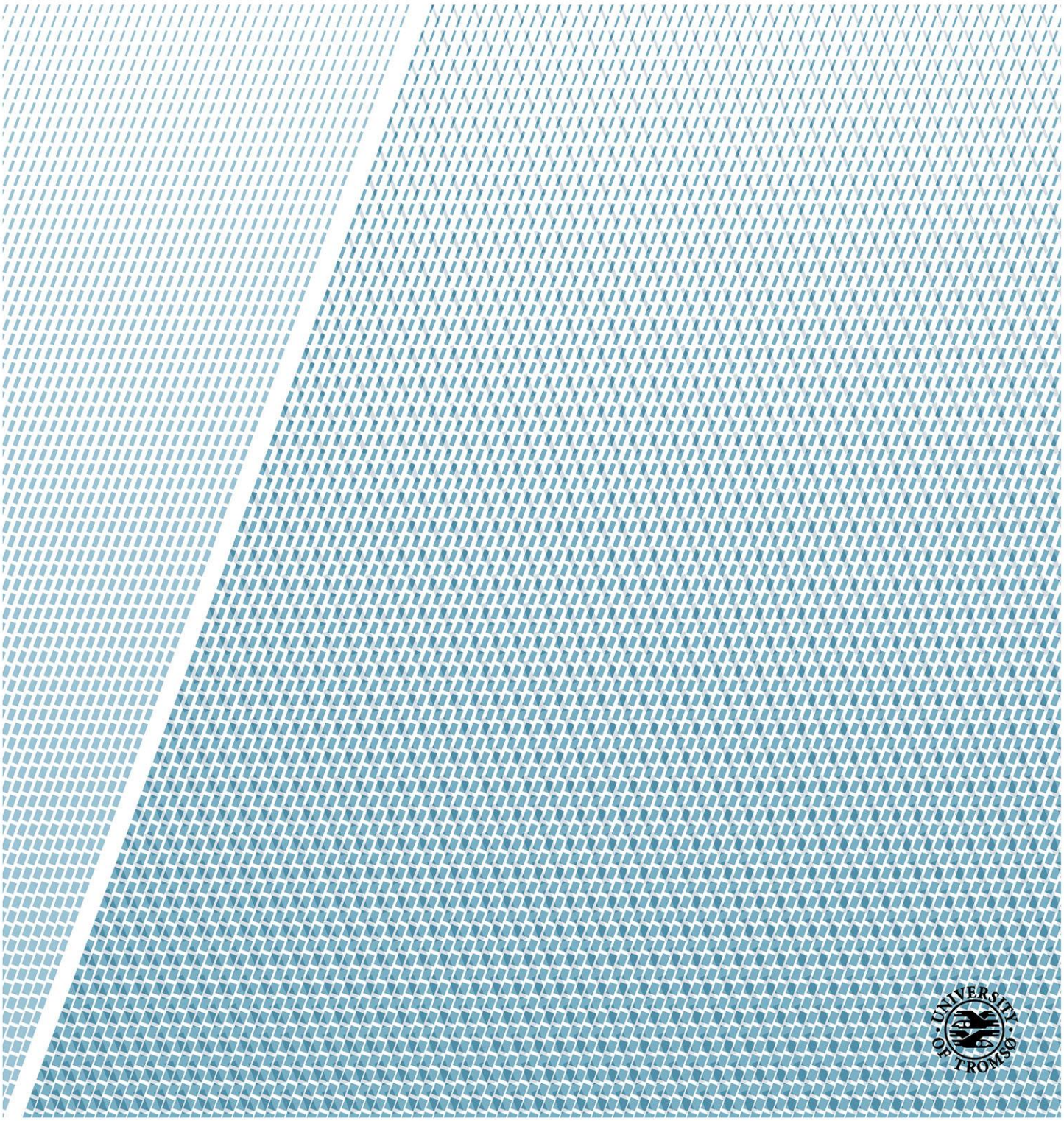

Acknowledgements

First, I would like to thank my supervisors, Steffen G. Bergh, Harald Hansen and Paul Armitage for all help during this study. I would specially like to express my gratitude to Steffen for all help, constructive criticism and motivation during the last year, I really appreciate it. I would also like to thank Morten Often for providing me with a car for the fieldwork, and NGU for paying my geochemical analyzes. Further, I would like to thank all my fellow students, with a special shout-out to Karina and Elise for their support, help and encouragement with my thesis.

Finally, thanks to my friends and family for all their support, especially my sister Sigrid, for proofreading the thesis. And last, but not least, I would like to thank Maren for everything from late-night dinners to help with microscopy.

Hallgeir Elvenes

Tromsø, May 28th 2015

Abstract

Ringvassøy is one of a chain of large coastal islands representing the Archaean to Paleoproterozoic West Troms Basement Complex (WTBC), west of the Caledonides. On Ringvassøy, a basement of mainly tonalitic gneiss is overlain by the Ringvassøy Greenstone Belt (RGB), which is metamorphosed up to middle amphibolite facies. Tonalitic gneiss in the west and southeast of the island has U–Pb zircon ages of 2.84–2.82 Ga, similar to U–Pb zircon ages of 2.85–2.83 Ga for metavolcanics in the RGB. Mafic dykes cutting the basement have U–Pb zircon and baddelyite ages of 2.40 Ga, with a titanite age (metamorphic overprint) of 1.77 Ga; the same dykes seem to occur in the RGB.

The focus of this study is a highly Fe-sulphide-mineralized, quartz-mica rich unit ('keratophyre'?), which is suggested to be auferious. This unit be traced from the western to eastern limits of the RGB and coincides with a geophysical resistivity anomaly. The unit was mapped and sampled to identify enrichments of Fe-sulphides and Au, in all types of encountered mineralizations. Structurally in the RGB, D_1 is represented by the main ductile foliation (S_1) parallel to primary bedding/layering, rare isoclinal folds, and foliation-parallel shears (S_1), and occurred between 2.8 Ga and 2.40 Ga. Most of the post-D_1 structures, which cut the mafic dykes, formed in greenschist-facies conditions possibly during the Svecofennian Orogeny (c. 1.80–1.75 Ga), and include: macroscale upright folds and related low-angle ductile shears (S_2), and moderately to steeply plunging folds associated with steeply dipping, ductile shears (S_3).

Samples of the quartz-mica rich unit were collected across and along strike, and include all observed variations in lithology and mineralisation. Samples were also collected from syn-tectonic mineralisation and quartz veins in. Geochemical data, combined with the S_1-concordant position of the quartz-mica rich unit throughout the RGB, offer the possibility that it originated as a stratiform unit in a volcano-sedimentary setting. The unit may then have been hydrothermally altered and mineralized in the vicinity of a black smoker complex. A gold mineralization is identified in the bordering lithologies, thus, presenting no relation to the quartz-mica rich unit. These findings again state the potential for gold in the RGB, and provide important knowledge for further prospecting.

Contents

1. Introduction

1.1. Context of study

During the last decade, the metal market has experienced various up- and downswings in the price of base and precious metals (www.lme.com); this has made life difficult for prospecting companies and the mining industry. Even considering variations, the general trend is a rising price for most economical minerals as a direct cause of the rising consumption and demand in the developing world. Norway has not been able to keep up the production of minerals compared to other Nordic countries, as oil has been the main priority and source of income. Still, northern Norway is regarded as a high-potential area for exploration and production of economical minerals forming part of the Precambrian Fennoscandian Shield and the Scandinavian Caledonides, and a development of the Norwegian mineral industry is hopefully on the rise. Because of this lacking industry, the Norwegian government initiated the MINN (Mineral recourses In Northern Norway) program in 2011 (Regjeringens mineralstrategi, 2013). The MINN-program is conducted by the Geological Survey of Norway (NGU), and is set to examine ore potential in known as well as unknown locations in northern Norway based on new gravity and magnetic data (NGU.no).

The Ringvassøya Greenstone Belt (RGB) in the Neoarchaean-Palaeoproterozoic West Troms Basement Complex (Figure 1.3) is one of the targets included in the MINN program. Its geology is similar to greenstone belts in other parts of Fennoscandia and the world, where the presence of both base and precious metals is a well-known fact among geologists and prospectors. In 2012, Store Norske Gull AS started high-intensity prospecting for gold in the north-western parts of the Ringvassøya Greenstone Belt (Motuza, 2000; Bergh & Armitage, 1998). This yielded promising results during the first field season, and a second field season was planned. As prospecting was foreclosed due to lack of revenue (similar to many other prospecting projects in this period), the second field season was not carried out. The results, however, stated great ore potential in the Ringvassøya Greenstone Belt, but a proper understanding of the genesis and relationship of various sulfide and precious element mineralizations in the greenstone belt is still lacking. This thesis is part of a collaboration effort between Store Norske Gull AS, NGU and The Arctic University of Norway(UiT), with the focus of testing and answering some of the many unresolved questions related to the Ringvassøya Greenstone Belt and its ore potential.

1.2. Goal of work

This thesis is a part of the ongoing project "Tectono-magmatic evolution of Archaean and Palaeoproterozoic volcanic and sedimentary rocks of the West Troms Basement Complex and related TTG (Tonalitic, Trondhjemitic and Granitic) gneiss provinces in North Norway", at the Department of Geology(UiT). The goal of this project is gathering geological knowledge about the West Troms basement complex, with the focus set on getting an understanding of the formation, age, petrology/metamorphosis, geochemistry, and structural and tectonical development, especially associated with Precambrian crustal deformation. A large amount of prospecting work has been conducted in the Ringvassøya greenstone belt for more than 100 years (Sandstad & Nilsson, 1998; Ihlen & Furuhaug, 2000; Fareth & Lindahl, 1981), and the existence of both stratiform (Fareth & Lindahl, 1981) and structurally controlled (Bergh & Armitage, 1998) mineralizations has been proven. Nevertheless, a link between the stratiform and the structurally controlled mineralizations is yet to be defined, as is a formational process for the different types of mineralizations (cf. Sandstad & Nilsson, 1998).

First, the aim of this particular study is to map, structurally and lithologically, a Fe-mineralized quartz-mica rich unit and surrounding lithologies in the northwestern parts of the Ringvassøya Greenstone Belt (Bergh & Armitage, 1998; Fareth & Lindahl, 1981; Sandstad & Nilson, 1999; Motuza, 2000). In order to discuss possible relationships and the origin of the lithologies, as well as try to evaluate any encountered mineralizations in terms of ore-potential. The latter is based upon Store Norske Gull's work in the area, which has indicated the potential for precious elements and provided a good basis for scientific investigations. Thus, a model that explains the relationship between possible precious element mineralizations and the quartz-mica rich unit is highly valuable and essential for future prospecting. To investigate this, detailed mapping and sampling (including lithologies and mineralization) in an east-west transect across the RGB, from Lassefjellet in the east and toward Innerelvdalen on the western side of Skogsfjordvatnet (Figure 1.1) has been conducted.

The structural and geological mapping was preformed with the focus on main lithological boundaries, mineralizations and shear-zones of different generations. Structural measurements from foliation, cleavage and micro- to meso-scale folds were gathered, and orientation and relative slip-directions for shear-zones related to the quartz-mica rich unit were obtained where possible. In locations with dense vegetation, interpretations were made based on geological knowledge. During the mapping, 45 chip samples for thin sections and geochemical analysis were collected within the study area (Figure 1.1). The locations of all 45 samples were plotted on GPS, and each sample-location was photographed.

Samples were hammered out manually, weighing in at about 1 kilogram, with an approximate size of two fists. During the gathering of chip samples, the following main criteria were emphasized:

(1) Representative specimens of the quartz-mica rich unit across and along strike to include all observed variations in lithology.

(2) Sampling of bordering lithology in order to investigate origin and possible relationships.

(3) Sampling of the mineralizations (both stratiform and structurally controlled) and quartz veins (parallel/truncating the main fabric) with wall rock.

1.3. Location of the study area

The Ringvassøya Greenstone Belt is located on the island of Ringvassøya, about 30 kilometers north of Tromsø (Figure 1.1). Most parts of the greenstone belt are relatively easily accessible, as Riksvei 863 runs through most of the 30 km long NW-SE striking belt. The degree of exposure is on the other hand sparse, due to the geographical location in the lowlands of Ringvassøya, where birch forest and heathers cover much of the surface. The study area of approximately 2km^2 is located in the north-western parts of the RGB, by the northern shoreline of the lake Skogsfjordvatn. (Figure 1.1)

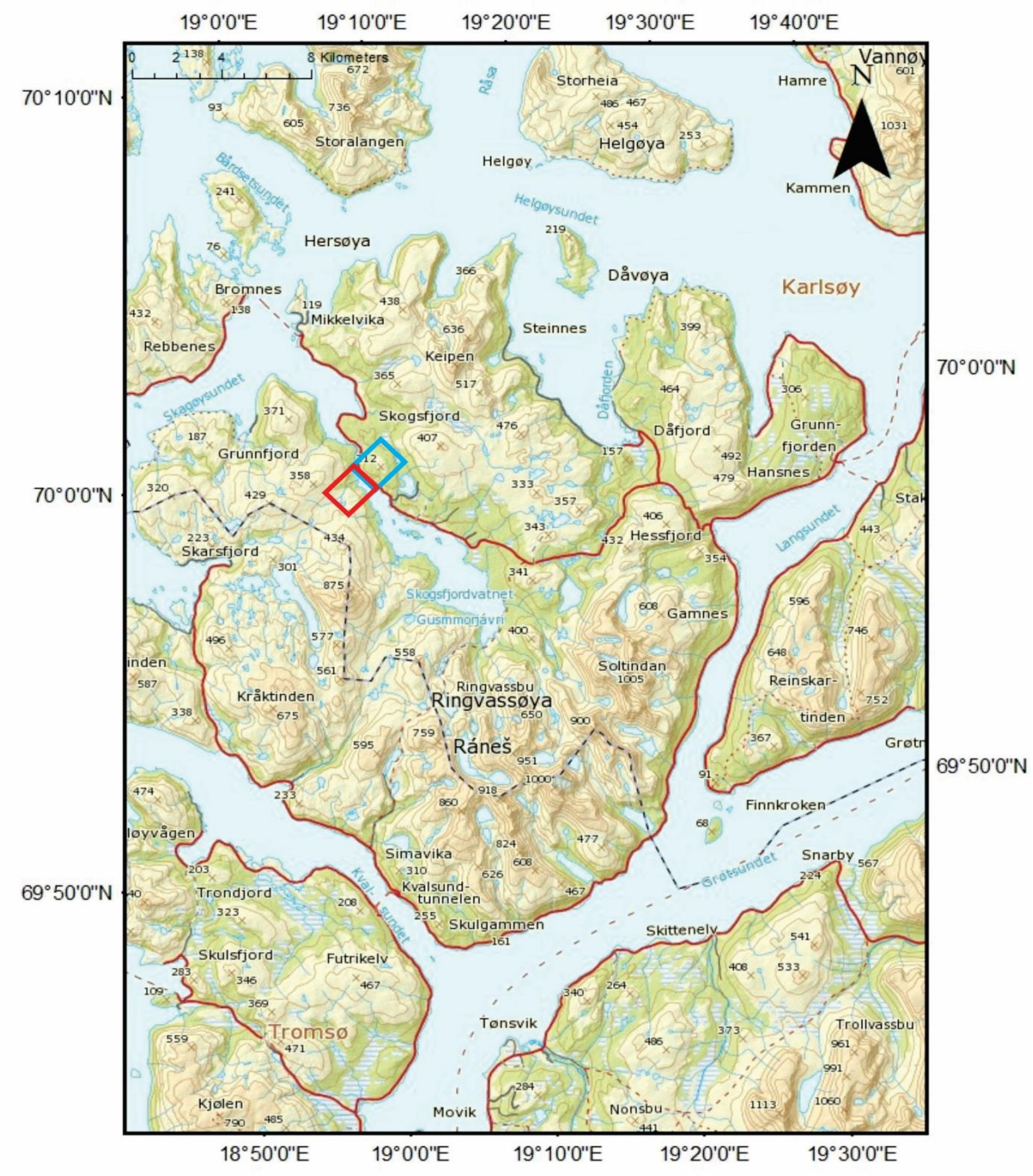

Figure 1.1: Topographical map of Ringvassøya, located in Troms County. The red square indicate the location of the Innerelvdalen map sheet and the blue square indicate the location of the Lassefjellet map sheet, combined outlining the study area. Both maps are presented in sub-section 2.1.3.

1.4. Regional geology

The West Troms Basement Complex and the Lofoten-Vesterålen Islands constitute a preserved part of the Archaean and Palaeoproterozoic conitinental crust (2.9-1.67 Ga) in northern Norway (Figure 1.2). Studies of a series of Archaean and Palaeoproterozoic geological units in the West Troms Basement Complex, including greenstone belts (Zwaan, 1995; Zwaan et al., 1998; Corfu et al., 2003; Kullerud et al., 2006; Bergh et al., 2007, 2010; Myhre et al., 2011), have highlighted and corroborated important aspects related to the tectono-magmatic evolution (cf. Bergh et al., 2010) of this cratonic-marginal province (Figure 1.3). A further correlation to the cratonic crustal provinces of the Fennoscandian Shield in the east remains enigmatic. Important questions regarding this correlation have been raised (Bergh et al., 2014), emphasizing also the structure and ore-potential of the WTBC's NW-SE trending metasupracrustal units (Armitage & Bergh, 2005; Zwaan, 1989; Motuza, 2000) as key components. Several greenstone belts exist in the WTBC (Bergh et al., 2010), but the only supracrustal unit of evidently Neoarchaean age, the Ringvassøya Greenstone Belt (Zwaan, 1989; Motuza, 2000) may provide a particularly important piece to this puzzle. Sharing several similarities with the greenstone belts of the Belomorian province (Hölttä et al., 2008; see sub-section 1.4.1), a better understanding of the structures, lithology and ore-potential in the Ringvassøya Greenstone Belt may help resolve questions regarding the West Troms Basement Complex's relation to e.g. the Fennoscandian Shield (Bergh et al., 2012).

1.4.1. Fennoscandian shield

From a geographical point of view, the Fennoscandian shield comprises large parts of Sweden, Finland, northwestern Russia and Norway. In terms of geology, the Fennoscandian Shield forms the northwestern crustal segment of the East European Craton, which is the largest exposed segment (ca 1,417,400 km2, Sundblad, 2003) of Precambrian crust in Europe (Figure 1.2).

The bedrock forming the shield includes domains ranging from 3.5 and 1.5 Ga, where the general trend is a successively younger bedrock from northeast to southwest. This age separation is a result of several orogenic events, i.e the Lopian, the Lappland-Kola (Svecokarelian), the Svecofennian and the Gothian orogenies (Hölttä et al., 2008; Lahtinen et al., 2008).

The Archaean domain and Palaeoproterozoic cover rocks

The Archaean domain, situated in the northeastern parts of the Fennoscandian Shield (Kola Peninsula, Karelia and northeastern Finland), is divided into four main provinces, i.e. the Karelian, the Belomorian, the Kola and the Norrbotten province (Gaál & Gorbatchev, 1987; Gorbatchev & Bogdanova, 1993; Hölttä et al., 2008; Lahtinen, 2012;). Palaeoproterozoic rifting and break-up between 2.5 and 2.0 Ga (Gorbatschev & Bogdanova, 1993; Lahtinen, 2012) has strongly affected the Archaean domain, causing dispersal and reworking. These rifting events are associated with the formation of tholeiitic dykes and sills, as well as volcanic and shallow-water sedimentary rocks (Laajoki, 2005; Vuollo & Huhma, 2005) in all provinces (Figure 1.2). The partly covered Norrbotten province, mainly dominated by Archaean and Proterozoic rocks, is believed to extend under the Caledonian orogenic belt in the northwest, where it crops out below the Lower Allochthon (Lahtinen, 2012).

The Archaean crust with highest intensity of Neoarchaean and Palaeoproterozoic deformation is the Belomorian province. Mainly consisting of Meso- and Neoarchaean TTG gneisses, greenstones and paragneisses, the Belomorian province is characterized by three age generations of greenstone belts, dating from 2.88 Ga to 2.66 Ga (Hölttä et al., 2008). All Belomorian greenstone complexes comprise rocks ranging from polymictic conglomerates and meta-sandstones to a wide specter of volcanic rocks with rhyodacitic to basaltic composition. The province is separated from the underlying Karelian province by a detachment zone (Mints et al., 2004).

Along the western border of the underlying Karelian province (Lahtinen, 2012), Palaeoproterozoic rifting resulted in the formation of 2.05 Ga bimodal felsic-mafic volcanic rocks of alkaline affinity, intercalated with deep-water turbiditic sediments (Lahtinen, 2012). Felsic volcanics aged 2.02 Ga also occur in association with oceanic island arc-type rocks in the Karelian province, regarded as the oldest candidate for Palaeoproterozoic subduction-related rocks, as no subduction-related magmatism has been recorded between 2.7 and 2.05 Ga (Lahtinen, 2012).

The oldest Kola province displays the fewest signs of Palaeoproterozoic deformation (Hölttä, 2008), as only the Keivy terrain show signs of heavy reworking. The Keivy terrain is characterized by felsic metavolcanic rocks dated at 2.87 Ga (Hölttä, 2008), and resembling the younger island arc-type rocks of the Karelian province.

Palaeoproterozoic orogenic rocks

The main Palaeoproterozoic orogenic evolution of Fennoscandia is divided into the Lapland-Kola orogeny (1.94-1.86 Ga) in the northern part, and the Nordic orogen (1.81-1.77 Ga) in the south, both involving rifting, opening and then renewed closing of oceanic and arc-marginal basins (Daly et al., 2006; Lahtinen et al., 2012). The latter event is a part of the Svecofennian orogeny 1.92-1.79 Ga (Lahtinen et al., 2005, 2008), responsible for the production of a large volume of Palaeoproterozoic crust in the Svecofennian province (Lahtinen et al., 2012). As the Lapland-Kola mobile belt (separating the Archaean and Svecofennian Domains) and the Svecofennian Domian both contain a considerable amount of Palaeoproterozoic rocks, the difference in character is remarkable. The high P-T features of the Lapland-Kola belt clearly reflect a collisional orogeny, whereas the Svecofennian Domain is much richer in felsic volcaninc and plutonic igneous rocks, accreted in an early stage of a collisional regime (Gorbatschev & Bogdanova, 1993; Lahtinen et al., 2012).

Meso-and neoproterozoic features and events

During the Mesoproterozoic Gothian (1.64-1.52 Ga) and Sveconorwegian (1.14-0.90 Ga) orogenies, the western and southwestern margins of the Fennoscandian Shield grew by Andean-type accretion (Bingen et al., 2008; Åhäll and Connelly, 2008). The Gothian(1.64-1.52 Ga) orogenic event formed the voluminous granite bodies(1.65-1.47 Ga) as well as calc-alcaline volcanites, e.g the Transscandinavian Igneous Belt(Larson & Berglund, 1992) in the southern Svecofennian Domain. As the Sveconorwegian orogeny involved crustal stacking and cumulating of crust in the southwest, it did not result in much formation of new crustal segments (Gorbatschev & Bogdanova, 1993).

Later reworking

Opening of the Iapetus Ocean (ca 600 Ma) resulted in a final continent-continent collision during the Scandian orogeny (430-390 Ma), followed by an orogenic collapse. This caused the formation of the allochthonous Caledonian orogenic belt, characterized by Phanerozoic rocks (500-430Ga)(Ramsay et al., 1985; Roberts et al., 2003, Lahtinen, 2012; Corfu et al., 2014). The Scandian orogeny also resulted in reworking of the older crustal segments of the Fennoscandian Shield.

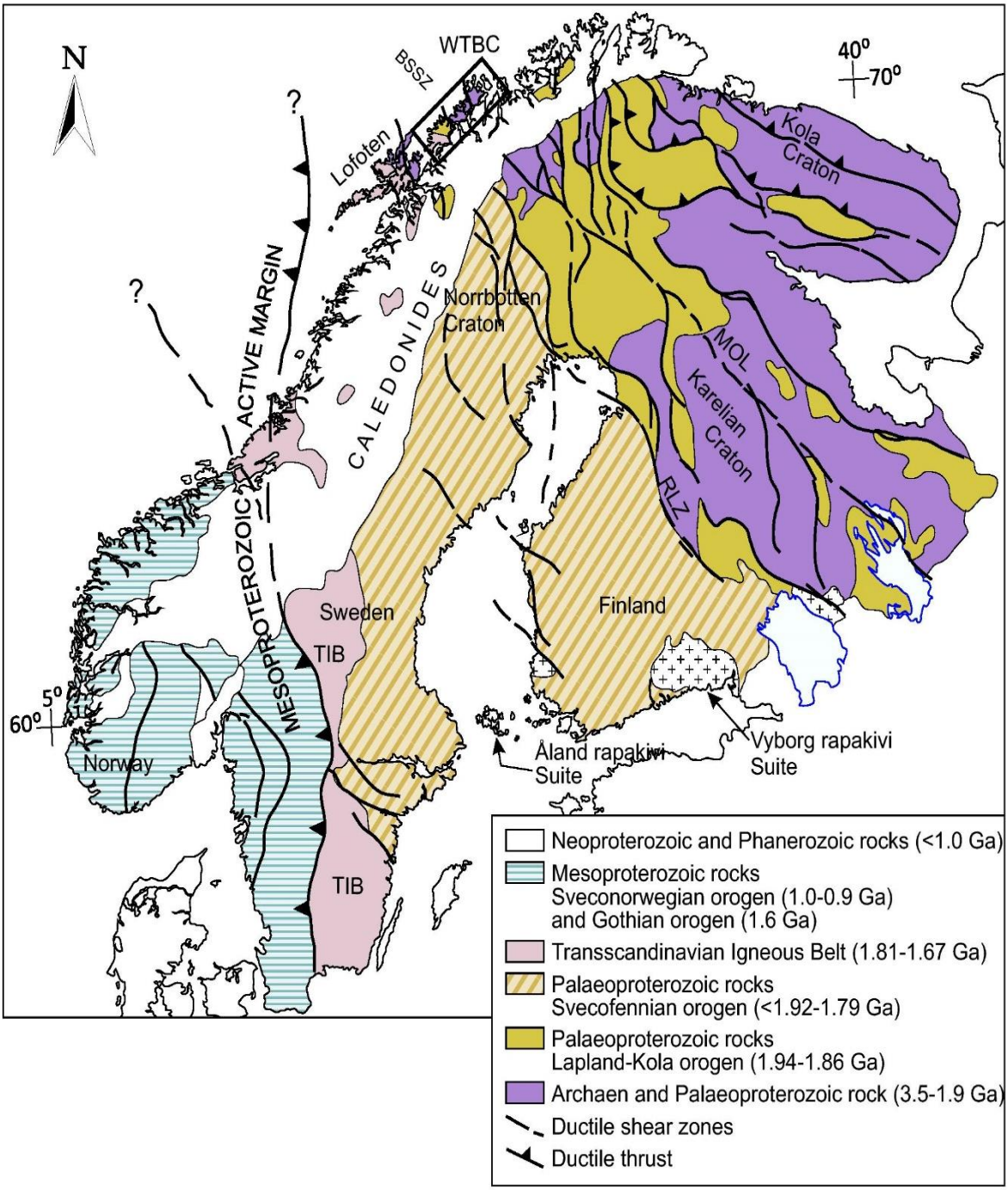

Figure 1.2: Regional geological overview of the Fennoscandian shield (Bergh et al., 2014). The black rectangle indicates the position of the West Troms Basement Complex.

1.4.2. West Troms Basement Complex

The West Troms Basement Complex (WTBC) makes up the bedrock geology of a chain of islands west of the Scandinavian Caledonides (Figure 1.3). Starting with the island of Vannøya in the northeast, Ringvassøya and Kvaløya in the central part, and the island of Senja in the southwest, bordering the southwestermost Lofoten and Vesterålen magmatic provinces (Zwaan et al., 1998; Corfu, 2004; Bergh et al., 2010). The complex was uplifted as a major horst due to Mesozoic rifting and normal faulting (Olesen et al., 1997; Indrevær et al., 2013), and erosion has later on exposed bedrock of Neoarchaean to Palaeoproterozoic age. Despite the proximity to the Caledonian mountain range and its orogenesis, Archaean and Palaeoproterozoic structures are well preserved within the WTBC (Bergh et al., 2010). The WTBC is thought to be either a part of the northwesternmost Fennoscandian Shield margin, or an exotic element from the Laurentian/Greenland margin (Bergh et al., 2014).

The bedrock of the WTBC can be divided into two distinct tectonic provinces separated by the Senja shear belt (Zwaan, 1995), and by a number of NW-SE trending meta-supracrustal/greenstone belts and mafic and felsic intrusives (Figure 1.3).

Archaean domains and Palaeoproterozoic structures

The backbone of the West Troms Basement complex is composed of Meso- and Neoarchaean rocks (Bergh et al., 2014). The vast majority is Neoarchaean tonalitic, trondhjemitic and granitic(TTG) gneisses (2.92-2.70Ga), well displayed in the northeastern domain, and displaying relict high-grade tectono-metamorphic assemblages. The TTG-gneisses (2.89-2.70Ga) on Ringvassøya in the north are separated by NW-SE trending metasupracrustal rocks of presumably early Palaeproterozoic age (Motuza, 2000; Bergh et al., 2007). As for the southwestern domain of the WTBC, a more granitic composition is prevailing in the bedrock. The ca 30 km wide Senja shear belt separates the two tectonic provinces, constituting a network of Palaeoproterozoic and possibly Svecofennian ductile shear zones trending NW-SE (Zwaan, 1995). The TTG domains of the WTBC are intercalated with mafic to ultramafic layers (Bergh et al., 2014), along with mafic to ultramafic intrusive dyke swarms (2.4Ga) (Kullerud et al., 2006)

Svecofennian deformation

Conspicuous ductile deformation and amphibolite- to greenschist facies metamorphic overprint characterize the entire WTBC; this was mainly caused by the Svecofennian tectonic event (1.8-1.7 Ga). The metamorphic grade varies from lower greenshist facies at Vanna (Bergh et al., 2007) in the northeast, to amphibolite facies in southwestern Ringvassøya(including western parts of the

Ringvassøya Greenstone belt) and central parts of the WTBC farther south. Thus, the metamorphic trend is increasing towards the southwest of the WTBC, with retrogressive greenschist facies metamorphic reworking only in the northeast (Zwaan, 1996). Younger bimodal plutonic suites (1.7-1.76 Ga)(Corfu et al., 2003) have later on intruded the WTBC.

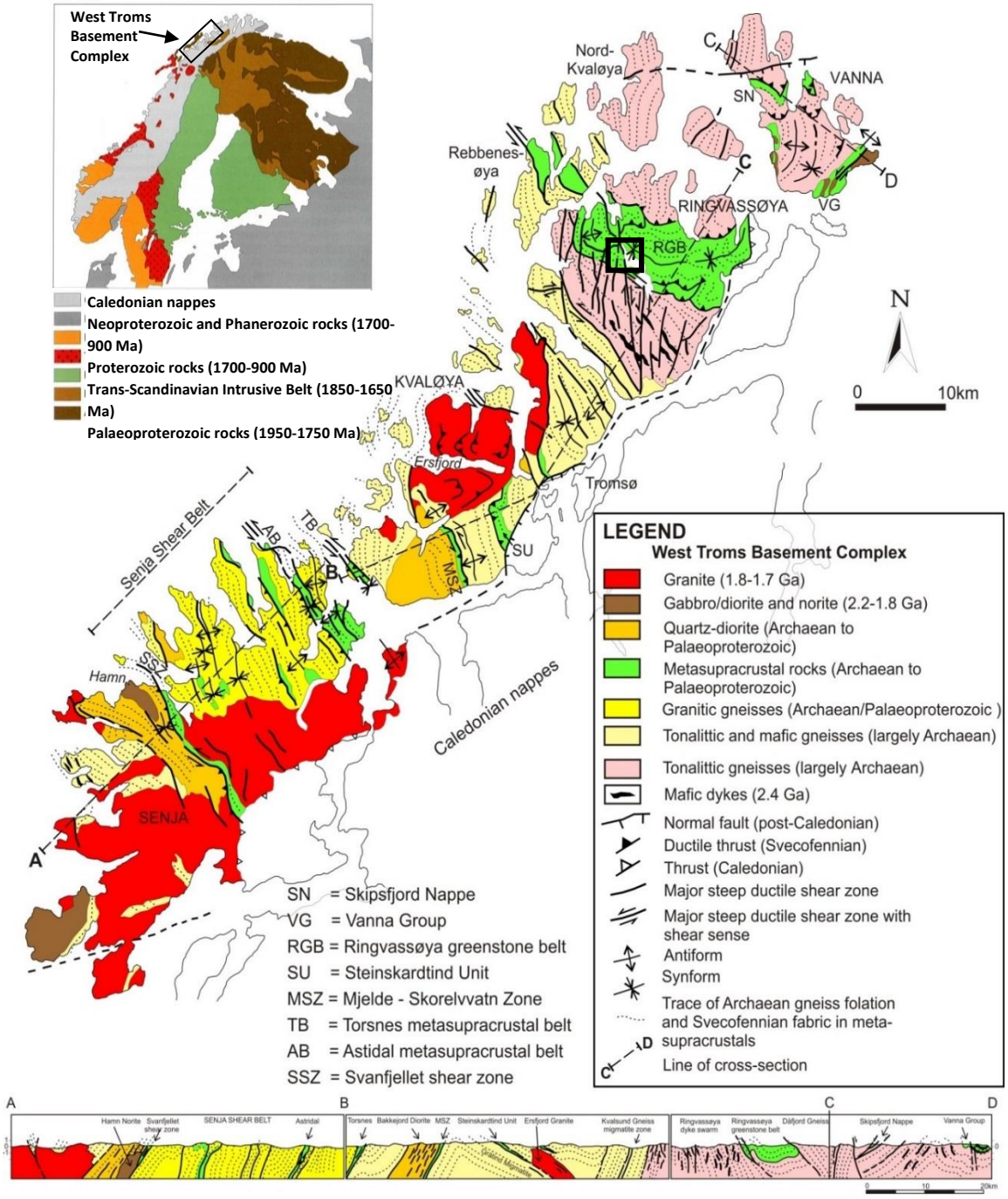

Figure 1.3: Map of the regional geology in the West Troms Basement Complex, and its relative location in Fennoscandia (Ramberg et al., 2006) on the index map, modified from Bergh et al. (2010). The black square indicates the location of the study area.

1.4.3. The Ringvassøya Greenstone Belt

Location and contact relations

The bedrock geology of the Ringvassøya island (Figure 1.4) can be divided into three main units: (1) Meta-tonalitic basement gneisses (TTG) assumed to be Meso- to Neoarchaean in age (Bergh et al., 2010; Myhre et al., 2011). (2) An overlying sequence of evidently Neoarchaean (Motuza, 2000) metasupracrustal rocks, known as the Ringvassøya Greenstone Belt, the age of RGB is however debated when compared with the Palaeoproterozoic ages of similar metasupracrustal units (e.g Torsnes 1.9Ga) in the WTBC (Myhre et al., 2013). (3) The overlying Lyngsfjell Nappe (Zwaan, 1989) in the east, consisting of Caledonian rocks. The TTG-gneisses are intruded by numerous mafic and felsic dykes, dated at c. 2.4 Ga (Kullerud et al., 2006), some of whom can be traced across the gneiss-greenstone contact into the Ringvassøya Greenstone belt.

With an extent of up to 15x40 kilometers, the NW-SE trending Ringvassøya Greenstone Belt is sandwiched in between segments of TTG-gneisses (Zwaan, 1989). On the northeastern side, the tonalitic Dåfjord gneiss domains are prevailing. Corroborated by a characteristic thrust contact to the supracrustal rocks, this unit of TTG-gneiss was likely emplaced on top of the Ringvassøya Greenstone Belt during the Svecofennian orogeny, and this presumed NE-SW shortening and thrusting resulted in large-scale syn-formal structure in the interior of the Ringvassøya Greenstone Belt(Bergh & Armitage, 1998; Bergh et al., 2010). In the southwest, a combined ductile reverse fault with strike slip overprint (Bergh & Armitage, 1998) separates the supracrustal rocks from various displaced tonalitic, granitic and mafic gneisses (Zwaan, 1989; Motuza, 2000).

The remains of an overlying Caledonian thrust nappe, the Lyngsfjell Nappe, is present in the northeastern parts of Ringvassøya. The nappe predominatly consists of sedimentary rocks ranging from low- to medium- grade metamorphic conditions. This particular part of the Lyngsfjell Nappe is referred to as the Hansnes group (Binns, 1983), and interpreted to have been thrusted in from the northwest over the WTBC suite during the Caledonian orogeny.

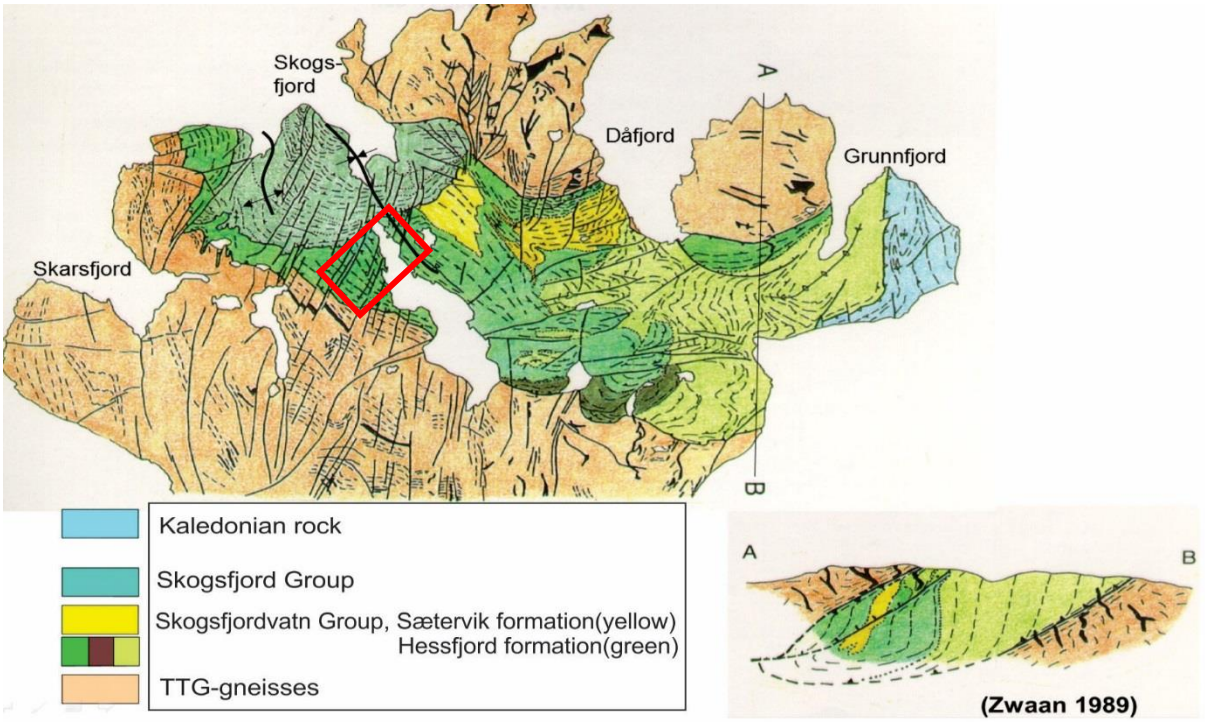

Lithology

Figure 1.4: Geological map showing the tectono-stratigraphic relationships and profile of Ringvassøya, modified from Zwaan (1989). The red square indicates the location of the study area

The Ringvassøya Greenstone Belt is divided into two main groups (Figure 1.4): the lowermost Skogsfjordvatn Group and the overlying Skogsfjord Group (Zwaan, 1989), separated by a tectonic contact, probably a low angle thrust fault (Bergh & Armitage, 1998). Overall, the belt is comprised of both felsic and mafic volcanic units, originating from a possible back-arc volcanic setting (Motuza, 2000). The Skogsfjord group is mainly dominated by garnet-quartz-feldspar hornblende schists (Zwaan, 1989), and is regarded as the group with the highest metamorphic grade. The underlying Skogsfjordvatn Group is divided into two formations:

(1) The lowermost Hessfjord (Figure 1.4) formation dominated by dark volcanic rocks, local layers of felsic meta-volcanics (keratophyre) and various meta-sedimentary rocks. Importantly, the various felsic meta-volcanic rocks (Keratophyre), amphibolites, mica schist, and quartzites contain very high concentrations of iron-sulfides, and some of them carry epigenic gold (Zwaan, 1989; Sandstad & Nilsson, 1998; Bergh et al., 2010). These sediment-hosted sulfide- rich lithologies make up a significant portion of the Skogsfjordvatn Group (Zwaan, 1989).

(2) The overlying Sætervik Formation (Figure 1.4) consists of various meta-sedimentary rocks and hornblende schists. The contact between the two groups is regarded as depositional and transitional, as the Hessfjord formation experiences an increase in sedimentary rocks upwards in the lithological package (Zwaan, 1989).

Metamorphism

Overall, the metamorphic grade of the Ringvassøya Greenstone Belt rocks is amphibolite facies in the western areas, with a gradual decrease toward greenschist facies conditions in the central and eastern parts of the (Motuza, 2000).

1.5. Greenstone belts and ore deposits

"Greenstone belts" is a widely used term for low-grade metamorphic mafic volcanic and/or volcano-sedimentary rocks related to the Precambrian (Blatt et al., 2006). The term *greenstone* comes from the distinct green hue to the color of greenschist facies metamorphic mafic minerals (e.g. chlorite), whereas *belt* refers to extensive zones of metamorphosed mafic to ultramafic and meta-sedimentary units arranged in between granite and gneiss basement rocks. In order to fulfill the greenstone belt definition completely, the zone of metamorphosed rock should be formed within the age span of Archaean to Proterozoic (De Wit & Ashwal, 1997).

Greenstone belts are often referred to as supracrustal belts; this is however a definition of their occurrence and formation rather than their composition. When Archaean cratons (e.g the Fennoscandian Shield) were subjected to extension, shallow rift basins formed. Subsequent volcanism filled in the basins with lavas of felsic to mafic composition, along with accumulation of various clastic and volcaniclastic sediments. Because the volcanic and sedimentary rocks were deposited on *top of* the prehistoric crust, the term *supra* (Latin; above) is adopted.

Greenstone belts are present on all of Earth's continents, in areas where Archaean crust is exposed on the surface. The general geologic interest in these ancient volcanic rocks is mostly due to their ability to carry ore deposits. Known to accommodate super-scale ore deposits of gold, silver, copper, zinc, REE(Rare-Earth Elements) and PGE(Platinum-Group Elements)(e.g. Sundblad, 2003; De Wit & Ashwal, 1997), these formations of rock are highly valued targets for modern day prospectors. For instance, the Archaean Abitibi Greenstone Belt (Corfu & Noble, 1992) in Canada, is one of the largest greenstone belts in the world; it has already generated 160 million ounces (5000 tons) of gold, whereas ongoing exploration is verifying significant in-situ deposits. Several other greenstone belts are also present significant ore-deposits, e.g. in the Yilgarn Craton of Western Australia (e.g Cassidy & Wyche, 2012). The greenstone belts in this particular part of Archaean crust are known to host approximately 30 percent of the world's known gold reserves, 20 percent of the world's nickel reserves and 80 percent of the world's tantalum, a REE used in various electronics(e.g Xie et al., 1993). Not only do considerable

amounts of greenstone-hosted ore-deposits in Australia and Canada, the Fennoscandian Shield (Lahtinen, 2012; Hölttä, 2008) is presenting similar features (e.g. Sundblad, 2003; Ojala, 2007).

After the Lopian orogeny(2.9-2.6 Ga), extensive Palaeoproterozoic rifting and breakup in the Arcean domains of the Fennoscandian Shield resulted in the formation of linear troughs as part of the former Kola Ocean (Berthelsen & Marker, 1986). Later on, during the Svecokarelian and Svecofennian tectono-thermal (orogenic) events (2.0-1.77 Ga), these basins were closed and deformed, now forming strongly deformed up to 1500 km long NW-SE- trending volcano-sedimentary belts encompassed by TTG-gneisses (Gaál & Gorbatschev, 1987; Gaál & Sundblad, 1990; Gorbatschev & Bogdanova, 1993). These greenstone belts all show significant fold-thrust belts and regional ductile shear zones, presumably products of the terminating Svecofennian orogeny (1.92-1.79 Ga).

Today, the NW-SE trending greenstone belts of Archaean to early Palaeoproterozoic age are present in Russia (Kola Peninsula), northern Finland, Sweden and Norway, and some of them are known to host Scandinavia's biggest deposits of precious minerals (Sundblad, 2003). Among those is the Suurikuusikko gold deposit, hosted by the Palaeoproterozoic Central Lapland greenstone belt (Patison, 2007). Discovered in 1986, it is regarded as the largest gold deposit in northern Europe (GTK.fi), with production yielding over 30 tons of gold and estimated in-situ resources to another 110 tons (Agnicoeagle.com). Archaean greenstone belts are also hosting gold deposits in Scandinavia, as exemplified by the Pampalo Au deposit situated in the Ilomantsi greenstone belt (Poutiainen & Partamies, 2003), estimated to hold 6300 kg of gold (GTK.fi).

A geological correlation between the Palaeoproterozoic greenstone belts in Finnish Lapland and in eastern Finnmark (the Karasjok and Kautokeino greenstone belts) is possible (Torske & Bergh, 2004; Bergh et al 2014), and may provide a clue to better understanding the genesis and linkage of important ore-hosting belts. Examples include the Kautokeino greenstone belt and the Kittilä greenstone belt (Hanski et al., 1997) that display very similar geological, structural and ore-related features. Correlation can further be based on the significant type of precious metals in both these greenstone belts, e.g. Suurikuusikko Au-Cu deposit in the Kittila greenstone belt and Biddjovagge Au-Cu deposit in the Kautokeino greenstone belt (Olesen & Sandstad, 1993; Sundblad, 2003). The Bidjovagge ore body has yielded 7000 kg of gold and some 24,000 kg of copper during several periods of mining (Sundblad, 2003), making this a significant mining operation by Norwegian standards.
A further regional comparison by Bergh et al. (2014) implies analogies between the Palaeoproterozoic Karasjok and Kautokeino greenstone belts (Bergh & Torske, 1988; Braathen & Davidsen, 2000), and

the youngest greenstone belts in the WTBC (Armitage & Bergh, 2005). This correlation gives rise to new hope in the ongoing search for precious metals in greenstone belts of the WTBC.

1.5.1. The history of prospectingon Ringvassøya

Ringvassøya has been a target for prospectors dating as far back as 1860(Bratrein, 1989). Towards the end of the 19th century, the prospector Robert Persson from Sweden had a workforce of 40-50 men digging prospecting pits in various locations around Skogsfjordvatn, including 12-15 small to medium size pits on Lassfjellet in the study area (Figure 1.5). The target of this prospection was mainly ore-deposits of pyrite and chalcopyrite, and the pits can still be seen in the slopes around Skogsfjordvatn.

Despite the huge investments and effort, none of the operations in the Skogsfjorden area reached a phase of production. The first know commercial operation on Ringvassøya was located in Grunnfjorden, where testing operations started as early as 1860s, and the so called "Grunnfjorden Verk" was opened in 1899 (Sandstad & Nilsson, 1998). Grunnfjorden Verk had English owners and the employees, up to 30 men, were mostly of Finnish background. The operation was situated on a pyrite deposit, and during the 5 years of production, 1200 tons of ore were produced and shipped to England for purification (Bratrein, 1989). In 1907, Gamnes Copper & Sulphides started mining a Cu-Zn deposit situated on Gamnes, on the eastern side of Ringvassøya. The production went on for two years before shutting down in 1909 (Sandstad & Nilsson, 1998). During the next 70 years, various companies with national and international background were defining known deposits as well as
prospecting in different locations on Ringvassøya, all with no documented results of economical findings (Bratrein, 1989; Sandstad & Nilsson, 1998).

The prospecting activity on Ringvassøya has varied in later years, but the optimism of finding mineral deposits of economic value has not diminished. Up until the 1980s, most companies trying their luck on Ringvassøya were mostly interested in sulfur-bearing rocks, and later on in copper and zinc mineralizations. But towards the end of the mid-20th century, Ringvassøya entered a new era of mineral prospecting, now with gold as the main targeted mineral. Companies like ASPRO/Sulfidmalm and Folldal Verk/Amoco Norway started advanced prospecting work, including soil sampling, panning of moraine material and stream sediments, chip sampling, geophysics, and drilling. The work was conducted on known as well as un-known targets throughout out the RGB. The so-called "Klondike lineament" at Holmvasshøgda, and know gold occurrences on Sørdalshøgda at Tverrfjellet and Hårskoltan in the Bjørnlia area, were the main focuses of the prospecting. The optimism was great,

and highly anomalous results of up to 44ppm Au in chip-samples and 300 grains of Au in washing pans were published (Lieungh, 1985). Despite good results and plans for upcoming field seasons, the high activity of private prospecting at Ringvassøya was down-scaled in 1985, and shortly after came to an end.

Even though ASPRO/Sulfimalm and Folldal Verk/Amoco Norway released their claims, NGU continued to pin their interest in Ringvassøya. As a part of the USB-project (Undersøkelse av Statens Bergrettigheter) initiated in 1973 (Sandstad & Nilsson, 1998), a report summarizing previous work was published (Svinndal, 1974). A great amount of work was conducted to assist the prospecting industry, and to better the scientific understanding of Ringvassøya's complex geology. The work, organized by NGU and various universities in Norway, consisted of regional mapping, investigations of various mineralizations and geochemical samplings (e.g. Svinndal, 1974; Rindstad, 1977; Minsaas, 1980). This continued sporadically until the early 1990s. In 1994, a total of 27 mineral deposits had been investigated, sampled and logged in NGUs ore database.

The only private company still to have claims at Ringvassøya during this period was Norsulfid, although the company did no noteworthy prospecting up until the release of the claims around 1990. In 1998, Sandstad & Nilsson published the report "Gullundersøkelser på Ringvassøya, sammenstilling av tidligere prospektering og feltbefaring i 1997" (Gold-related investigation on Ringvassøya, a summary of prospecting-results and field reconnaissance in 1997), including results from their fieldwork in 1997 and consideration of previous work regarding gold prospecting on Ringvassøya. In the report, the authors confirmed the potential of economical gold mineralizations on Ringvassøya, and stressed the need of a better understanding of how the mineralizations relate to structures and models to make prospecting more efficient.

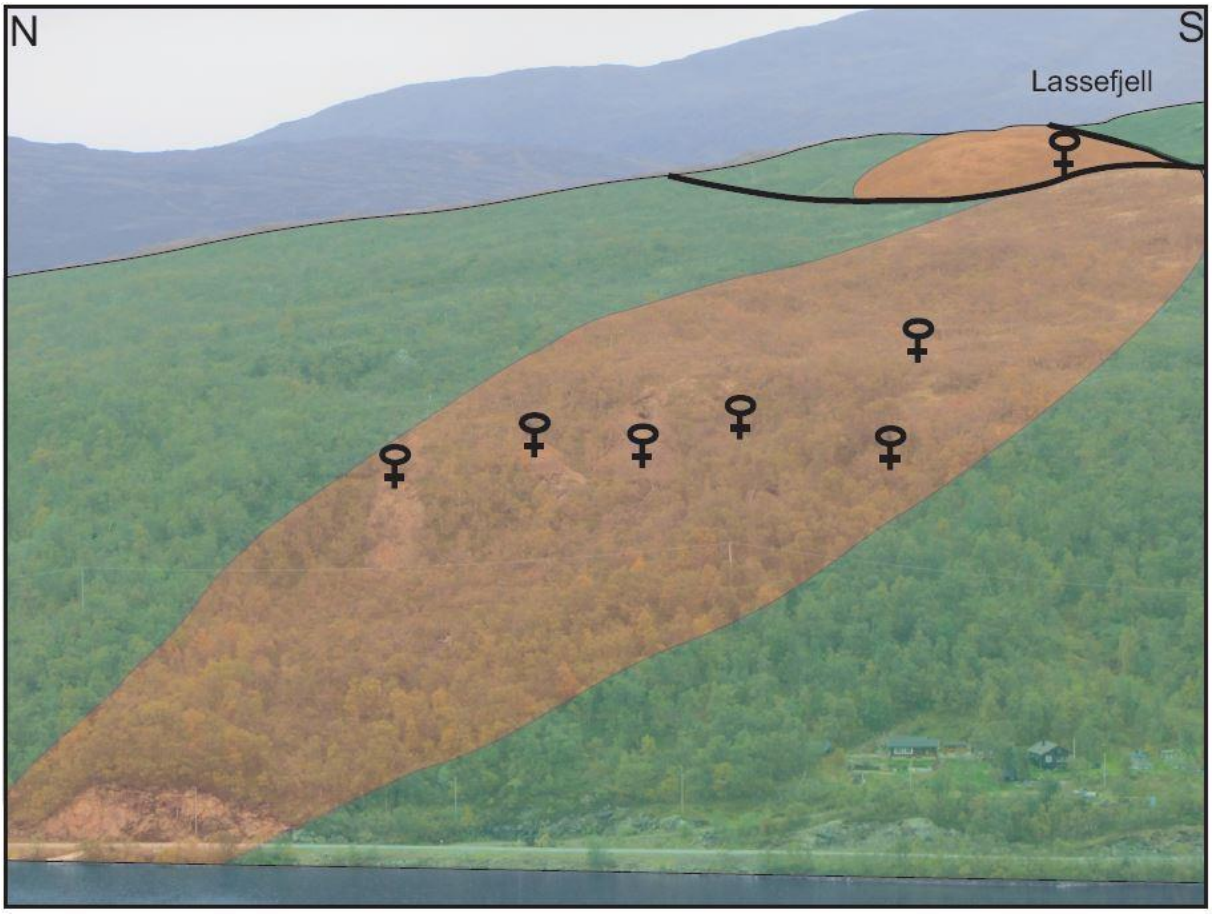

Figure 1.5: Overview of Lassefjellet. The interpreted amphiblotic terrains are displayed by green shading, and the quartz-mica rich unit with orange. Location of prospecting pits are presented with venus symbols.

1.6. Definitions and terms

The following terms and nomenclature are used troughout the thesis.

Mineralization

The author refers to mineralization as an assemblage of minerals associated with economic benefits (in this context: precious elements and iron-sulfides).

Keratophyre

The term keratophyre is a matter of discussion, and the nomenclature has changed trough times. According to literature, the most common definition is “a leucocratic sodic intermediate albite-phyric volcanic rock” (Schermerhorn, 1973). Schermerhorn has also defined the term quartz-keratophyre, classified as a leucocratic sodic felsic quartz-albite-phyric (*type one*) or albite-phyric (*type two*) volcanic rock. The distinction between keratophyre and quartz-keratophyre hinges upon the presence of free

quartz in significant amounts. Often, inspection of the groundmass can clearly decide whether a rock is keratophyre or a type two quartz-keratophyre (Schermerhorn, 1973).

Cleavage and schistosity

The concept of cleavage and schistosity are widely used as general terms for foliations thought to be of secondary origin. Cleavage is generally used for fine-grained rocks up to the scale where individual cleavage-forming minerals can be distinguished with the naked eye; schistosity for more coarse-grained secondary foliations (Passchier & Trouw, 2005).

Texture and structure

Texture refers to the geometrical aspects of the mineral of the rock, including size, shape and arrangement. Structure usually refers to the presence of compositional layering, folds, foliation and lineations in the exanimated rock (Passchier & Trouw, 2005).

2. Petrographic and structural descriptions

2.1. Introduction

The following section features petrographic and structural description of the targeted mineralized quartz-mica rich unit, and adjacent lithologies and mineralizations of the study area. A general description of quartz veins and mafic intrusions is also included, as these are important kinematic indicators and tend to be related to mineralizations (see below). All descriptions are based on field observations and petrographic studies of sampled specimens (Appendix A).

The mapped area of approximately 2 kilometers^2 is located at the northern termination of Skogsfjordvatn (Figure 1.1) and includes both main groups of the RGB, the Skogsfjordvatn Group and the overlying Skogsfjord Group (Zwaan, 1989; Figure 1.4). The area comprises hornblende schists, various amphibolites, scattered meta-sedimentary units and the targeted quartz-mica rich unit (Bergh & Armitage, 1998; Motuza, 2000; Zwaan, 1989). Approximately 9/10 of the investigated area is stratigraphically situated within the Hessfjord Formation of the Skogsfjordvatn Group, with the last tenth including the Skogsfjord Group strata (Figure 2.2 and 2.3). The two major groups are presumably separated by a low angle ductile shear zone (Bergh & Armitage, 1998), displayed as a obliquely truncating shear-zone exposed in the northwestern regions of the study area (Figure 2.2). Further introduction to lithologies and structural relations are included in each sub-section.

As all lithologies of the study area has undergone greenschist to amphibolite metamorphic conditions (Zwaan, 1989; Bergh & Armitage, 1998), no primary structures are visible in hand specimens or in thin section. The observed foliation is therefore classified as secondary (Bergh & Armitage, 1998; cf. Passchier & Trouw, 2005) and presumed to have formed parallel to the primary bedding (Bergh & Armitage, 1998). All described structures are related to the three main deformational events, D1-D3 (see sub-ection 2.1.1), and deformed in a ductile manner (Bergh & Armitage, 1998).

2.1.1. Methodology

Thin sections and microscopy

When the samples had been logged and prepared, 37 of the total 45 gathered specimens were cut to appropriate size (3.5x-2.5x-0.5 centimeters) for thin section polishing. The geological lab at the Department of Geology, UiT, conducted the preparation and polishing of the thin sections. Microscopy was carried out under plain and cross-polarized light, by the aid of a Leica DM4500P microscope. On thin sections containing sulfides and oxides the additional reflected-light mode was used. Published photographs are taken with a Canon EOS 650D camera mounted onto the microscope.

2.1.2. Brief summary of currently known structural relations on Ringvassøya

The structure of the Ringvassøya Greenstone Belt is in topographic maps displayed as a broad arcuate or bowl form with an average N-NW trend in the northwest, E-W trend in the central parts and NE trend in the eastern parts (Bergh & Armitage, 1998). This structural pattern (Figure 2.1) is suggested to be a result of at least three main phases of deformation (D1-D3, Figure 2.1), as deducted from internal meso-scale structures and their cross-cutting relationships in the RGB (Bergh & Armitage 1998). These three phases of deformation produced three distinct groups of ductile structures, including (Figure 2.1):

-D1 structures: The main S1-foliation is defined by the preferred dimensional alignment of micas, quartz and feldspar in the gneisses, and hornblende-biotite, locally garnet-porphyroblasts in the meta-volcanic rocks (Bergh & Armitage, 1998). One can also observe stretching lineations trending NE-SW on well-developed S1-foliation surfaces referred to as L1. The main fabric (S1-foliation) is considered to have formed axial-planar to mesoscale NW-SE trending recumbent isoclinal and intrafolial folds (F1), and bedding surfaces can only be found in tight F1 hinge zones (Bergh & Armitage, 1998).

-D2 structures: Macro- and meso-scale open to tight asymmetric folds are causing a regional variance in the attitude of the main S1-foliation. These macro- to megascale folds are referred to as F2 folds and their axial trends are mostly NW-SE parallel to F1 folds. Subsequent to the macrofolding shortening event, foliation-parallel to low-angle foliation-truncating mylonitic shear zones with numerous internal kink bands and oblique cleavages formed as possible, “out-of-the syncline” shear zones in relation to the macro-scale F2 folds. These shear-zones, referred to as S2, are related to ductile thrust movement between lithological groups in the RGB (Bergh & Armitage, 1998).

-D3 structures: The third main deformation event is thought to be responsible for the arcuate bending of the entire Ringvassøya Greenstone Belt to a NE trend in the southeast (Figure 2.1), and to be due to NW-SE shortening and lateral shearing (Bergh & Armitage, 1998). On a smaller scale this event caused the development of NNE-SSW trending, subvertical, high-angle (steeply dipping) oblique-truncating dextral and sinistral strike-slip shear zones that cross-cut the D1 and D2 structures, and these are later on referred to as S3 faults (Bergh & Armitage, 1998). Closely related to the S3 faults, steeply plunging drag folds (F3) with S- and Z-shaped geometries are often present, indicating that they formed by lateral (strike-slip) shearing parallel to the NW-SE shearing direction during the third deformational event (Bergh & Armitage, 1998; Bergh et al., 2010).

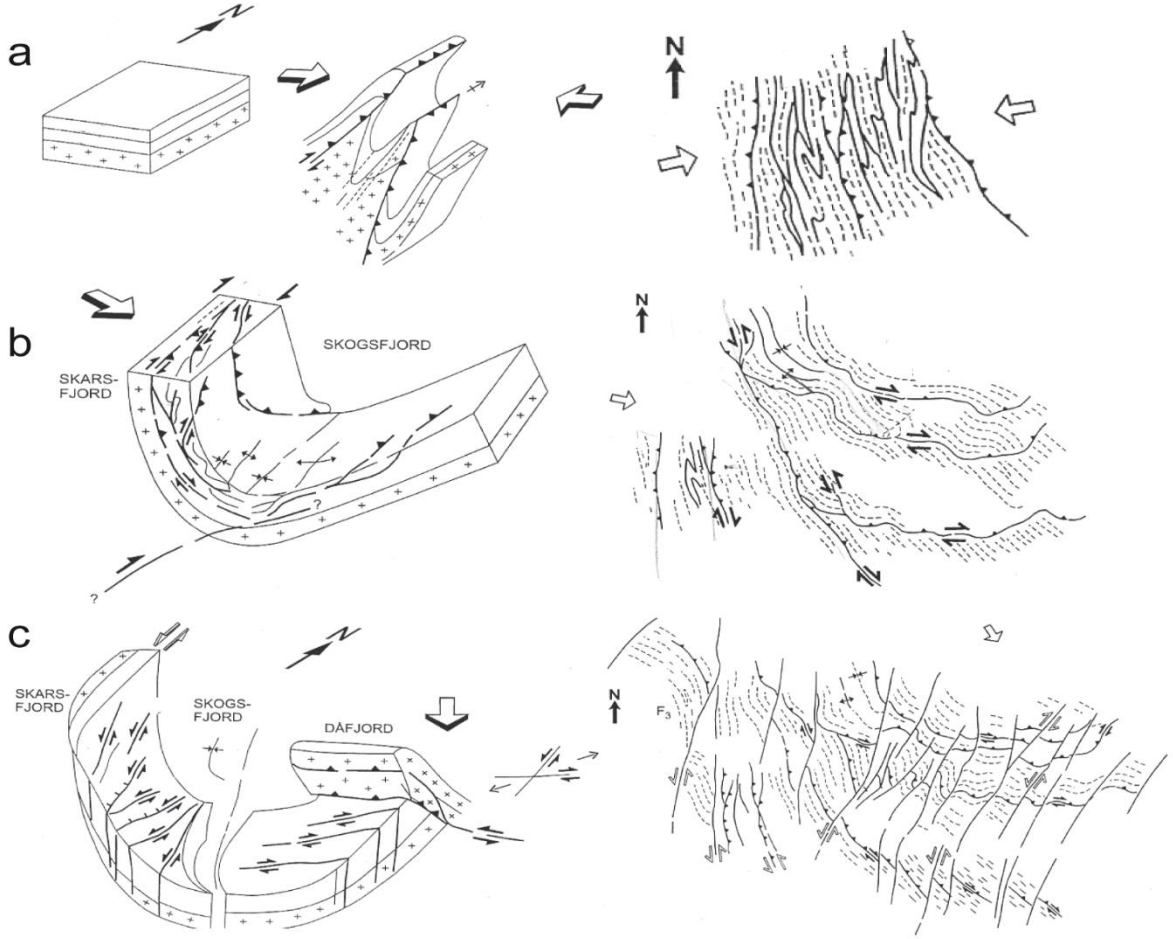

Figure 2.1: Tentative Svecofennian tectonic model for RGB and underlying TTG-gneisses.(Bergh & Armitage, 1998; Bergh et al. 2010). Left; schematical interpretations of the main structures. Right: Resulting map pattern. A) E-W compression generating tight isoclinal folds(F1) and localized ductile shear-zones(S1) along the gneiss-greenstone boundary, and main foliation(S1) in the greenstone belt. B) ESE-VNV compression resulting in regional asymmetrical folding (F2) of the main foliation(S1), and formation of low-angled out-of-the syncline thrust-faults(S2) in the hinge zones of the F2-folds, and dextral shearing(S1-S2) along the western limb(foliation) of the macro fold and TTG-greenstone contact. C) Formation of vertical cross-cutting conjugating shear-zones(S3) and related drag-folds(F3) with axial-planar cleavage, possibly related to the SE-directed thrusting from the Dåfjordgneiss.

2.1.3. Regional overview

Figure 2.2 and 2.3 below show the mapped horizontal extent of the quartz-mica rich unit on both sides of the Skogsfjordvatn lake (i.e Lassefjellet in the east and Innerelvdalen in the west). The targeted quartz-mica rich unit (orange) is displayed as conformable, interbedded in foliated amphibolites (green) of the Skogsfjord group. All presented lithologies are heavily influenced by structures related to three generations of deformational events (D1-D3), viewed as offset and deformed. Further description of the lithologies, structures and relationships are given throughout this chapter.

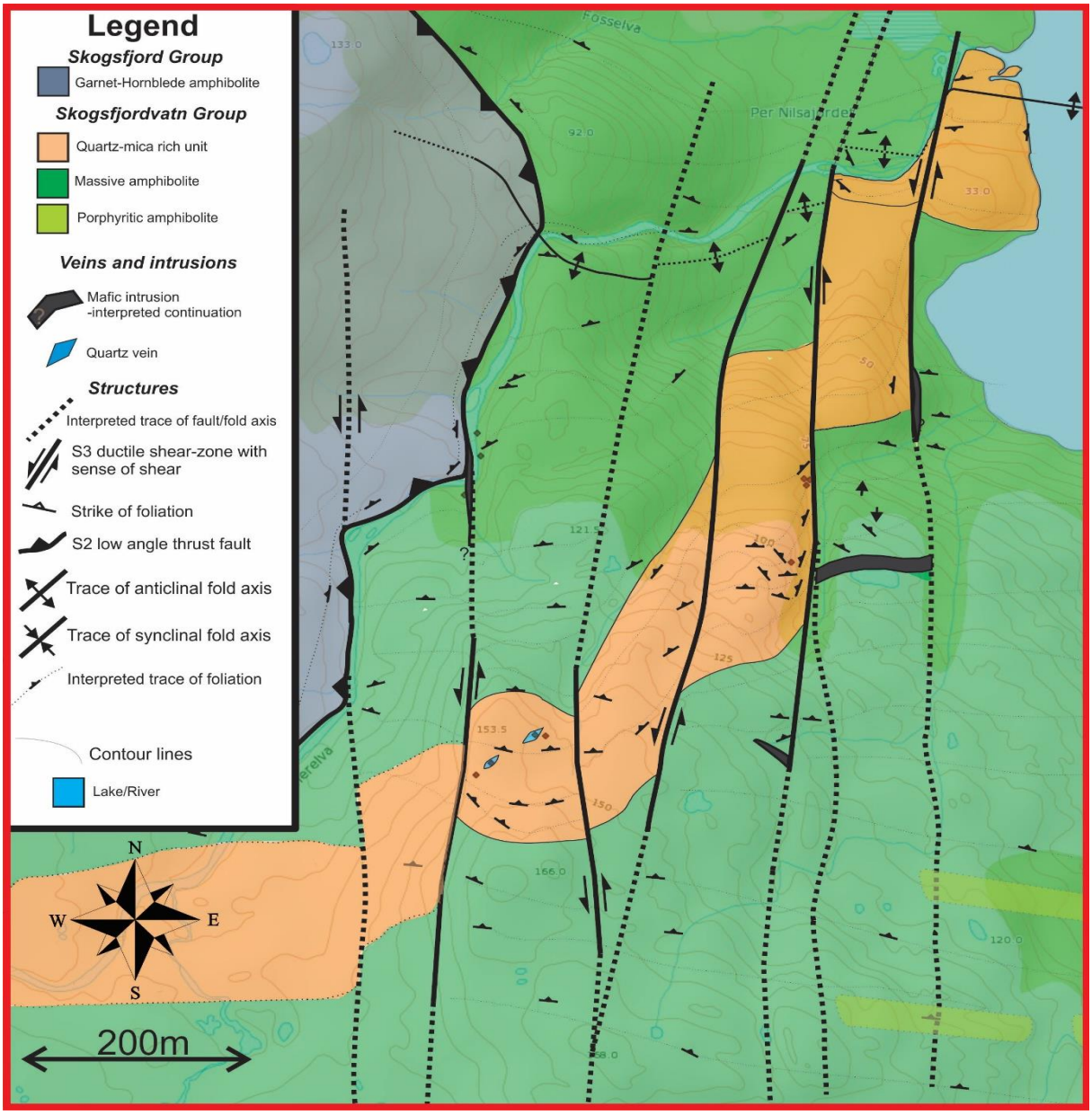

Figure 2.2: Detailed lithological and structural map of Innerelvdalen. The quartz-mica rich unit appears interbedded in the foliated amphibolite, highly influenced by structures related to three deformational events. It should be noted that the western segment of the quartz-mica rich unit is an interpreted continuation, as the unit only crops out in a few locations. The change in color within each lithology is presented to give a general impression of exposed bedrock, i.e. the darker shading indicates <25% exposure and the lighter >75% exposure. For location in the RGB, see Figure 1.1.

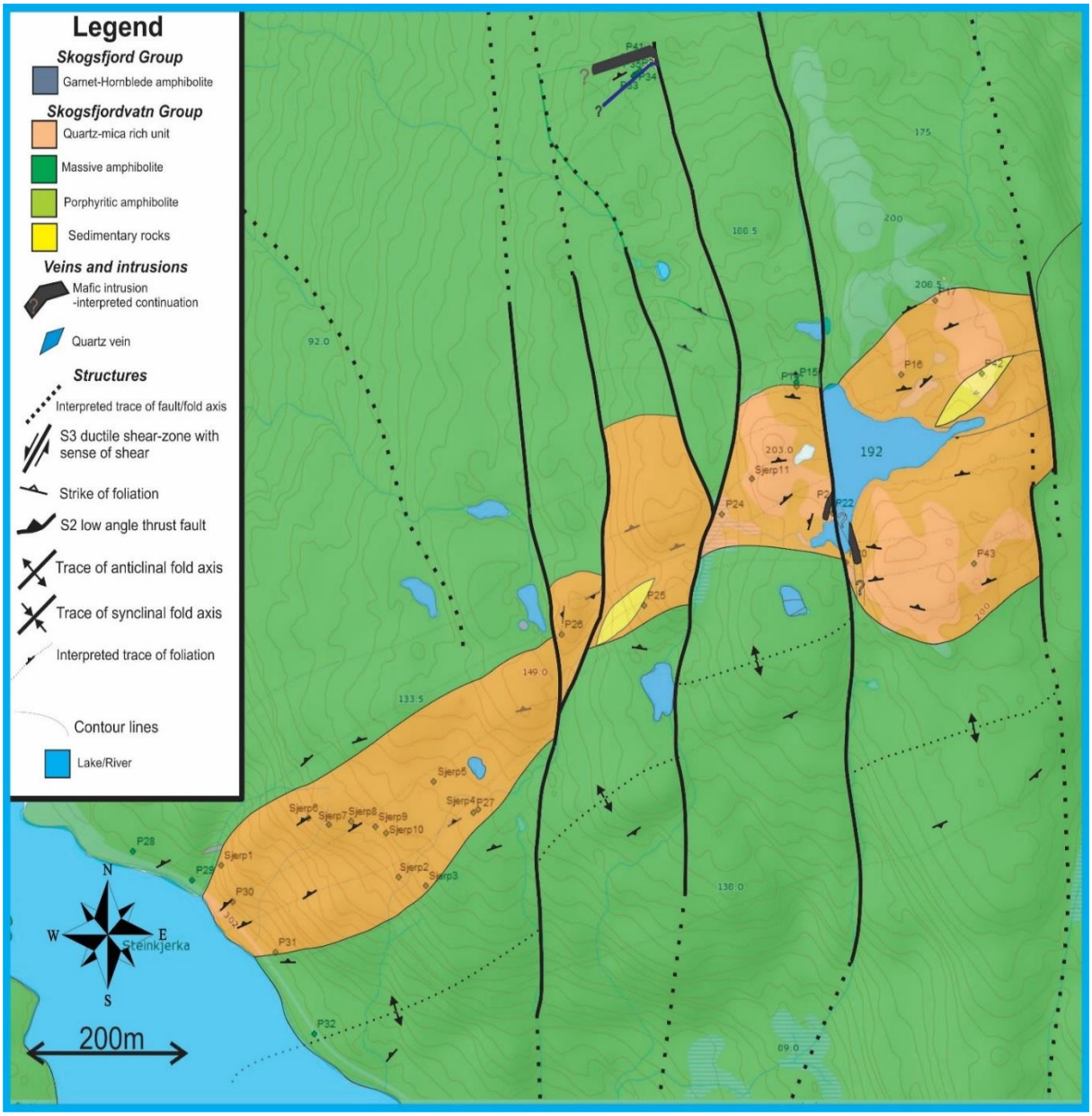

Figure 2.3: Detailed lithological and structural map of Lassefjellet. The quartz-mica rich unit appears interbedded in the foliated amphibolite, highly influenced by structures related to three deformational events. The change in color within each lithology is presented to give a general impression of exposed bedrock, i.e. the darker shading indicates <25% exposure and the lighter >75% exposure. For location in the RGB, see Figure 1.1.

2.2. Skogsfjordvatn Group

The Skogsfjordvatn Group comprises two formations. The uppermost, defined as the Sætervik formation, is mainly composed of meta-psammites, alternating hornblende-chlorite schist and intercalated amphibolite layers (Zwaan, 1989), while the lowermost Hessfjord formation is characterized by various types of amphibolite and keratophyre(Zwaan, 1989), the latter is further defined as the *quartz-mica rich unit*. With only the latter being present within the study area, this thesis emphasizes investigation of lithologies and structures within this formation (Figure 2.2 and 2.3).
The two formations are separated by a conformable and transitional contact (Zwaan, 1989). This contact has not been investigated further, as it is located in the eastern terrains of the RGB (outside the study area). The nomenclature and tectonostratigraphy proposed by Zwaan (1989) is maintained throughout this thesis.

2.2.1. Foliated amphibolite

The most common and widespread rock of the study area is a dark grey/black phaneritic amphibolite, displayed on both sides of the interbedded quartz-mica rich unit, and further defined as the country rock of the studied area (Figure 2.2 and 2.3) . The total extent of this dark colored rock body crops out far beyond the borders of the investigated domains, and thus its northwestern termination is encountered within the study area, where the lithology borders to the overlying Skogsfjord group. The boundary between these two units is defined by a low angle ductile shear zone, considered by Bergh & Armitage (1998) to be a thrust fault (see sub-section 2.1.2), well exposed along parts of the Innerelv river (Figure 2.2). Furthermore, the unit presents a conformable contact to the quartz-mica rich unit situated in the central parts, with a common trend of gradual bleaching progressing towards the lithological border. This bleached zone is defined by a gradual increase of light colored minerals presenting a leucocratic mineral matrix, normally extending up to 20 meters from the lithological contact (further description of the zone is presented below).

A typical outcrop of the foliated amphibolite looks relatively massive, displayed as a dark grey/black colored rock with a distinct green hue, often covered by smooth weathered surface. Even due to the massive appearance, all hand specimens present relatively well-developed foliation surfaces, where the alignment of hornblende and plagioclase form continuous foliation planes. The presence of aligned plagioclase and hornblende appear to vary in different locations, generally ranging from moderate to high degree of foliation. With the latter observed in thin section as subhedral hornblende and

plagioclase grains aligning to form parallel continuous cleavage, the moderate variations display more randomly distributed auhedral to subhedral hornblende and plagioclase grains in roughly spaced cleavage domains. The overall grain distribution is inequigranular, with large grains of hornblende in a fine grained equigranular matrix of plagioclase, all presenting lobate grain boundaries (Figure 2.4a,b). As the main mineral assemblage includes plagioclase and hornblende, the latter is by far the dominant matrix mineral, resembling approximately 80% of the ground mass (Figure 2.4a,b). The remaining plagioclase is represented as subhedral grains, commonly overgrown by smaller grains of epidote in the grain boundaries. Hornblende is mainly poikilitic, containing inclusions of quartz and plagioclase (Figure 2.4a). Quartz is mainly observed as a secondary mineral in the rock, represented by thin veins or small lenses (<5mm) often in association with carbonate (Figure 2.4d). Minor amounts of anhedral pyrite are also observed in the mineral matrix (Figure 2.4c), often with increasing distribution on the vicinity of quartz-mica rich unit.

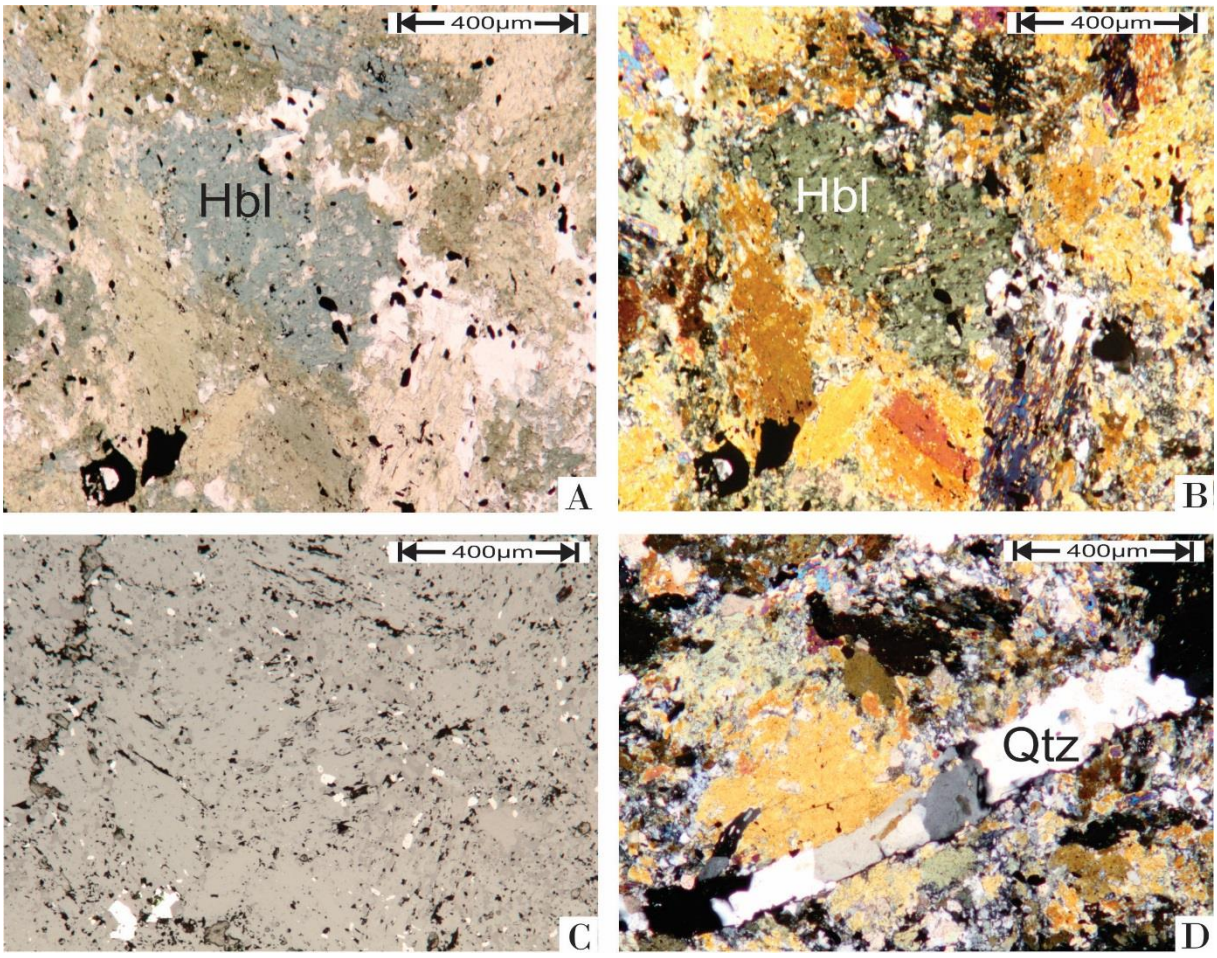

Figure 2.4: A) Foliated amphibolite viewed in plane-polarized light. Note the scattered opaque minerals and poikilitic hornblende with inclusions of feldspar (presumably plagioclase) B) Foliated amphibolite viewed in cross-polarized light. Note the very irregular grain boundaries. C) Foliated amphibolite viewed in reflected light. The opaque mierals are here determined to be pyrite. D) Quartz-carbonate vein with thickness of approximately 200 microns, note how the feldspar is altered into sericite(high interference colors) in the vicinity of the vein. All pictures originate from sample HE-34.

Thin section studies of the bleached type of foliated amphibolite described above, reveal high contents of fine-grained quartz and muscovite that are making up for the leucocratic mineral assemblage. Anhedral fine-grained muscovite appears to have near totally displaced the polygonal plagioclase, observed as intense serritication at the boundaries of the few remaining plagioclase grains. The initial inequigranular distribution of grains in the foliated amphibolite is further changed to a seriate apperance, with large hornblende grains in a fine grained matrix of serricite and quartz, all displaying interlobate grain boundaries. The amount of scattered anhedral grains of pyrite randomly distributed in the mineral matrix has also increased dramatically, making up for about 10 percent of the mineral matrix.

2.2.2. Porphyritic amphibolite

Mapped to a relatively limited extent, this particular type of amphibolite is only observed in a few localities to the south of Innerelvdalen (Figure 2.2). The outcropped appearance is on the other hand easily recognizable, displayed as a dark grey rock with distinct white mineral patches. These white patches of roughly 5-20 millimeter in size consist of feldspar, occurring within a fine-grained hornblende-rich matrix (Figure 2.5). The outcrops are rarely over 20 meters long and 5 meters wide, all presented as elongated bodies, intercalated in the surrounding foliated amphibolite (see sub-section 2.2.1; Figure 2.2) parallel to the main foliation. The patches of plagioclase occur as stretched, also orientated parallel to the main foliation of the surrounding foliated amphibolite. Further petrographic investigation of this rock unit is not conducted, as no specimens for thin-section analysis were gathered.

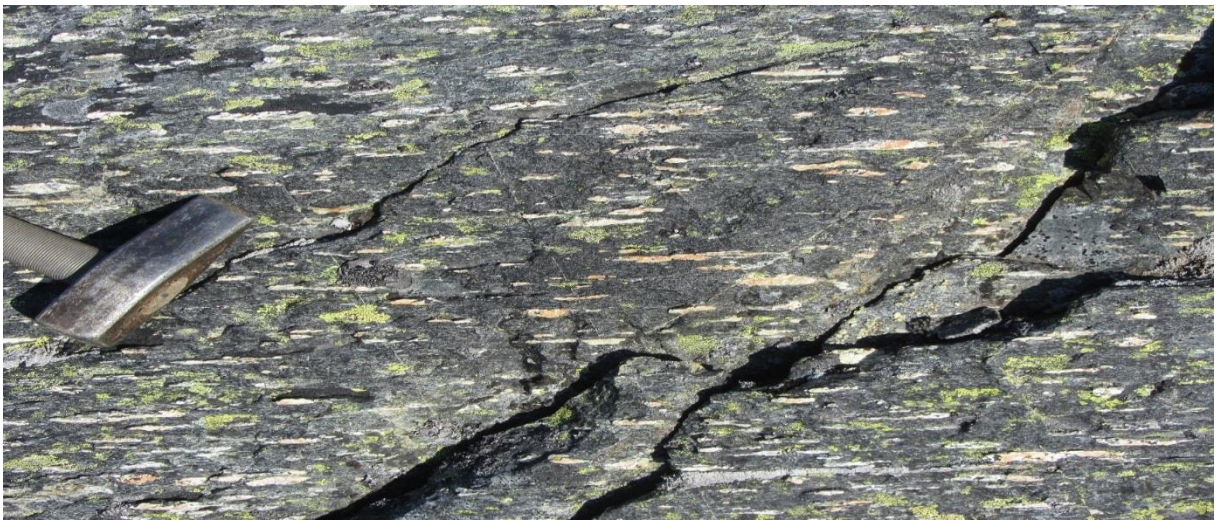

Figure 2.5: Porphyritic amphibolite, outcropping in the southwestern domains of the study area. Plagioclase patches are aligned parallel to the S1-foliation of the surrounding foliated amphibolite.

2.2.3. Quartz-mica rich unit.

Covering about 1/5 of the study area, the main target of investigation is displayed as a light colored quartz and white mica-rich sulfide hosting lithology, mapped from the top of Lassefjellet in the east to Innerelvvatnet in the west (Figure 2.2 and 2.3), previously mapped to a further extend westwards of approximately 10 kilometers (Bergh & Armitage 1998). This E-W striking unit occurs as conformable and interbedded in the foliated amphibolite, displaying no disconformity changes in the attitude of the foliation across the lithological border. The width of the unit varies from 20 to 70 meters, with a general attitude of lesser thickness in the areas of lower altitude along the shore of the Skogsfjordvatn lake (Figure 2.2 and 2.3). Despite the limited amount of exposed bedrock in the study area, the unit's distinct weathered surface is easily recognizable, displayed as reddish brown oxidized surface (Figure 2.7a,b). This characteristic appearance also makes it a good marker horizon, favorable for structural mapping related to the thesis objectives.

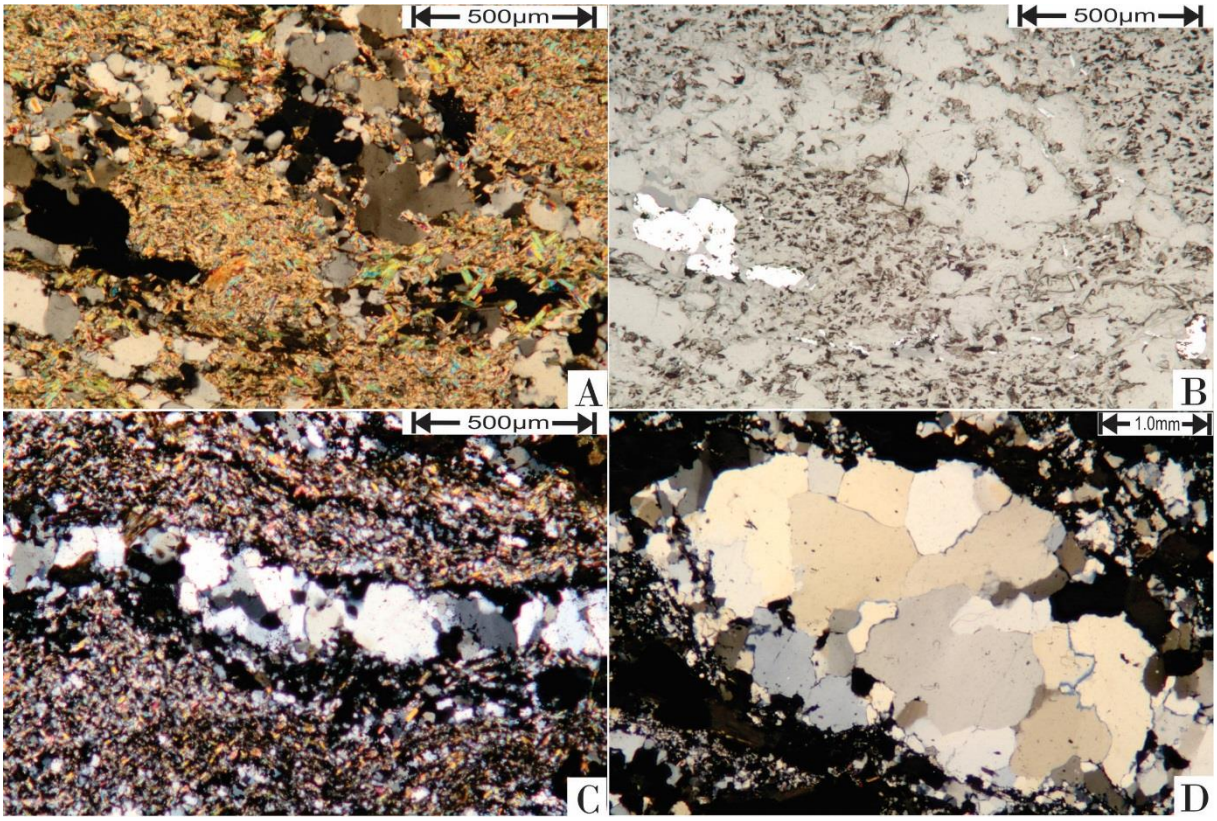

Figure 2.6: All pictures originate from the quartz-mica rich unit, picture A, B and C is taken of sample HE-P32, and picture D is taken of sample HE-P9. A) Quartz and pyrite in a sericite matrix, viewed in cross-polarized light. B) Same picture as A, viewed in reflected light. Note the grain of pyrite(white) in the quartz-sericite matrix. C) Wriggly layers of quartz(white) and pyrite(black) in a textural equilibrium within the cericite matrix, forming the observed cleavage of the quartz-mica rich unit. Viewed in cross-polarized light D) Porphyroclast of quartz, commonly observed in the weathered specimens. Viewed in cross-polarized light.

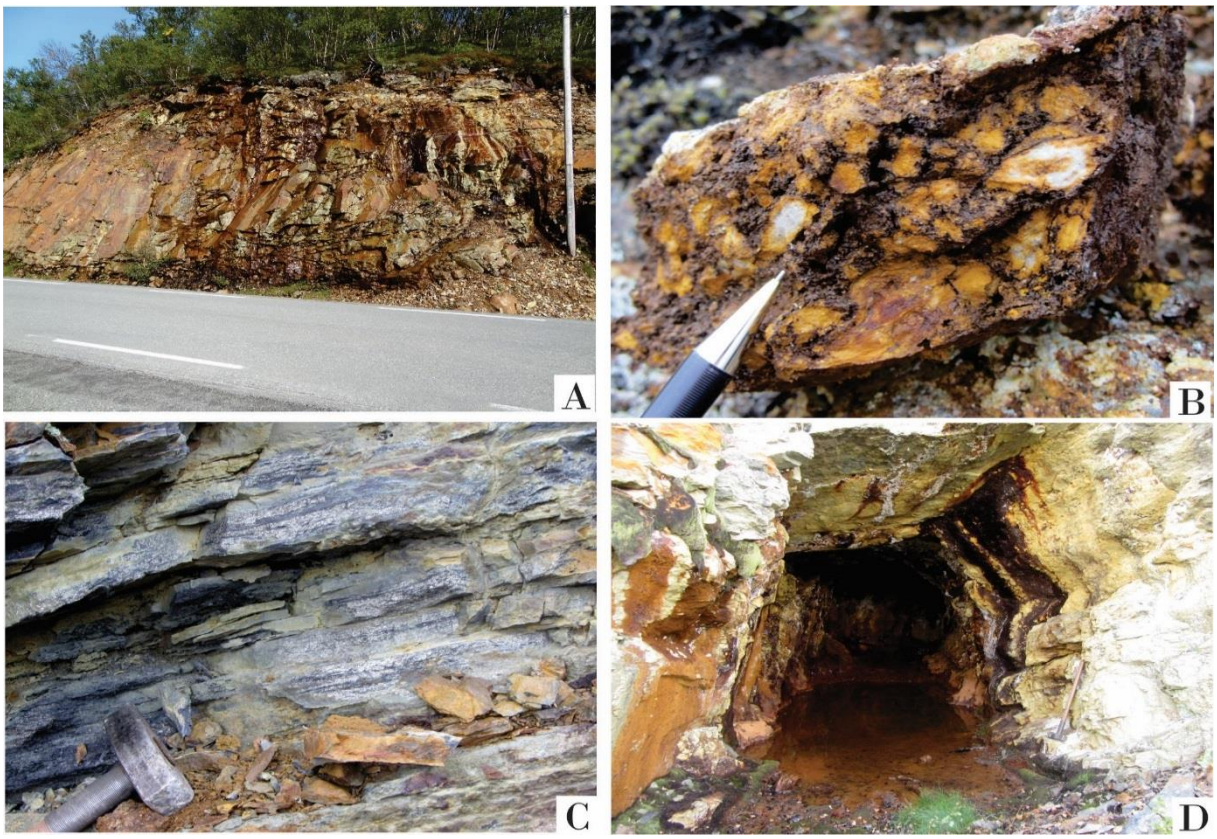

Figure 2.7: Road-cut exposing a relatively unweatherd cross section of the quartz-mica rich unit, total with of the unit is 30 meters. B) Weathered surface of the quartz-mica rich unit, displaying an oxidized matrix of sericite and pyrite, with porphyroclasts of fine grained plagioclase. C) Layered disseminated pyrite-pyrrhotite mineralization, observed parallel to the foliation of the quartz-mica rich unit. D) Prospecting pit in the quartz-mica rich unit on Lassefjellet, 1,5x2 meter and about 5 meters long.

In a traverse along a road-cut just south of Lassefjellet (Figure 2.3), the only relatively fresh and non-weathered outcrop of the quartz-mica rich unit is displayed as a 30 meter thick light-colored lithology (Figure 2.7a) interbedded in foliated amphibolite. This light colored aphanitic rock in the center of the road-cut presents the most pristine texture obtained from an outcropped specimen of the quartz-mica rich unit. Samples from the outcrop display a banded gneissose texture, including zonal layers of quartz grains (<20%) separated by a fine-grained muscovite (sericite) dominated matrix (>70%) (Figure 2.6a). The observed cleavage of the rock is defined by this spaced zonal alignment of these anhedral quartz grains, forming continuous wriggly parallel cleavage domains (cf. Passchier & throuw 2005; Figure 2.6c). Minor amounts of plagioclase are observed in the mineral matrix, often presenting strong features of sericitation along the interlobate grain boundaries. Small grains of chloritizised biotite are also scattered throughout the matrix, making up from a very small portion of the total mineral assemblage. Scattered anhedral grains of pyrite are abundant in the rock (Figure 2.6b), often appearing in textural equilibrium with the quartz grains (Figure 2.6c).

The overall impression of the relatively unaltered exposure also includes a transition-zone between the two distinct units. Earlier described as gradual bleaching of the foliated amphibolite in the vicinity of the quart-mica rich unit (see sub-section 2.2.1), another type of transitional trend is present in the lithological border-zones of the quartz-mica rich unit (Figure 2.2 and 2.3). Observed as a grey tint to the otherwise light color, the mesocratic zone is visible up to 5 meters in to the quartz-mica rich unit. Thin section studies reveal an increasing amount (up to 15 %) of subhedral hornblende in the quartz-sericite matrix, whereas fine-grained anhedral quartz make up for a higher degree (>50 %) of the matrix minerals compared to the general mineral composition. This transition type of the quartz-mica rich unit also displays more inequigranular grain sizes, with anhedral hornblende grains randomly distributed in a fine-grained quartz-dominated matrix.

Apart from the unweathered rock in the road-cut (Figure 2.7a), all other outcrops of the quartz-mica unit are characterized by a weathered oxidized surface with a characteristic bonded texture like the unweathered counterparts. The oxidized outcrops are encountered from Lassefjellet in the east to the top of Innerelvdalen in the west (Figure 2.2 and 2.3), displaying a total horizontal extent of approximately 2 kilometers along strike. On Lassefjellet (Figure 2.3), the bonded texture is substituted by a more porphyric igneous texture similar to that of the porphyritic amphibolite (Figure 2.5). This porphyritic texture present porphyroclasts of plagioclase in the fine grained oxidized pyrite-muscovite matrix (Figure 2.7b). Smaller porphyroclasts of quartz also appear in the matrix (Figure 2.6d), differing from the normally observed layered appearance of quartz grains in the unweathered type (Figure 2.6c).

2.2.4. Structure of the Skogsfjordvatn group lithologies

D1 structures

All of the Skogsfjordvatn Group lithologies, including all variations of amphibolite and weathered, deformed/altered and unweathered types of the quartz-mica rich unit are foliated in various degrees. The main foliation (S1) is well developed within the quartz-mica rich unit, as in the surrounding massive amphibolite. In the quartz-mica rich unit, alignments of quartz and locally pyrite form spaced zonal cleavage patterns (cf. Passcier & Trouw, 2005), contrary to the foliated amphibolite, presenting spaced to continuous cleavage by the alignment of hornblende and plagioclase grains. The foliation strikes from SW-NE to NNW-SSE (Figure 2.8d) in all domains, on average presenting a strike of WNW-ESE with a gentle to moderate dip to the NNE. In the east, towards the top of Lassefjellet, the general strike of the main foliation is W-E with a dip to the north (Figure 2.8a), similar to the strike present in the top of Innerelvdalen (Figure 2.8c). However, a few outcropped appearances of the foliated amphibolite in

southern slopes of Lassefjellet display an E-W strike with dip-direction to the south (Figure 2.8a). In prospecting pits on Lassefjellet (Figure 2.7d), the main S1-foliation presents axial-planar micro- to mesoscale gently NW-plunging recumbent isoclinal and intrafolial folds (F1), often observed in the S1-parallel sulfide mineralization (Figure 2.7c). Stretching lineations(L1) trending perpendicular to the main S1-folaiation are also observed on well-developed S1-foliation surfaces in the foliated amphibolite, most abundant in the domains of foliated amphibolite in Innerelvdalen.

Abrupt changes in the attitude of the foliation do occur locally within the quartz rich unit and the foliated amphibolite, these local changes may be related to the presence of steep to vertical shear-zones (Figure 2.2, 2.3 and 2.8f) striking NNE-SSW and macro scale folds (F2)(Figure 2.2, 2.3 and 2.8e,g,h). These steep NNE-striking shear zones consistently cut the main S1-foliation (Figure 2.2 and 2.3), developing moderately N-plunging, likely shear-related F3-folds in the proximity of the shear-zone boundaries (Figure 2.2 and 2.8f). The scale of observed drag-folding of the S1-foliaton is 5-15 meters on each side of the shear zones, perfectly displayed on the west side of the a N-S striking shear zone in Innerelvdalen (Figure 2.2). The shear-related F3-folds cause reorientation and flexure of offset lithologies, resulting in these local variations of the main foliation. On the weathered surfaces of the quartz-rich unit in Innerelvdalen (Figure 2.2), axial planar cleavages are observed, and these features display close to vertical dip and N-S strike parallel to the shear zone (Figure 2.2).

D2 structures

Overall, the studied areas of Lassefjellet and Innerelva (Figure 2.2 and 2.3) both lie within the central part of a regional NW-SE trending F2-synform in the RGB (Zwaan 1989; Bergh & Armitage 1998). This attitude is reflected in a gentle NE dip of the main foliation in Innerelvdalen and a gentle NW dip in Lassefjellet (Figure 2.8), indicating a gently N-plunging macrofold β-axis (F2)(Figure 2.8d). The moderate SW-directed dip of the main S1-foliation in the southern amphibolitic domain on Lassefjellet, combined with the NNW-dip in the northern parts, outlines the character of a WSW-ENE trending macroscale open antiform with a gently plunging β-axis (Figure 2.8a). A mesoscale F2- fold in the lowermost prospecting pit in the quartz-mica rich unit on Lassefjellet present the same style and orientation as the macroscale open antiform (Figure 2.8e), considered to have formed parasitic to the F2-macrofold. A similar mesoscale F2-fold is also observed in the lower part of the quartz-mica rich unit in Innerelvdalen, the open asymmetric F2-fold presenting a WNW-trend with gently upright to plunging β-axis (Figure 2.8g).

Small-scale folds (F2) in the foliated amphibolite are not common, except an open gently NNW plunging F2-fold located in the northern parts of the massive amphibolite (Figure 2.8h). In addition, a

low angled S2-shear-zone is observed striking parallel to the WSW-dipping limb of this NNW plunging F2-fold earlier described, and the sense of shear of the S2 shear-zone as well as the geometry of the F2-antiform resembles parts of out of the syncline faulting. The most prominent example of a S2 low angle ductile shear zone, is a low-angle gently NE-dipping thrust fault separating the Skogsfjord Group garnet-hornblende schist and the Skogsfjordvatn Group foliated amphibolite (Figure 2.2). A dominantly SE-ward, oblique-dextral strike-slip motion was deducted from the vergance and orientation of various kinematic indicators (e.g meso-/micro-scale asymmetric tight folds with axial planes dipping to the NW) on the phyllonitic surface of a N-S striking mafic dyke body sub-parallel to NW-SE striking shear zone (see sub-section 2.4.2).

D3 structures

Shear related sub-vertical to moderately N-plunging, likely drag related F3-folds are encountered in the study area, always observed in the vicinity of N-NNE-striking steep to vertical ductile S3 shear zones. The F3-folds are most prominent in the quartz-mica rich unit in Innerelvdalen, where the main S1-foliation is highly reworked into a north trending drag-related pattern with steeply plunging β-axis (Figure 2.2 and 2.8f) . Deducted from the folded orientation of S1-foliation, all investigated F3-fold corroborate to a sinistral movement in the bordering S3-shear zone. These well-developed sets of N to NNE-striking steep to vertical ductile shear-zones (S3) strongly affect the map pattern by crosscutting and offsetting the main foliation and all other structures (Figure 2.2 and 2.3). The width of the macro-scale S3-shear zones varies from one to 10 meters, with a length of up to a kilometer. Many such shear zones laterally offset the quartz-mica rich unit by up to 100 meters (Figure 2.2). The style, geometry and sense of shear (in most cases sinistrally) of these shear zones are consistent trough out the study area (cf. Bergh & Armitage, 1998). The easternmost NNE striking S3-shear-zone on Lassefjellet exhibits a dextral separation (Figure 2.3), thus being the only investigated shear zone with a prominent dextral sense of shear. The N-NNE strike of the shear zones is not directly observed, but deducted from the vergence and orientation of various kinematic indicators e.g., mesoscale to microscale drag folds and stretching lineations on fault surfaces elsewhere. Locally, displacement of dykes and lithological units corroborate the sense of shear (Figure 2.2).

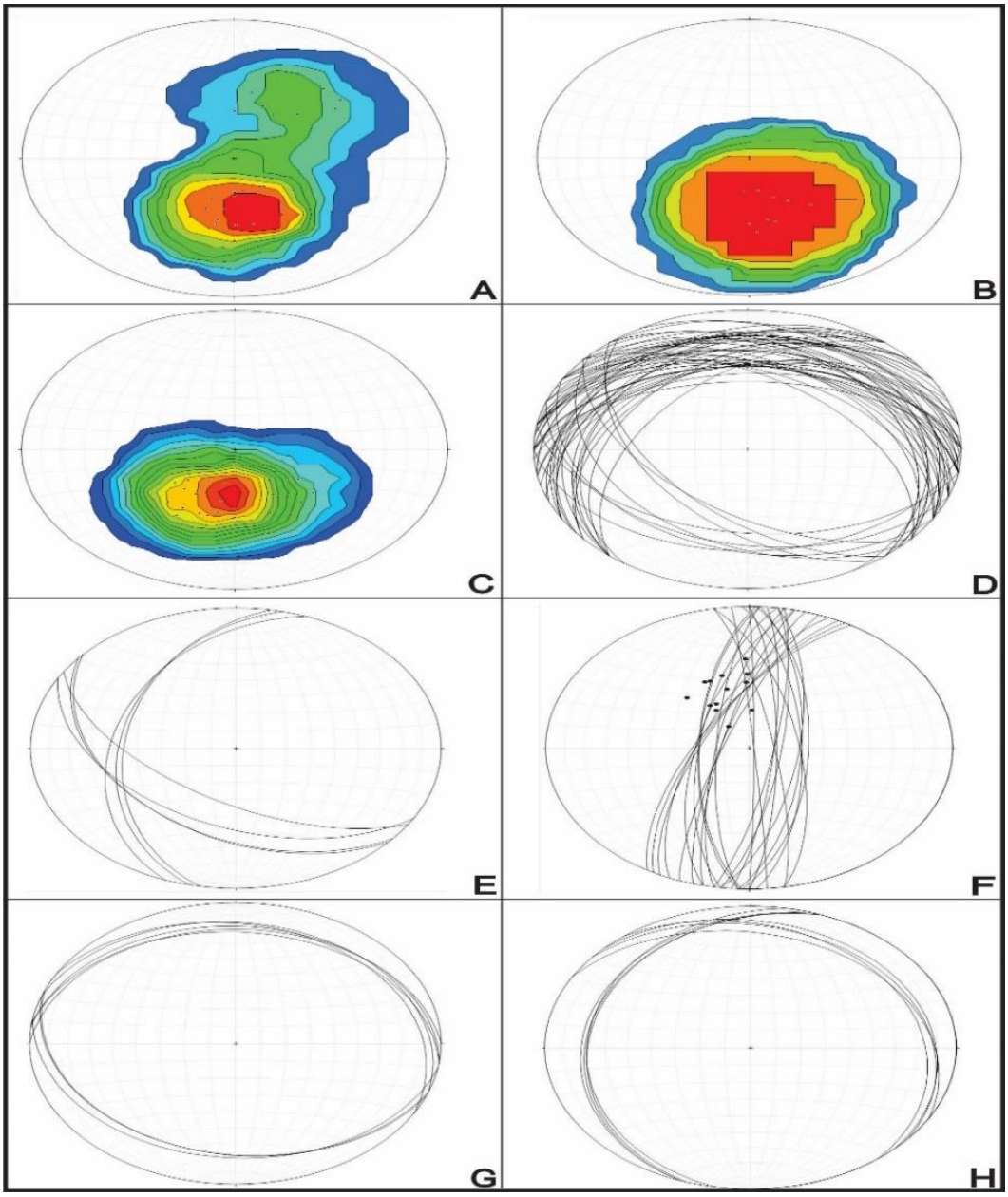

Figure 2.8: Stereoplot showing countoured poles of the main foliation(S1) from central and upper (eastern) parts of Lassefjellet. B) Stereoplot showing the countoured poles of the main foliation(S1) of the lower (western) parts of Lassefjellet. C) Stereoplot showing the contoured poles of the main foliation(S1) in Innerelvdalen. D) Stereoplot showing planes of the main foliation(S1) in the entire study area, note how the two sets of planes represent the fold-limbs of a mega-scale fold(F2). E) Stereoplot showing the two limbs of an anti-form structure in the lowermost prospecting pit on Lassefjellet. F) Stereoplot of the S3 ductile shear zones, poles represent axis of steeply plunging drag-folds(F3) G) Stereoplot showing the fold-limbs of a upright F2-fold in the lower domains of the quartz-mica rich unit in Innerelvdalen (Figure 2.2). H) Stereoplot showing fold-limbs of a gently plunging F2-fold in the foliated amphibolite in Innerelvdalen (Figure 2.2).

2.2.5. Meta-sedimentary rocks

A homogenous, weakly foliated, reddish-brown-colored type rock has been mapped as part of the Skogsfjordvatn Group (Figure 2.3). The rock occurs as lens-shaped bodies, ranging from 5-15 meters wide and up to 30 meters long, arranged parallel to the foliation of the quartz-mica rich unit near the peak of Lassefjellet. In thin section, the lithology displays a phaneritic coarse-grained intergranular to weakly granoblastic texture (Figure 2.9a,b). Studies reveal over 90% anhedral quartz grains with interlobate grain boundaries. All in an inequigranular matrix, embedded with veins of iron oxides, mainly hematite (Figure 2.9a,b). The rock gives the impression of a meta-sediment, mainly due to its clastic structure with semi-rounded quartz grains separated by hematite (Figure 2.9a,b).

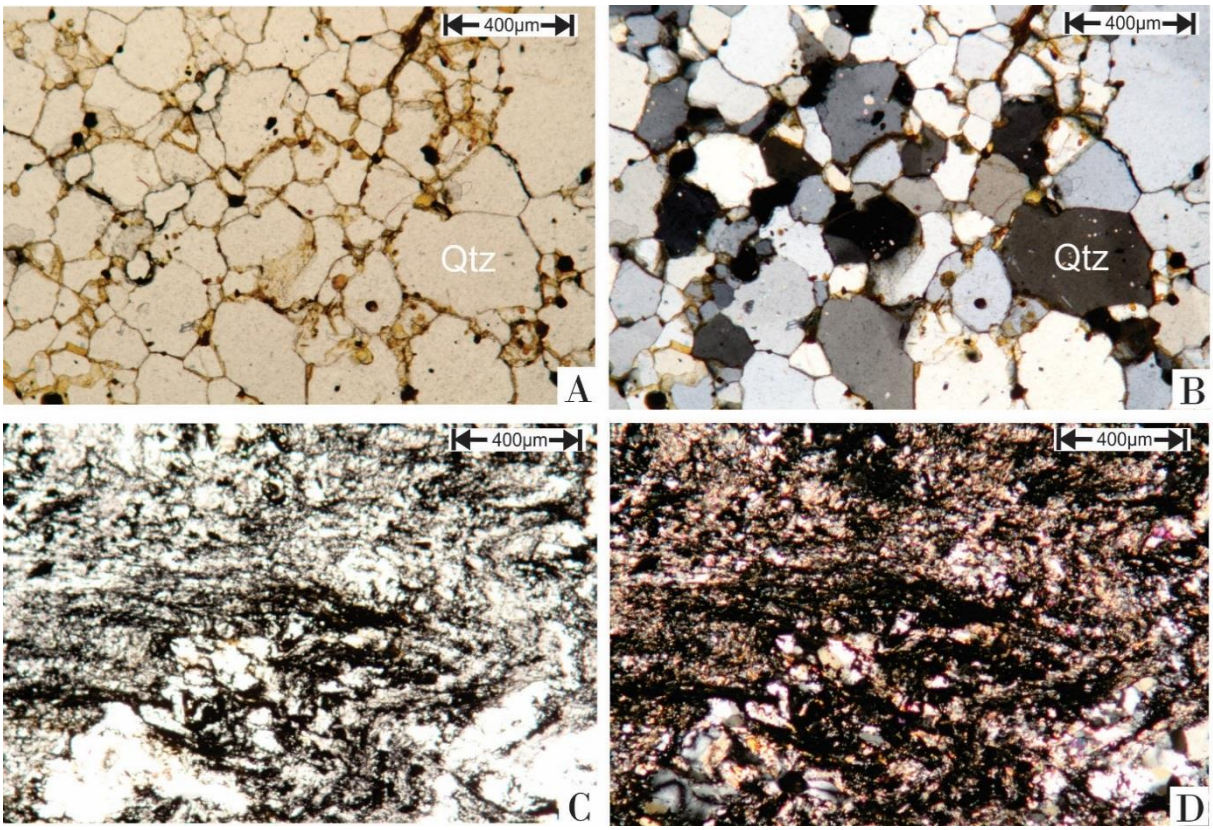

Figure 2.9: Thin section of sedimentary units. A and B originate from sample HE-P18, C and D from sample HE-P44. Photo A and C are taken in plane-polarized light, photo B and D are taken in cross-polarized light. A) Anhedral quartz grains, separated by veins of iron oxide (probably hematite). Note how the texture appear similar to a classical quartzite. B) Same motive as picture A, note how the mineral matrix is dominated by quartz. C) Aphanitic rock with matrix of sericite(white) and opaque minerals, the latter does not display as a metal when observed in reflected light. D) Same motive as ture C, the sericite display light interference colors in cross-polarized light.

Similar lens- shaped bodies also appear as grey to black colored varieties with a higher degree of foliation, observed on top of Lassefjellet (Figure 2.3). These particular rocks are aphanitic, with a dull tint to the color and no visible grains to the unaided eye (Figure 2.9c,d). A well-developed slaty cleavage is evident in these lens-shaped bodies, displaying a strike parallel to the foliation of the surrounding quartz-mica rich unit. Muscovite and opaque minerals form a fine grained matrix with a slaty texture, and this high content of fine grained opaque minerals (Figure 2.9c,d), combined with the laminated appearance, argues for the sedimentary affinity.

2.3. Skogsfjord Group lithologies

The Skogsfjord Group is comprised by two main lithologies, garnet-quartz-feldspatic meta-sandstones and hornblende-rich schists, together defined as the uppermost lithotectonic unit in the RGB (Zwaan, 1989). Zwaan (1989) further argues that the metamorphic grade here is generally higher than in the Skogsfjordvatn Group, with mineral assemblages of hornblende and garnet being common features. In the study area, as well as in the RGB, this unit makes up the uppermost and northwestern parts, separated from the Skogsfjordvatn Group by a low-angle ductile thrust fault (Bergh & Armitage, 1998), well exposed in the northwestern part (Figure 2.2 and 2.10). Since this group only makes up a small portion of the study area, the garnet-hornblende schist is the only mapped and studied lithology of the Skogsfjord Group.

2.3.1. Garnet-hornblende schist

The schistose garnet- and hornblende-rich type of amphibolite is observed in the northwestern regions of the study area, where it crops out along the shoreline of Innerelva (Figure 2.2). The strike of the main foliation (S1) of the rocks is on average W-E with a moderate dip to the northwest. The contact zone between the garnet-hornblende amphibolite and the underlying foliated amphibolites of the Skogsfjordvatn Group is outlined as a zone with chlorite-rich phyllonitic schists (see sub-section 2.4.2) with well-displayed indicators of movement direction towards the southeast. The garnet-hornblende schist is characterized by a dark grey/green to black color on fresh outcrops, with a pale grey/black color on weathered surfaces. The garnet content is roughly 10%, highly visible in the hand specimen without any aids; this clear visibility in hand specimens has been an important factor in the differentiation between garnet-hornblende schist and foliated amphibolite domains. The main mineral assemblage in this highly foliated coarse grained type of amphibolite is amphibole (presumably hornblende) and garnet, with minor amounts of feldspar. No samples were gathered from this lithology, and thus the mineral content described above is based on field observations.

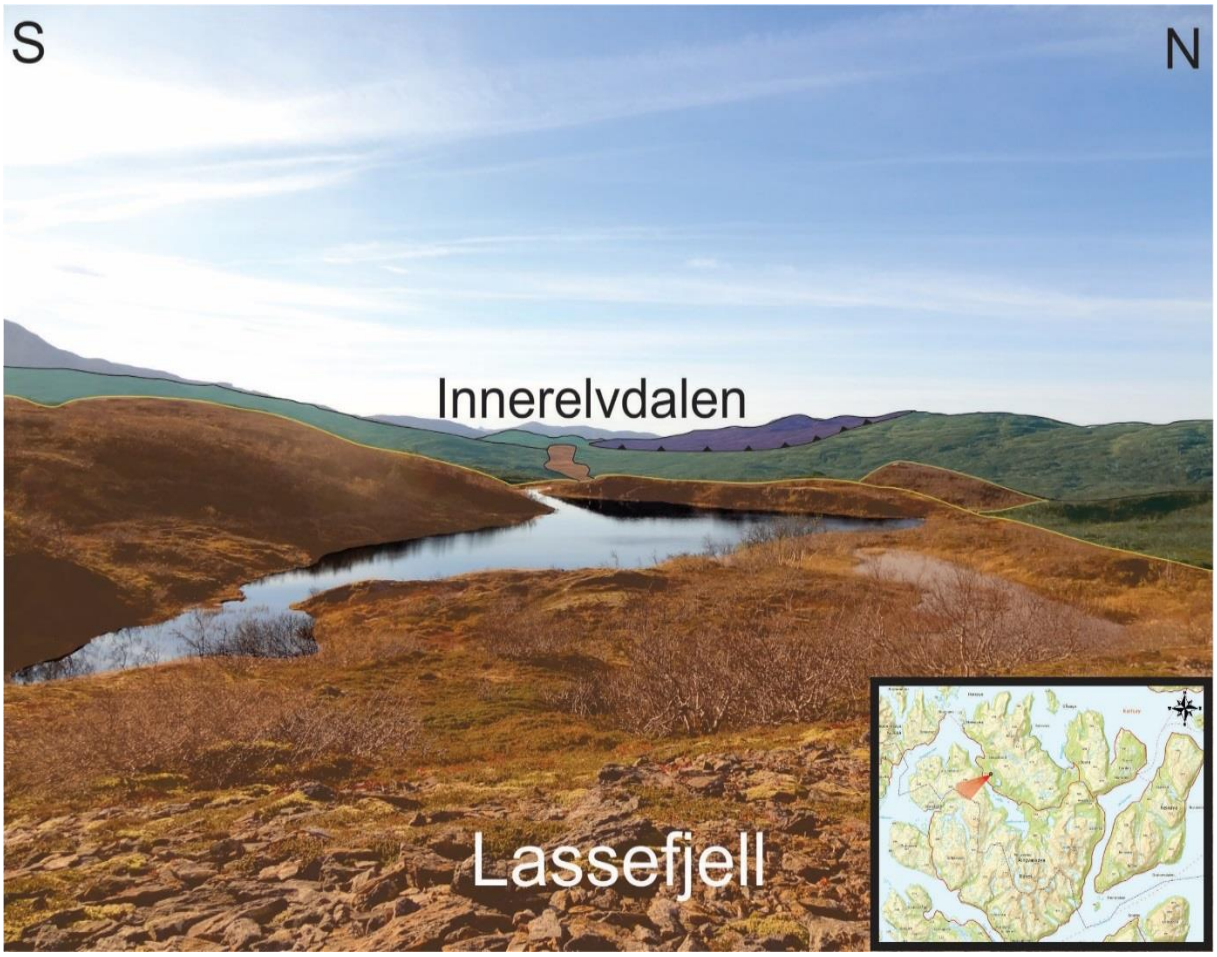

Figure 2.10: Overview of the study area, including interpreted lithology and index-map with point of view. Green shade represent the domains of foliated amphibolite, orange shade represent the quartz-mica rich unit, and the blue represent the overlying Skogsfjord Group.

2.4. Mafic dykes and quartz veins

Mafic dykes are included in this study for the main purpose of being kinematic indicators in relation to influential structures, and quartz veins and wall rocks are sampled in attempt to localize gold occurrences. With quartz veins observed both parallel to and crosscutting the main foliation, the study further attempts to investigate a possible linkage between the veins fabric relation and ability to carry potential gold.

2.4.1. Mafic dykes

Dark grey to black obviously intrusive mafic dykes are relatively easy detectable in the quartz-mica rich unit (Figure 2.2 and 2.3), as their distinct dark grey to black color stands out from the lighter colored quartz-mica unit. In the amphibolites, however, the mafic dykes are harder to detect as they tend to be more similar in color, and due to the sometimes poorly developed foliation in amphibolitic regions. The mafic dykes are very resistant to weathering, thus making up prominent ridges in the otherwise relatively flat landscape. The average thickness of the elongated dyke bodies range from 1-2 meters, with a traceable lateral extension of 2 to 30 meters. Microscopic investigation characterizes the dykes as amphibolite, i.e. a mineralogical assemblage of large subhedral amphiboles (Figure 2.11a,b) with an equigranular distribution, where minor amounts of plagioclase commonly are replaced by epidote in the matrix.

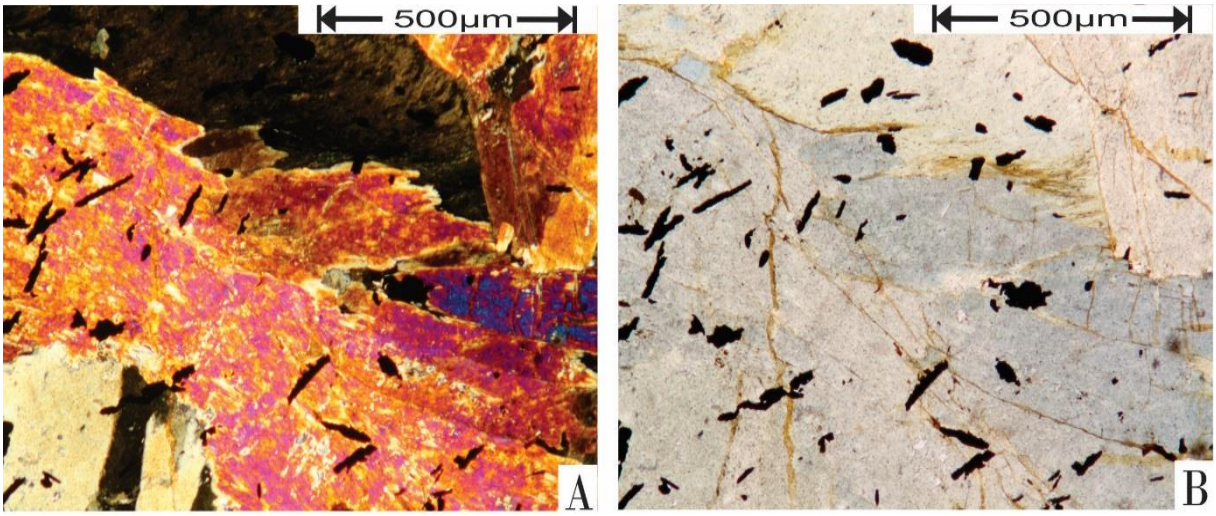

Figure 2.11: Thin section of mafic dyke. Sample HE-P43 A) Picture presenting presenting large subhedral grains of hornblende. Viewed in cross-polarized light. B) Same motive as A, viewed in plane polarized light. Note the scattered grains of opaque minerals (pyrite) overprinting other minerals, also note how the hornblende grains are more pristine and undeformed than in the foliated amphibolite.

2.4.2. Mafic dykes: phyllonites

A majority of the mapped mafic dykes occur in the vicinity of steep N-S striking S3-shear zones and low-angle ductile S2-thrust faults (Figure 2.2 and 2.3), and in such cases the dykes are offset and variously deformed into highly schistose, phyllite/schist -looking rocks, i.e. mafic mylonites (phyllonite). The most prominent example of such a mylonitic shear zone has been mapped at Innerelvdalen, where a mafic dyke body is striking NNE-SSW, sub-parallel to the oblique truncating shear zone separating the Skogsfjord Group and the Skogsfjordvatn Group (Figure 2.2). The western rim of this mafic dyke is heavily reworked, presenting a 50-centimeter thick phyllonitic texture (Figure 2.12a,b). This phyllonite rim proves as an excellent kinematic indicator, presenting great examples of micro- to mesoscale structures corroborating S1-S2 deformational events (Figure 2.13). The main mineral assemblage in the phyllonite is somewhat similar to the femic composition of the lesser deformed mafic bodies, i.e amphiboles, plagioclase and epidote. On the other hand, the percentage of quartz, chloritizised biotite, calcite, and iron sulfides is higher than in the un-deformed counterpart. The observed foliation is defined acicular grains of chlorite and biotite, intrafolial subhedral amphiboles and elongated bodies of subhedral quartz grains. (Figure 2.13). This main foliation is later on folded (F2) into tight asymmetric kink-folds (Figure 2.13), with fold axis dipping gently to the SSW. The sets of kink-folds are continuously folding the main fabric (S1), displaying a top to the SE movement, parallel to the suggested movement direction of the obliquely truncating S2-shear zone.

Figure 2.12: Phyllonitic outer rim on a mafic sub-parallel to the oblique truncating S2-shear zone separating the Skogsfjord Group and the Skogsfjordvatn Group. A) Total outcrop of the rim, roughly 50 centimeter thick and 2 meters long. B) Outcrop displaying sets of kink-folds(F2) continuously folding the main fabric (S1), displaying a top to the SE movement.

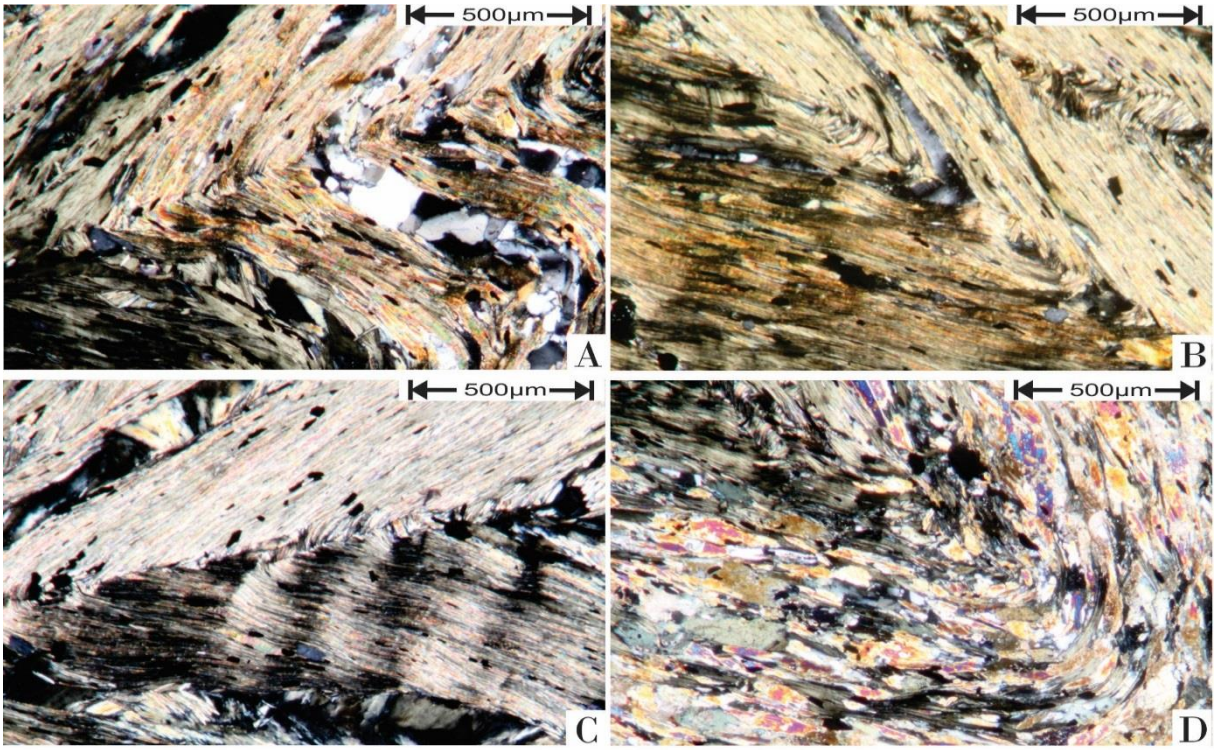

Figure 2.13: Thin section photos of the outer phyllonitic rim displayed on the last. Pictures originate from sample HE-P11 in cross-polarized light. A) Kink folded main S1-foliation of chlorite and elongated amphibolte, note the folded S1-folation parallel bands of quartz. B) Kink folded tight penetrative fabric of mainly chlorite. C) Similar kink-folded S1-foliation as in picture A and B. Note the weak zonal crenulation cleavage perpendicular to the main S1-folation, and intrafolial opaque minerals (pyrite). D) Tightly folded S1-foliation made up of elongated grains of amphibole.

2.4.3 Quartz veins

Extensive quartz veining is present in all the mapped lithologies, parallel to the main S1 foliation as well as truncating the main S1-fabric. The S1-parallel quartz veins are by far the most abundant, with thicknesses ranging from a few (Figure 2.14a) to 40 centimeters, and traceable up to 5 meters along strike. The most prominent example of foliation-parallel quartz veins is observed in the domains of foliated amphibolite north of Lassefjellet, presenting a 40 centimeter thick quartz vein, with 50 centimeter bleached amphibolite on both sides (Figure 2.3). Veins truncating the S1-foliation occur in relation to structures, though minor veins (>2centimeters) forming anastomosing patterns are observed in the foliated amphibolite. Most of the observed foliation truncating quartz veins are present in the steep to vertical F3 folds, in the vicinity of N-S striking S3 ductile shear-zones (see sub-section 2.2.4). These veins are striking parallel to the axial planar cleave of the interpreted drag-folded main S1-foliation, all presenting thicknesses of a couple of centimeters and traceable up to a meter. As the fabric truncating quartz veins are only localized in relation to the drag folded foliation, their extent in the study area is far lower than their foliation parallel counterparts.

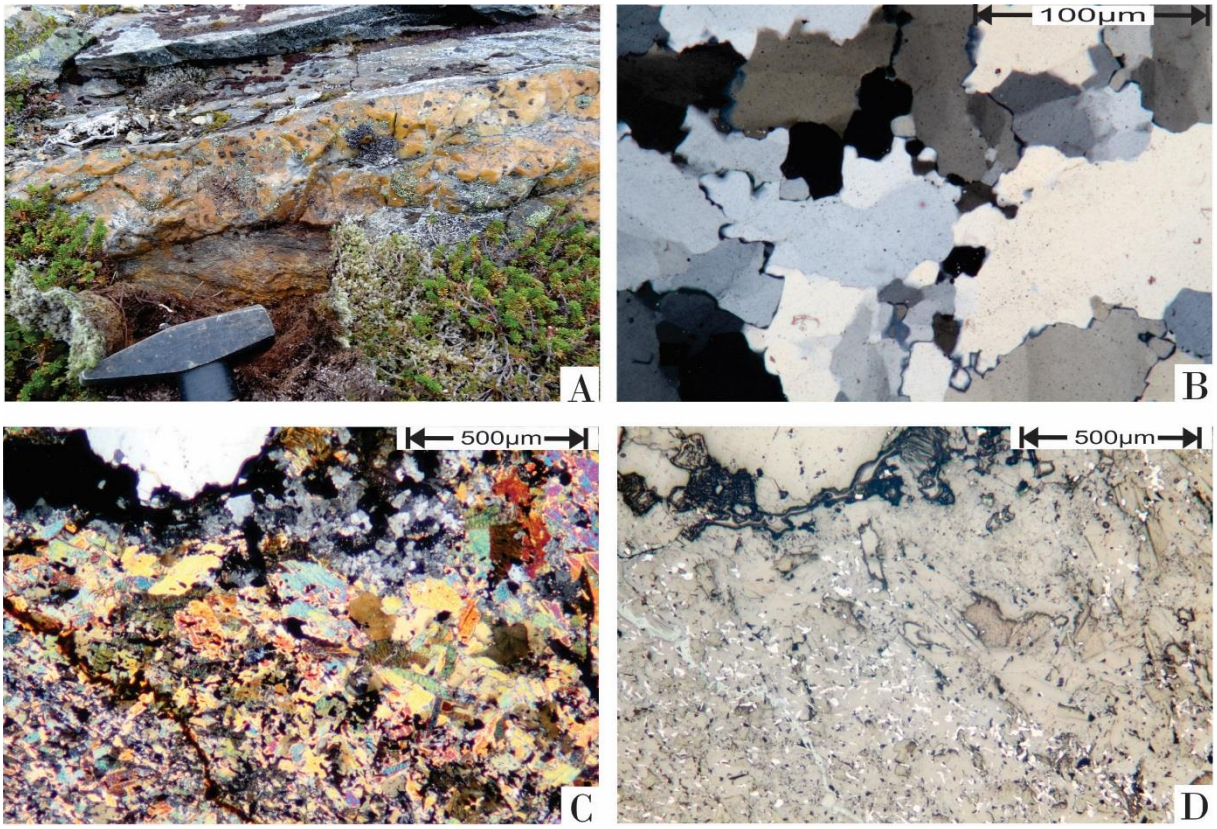

Figure 2.14: Quartz veins. A) Foliation parallel quartz vein, the brown color is due to contamination of iron sulfides. B) Inequigranular homogeneous crystal lattice of anhedral quartz grains with interlobate grain boundaries. C and D) Mineralized wall rock of foliation parallel quartz vein(not the one in picture A), displaying amphiboles(high interference colors) and arsenopyrite(white grains in picture D). More pictures of this wallrock is presented in sub-section 2.4.3.

In thin section, both the S1-parallel and -truncating quartz veins overall express an inequigranular homogeneous crystal lattice, defined by anhedral quartz grains with interlobate grain boundaries (Figure 2.14b). The S1-parallel quartz veins usually display a crystal lattice with well-developed undulatory extinction, a common evidence of dislocation glide, suggesting movement along the foliation-planes. A few of the sampled quartz veins, both foliation parallel and truncating, display vein-patterns of secondary minerals separating the quartz grains, this is typically iron oxides (hematite) giving the quartz a reddish tint to the otherwise white color (Figure 2.14a).

2.5. Mineralized rocks and fabric relations

2.5.1. Foliation parallel mineralization

The quartz-mica rich unit carries a high population of iron sulfides, both scattered within the mineral matrix, and as conformable disseminated to massive sulfides beds parallel to the dominating S1-foliation (Figure 2.7c). The sulfide beds are abundant in the quartz-mica rich unit, with thicknesses ranging from 1 centimeter up to two meters, with a flow-like appearance they are impregnating the host rock partly or completely. Thinner variations of this foliation-parallel sulfide mineralization often display isoclinal, intrafolial F1-folds, repetitively folding the sulfide layers, these also display a disseminated texture, with muscovite and quartz in the pyrite matrix (Figure 2.15a,b). The thicker sulfide beds display a more massive texture in central parts, and a gradual trend of quartz/muscovite dissemination towards the rims. In the massive central parts, one can observe rounded silicate blebs within the sulfide globules and sulfides being in capsuled in quartz gains (Figure 15bc,d). Towards the disseminated rims, an increasing amount of quartz and muscovite is present in between the pyrite grains. Massive central parts of the sulfide beds display no foliation, whereas the more disseminated rim zones and thinner beds display somewhat aligned quartz grains, causing the ore bodies to present a slightly foliated structure (Figure 2.7c). The mineral content is comprised by interlobate iron sulfides, represented by semi-rounded sulfide globules of mainly pyrite (>90%), along with phyrrotite, occasional chalcopyrite in fractured pyrite grains and anhedral quartz/muscovite(higher content in the disseminated variations, Figure 2.15).

A second and far less common type of foliation parallel mineralization is observed in a single outcrop of massive amphibolite, close to the garnet-hornblende schist (Skogsfjord Group). This particular mineralization is displayed as reddish brown tabular bodies of up to 20 centimeter, aligned in mullion structures parallel to the NW striking foliation of the massive amphibolite. Pyrite, chalcopyrite and sphalerite make up the mineral content in this type of mineralization, all anhedral in an inequigranular matrix. This mineralizationhas not been further investigated due to its sparse extent, and to lack of sampled material.

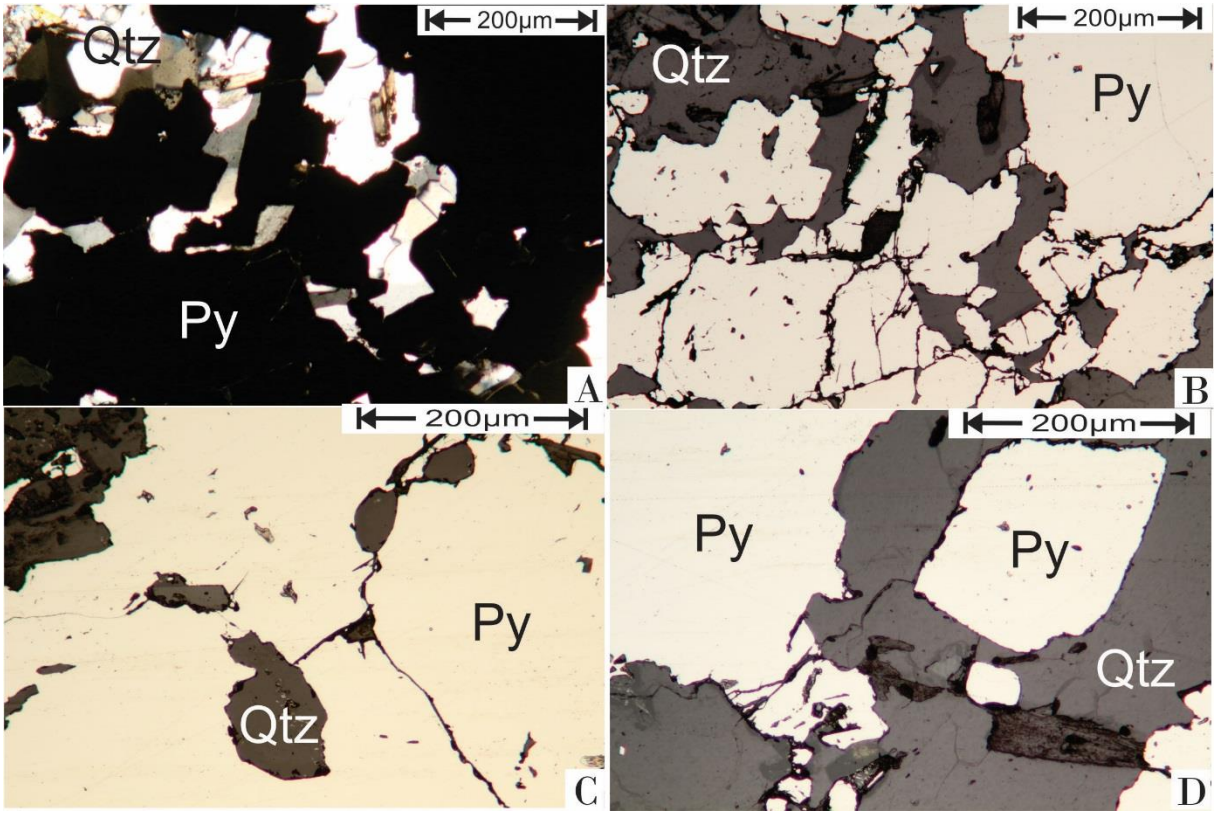

Figure 2.15: Foliation parallel mineralization sulfide mineralization. Picture A and B originate from sample HE-P28, B C and D from sample HE-P27. A) Thin section photo of disseminated sulfide mineralization of pyrite, quartz and minor amounts of muscovite, captured in plane-polarized light. B) same motive as picture A, viewed in reflected light. Note how the pyrite grains are deformed and fractured. C and D) Massive mineralization observed in reflected light. Note the rounded silicate blebs within the sulfide globules and sulfides being in capsuled in quartz gains

2.5.2. Mineralization related to structures (folds and faults)

Folds

The only prominent macro-scale example of fold-related sulfide mineralization is present in the lowermost prospecting pit within the quartz-mica rich unit on Lassefjellet (Figure 2.3). The outcrop displays a symmetrical moderately plunging open antiform-structure (F2), with fold axis dipping gently to the west (Figure 2.8e). The sulfide mineralization in this fold structure is presented as a folded foliation-parallel layer of pyrite grains in a careuos texture, similar to the observed foliation-parallel mineralization. Slight signs of sulfide accumulation is present in the hinge zone, defined by a thickening of the folded sulfide layer. Other mapped macro-scale upright to gently plunging F2 folds and steep to vertical F3 fold show no little signs of iron sulfide accumulation in the study area. Thus, for regional comparison, assemblage of iron sulfides in the cleavage domains of the F3- fold and fold hinges has been observed at Nordkjosvatnan (Bergh & Armitage, 1998).

Shear zones

All shear-related investigated mineralization, apart from scattered pyrite in the phyllonitic body (Figure 2.13), is located in the quartz-mica rich unit, along the trace of the N-S striking steep to vertical S3 ductile shear zones. Displayed as epigenetic tabular bodies of sulfide minerals, the mineralization is arranged parallel to the shear zone. This type of mineralization only occurs locally, where the S3-shear zones are piercing through the conformable sulfide mineralization of the quartz-mica rich unit. A total extent of this type of mineralization is problematic to define due to the high degree of coverage in the traces of the S3- shear zones, but even so, these tabular iron sulfide bodies are observed scattered up to 50 meters in the shear zone direction on Lassefjellet (Figure 2.3). The petrography and texture of these tabular iron sulfide bodies are very similar to the foliation-parallel S1 mineralization described above, with pyrite globules (>90%) and anhedral quartz grains in an inequigranular matrix.

2.5.3. Vein-related mineralizations

Vein-related mineralization is defined as a separate type of mineralization in the study area, due to lack of relation (both mineralogical and locational) to the massive sulfide mineralizations described above. The term *vein-related* is used to emphasize the occurrence in the wall rock on either side of a quartz vein, rather than in the actual quartz vein.

The only observed vein-related mineralization occurs in the bleached wall rock (Figure 2.14c,d) on either side of a 40 centimeter thick foliation-parallel quartz vein, situated in the amphibolitic domains north of Lassefjellet (Figure 2.3). The mapped lateral extent of the vein is roughly 10 meters, although further extent is anticipated, as the outcrop is partly covered by heather. The vein itself displays a light milky color, with an inequigranular matrix of anhedral quartz grains expressing undulatory extinction (see sub-section 2.4.3). The bordering zone of mesocratic amphibolite displays a pale grey color with a light green hue, similar to the zone observed in the vicinity of the quartz-mica rich unit (see sub-section 2.2.1), extending approximately 50 centimeters into the foliated amphibolite. The main mineral content of the bleached amphibolite is defined by subhedral hornblende (Figure 2.14c), heavily sericitized plagioclase, anhedral quartz (Figure 2.14c), subhedral foliation parallel aresenopyrite (Figure 2.16a,b,c), hexagonal tourmaline porphyroblasts (Figure 2.16d), anhedral carbonate, and chloritized biotite, ranged after the degree of presence. By a closer examination of this inequgranular mineral matrix, scattered gold grains (<5microns) are also observed (Figure 2.14e,f), often close to the arsenopyrite (<100 microns) grains (Figure 2.16e,f), suggesting a possible link between the two minerals (see sub-section 4.6.3). It should however be noted that the gold grains have not been

subjected to SEM-analysis, and this is therefore only a suggestion based on petrographic observations. With the mineralization defined as an arsenopyrite-gold occurrence, its grade and origin will be further emphasized in the next chapters.

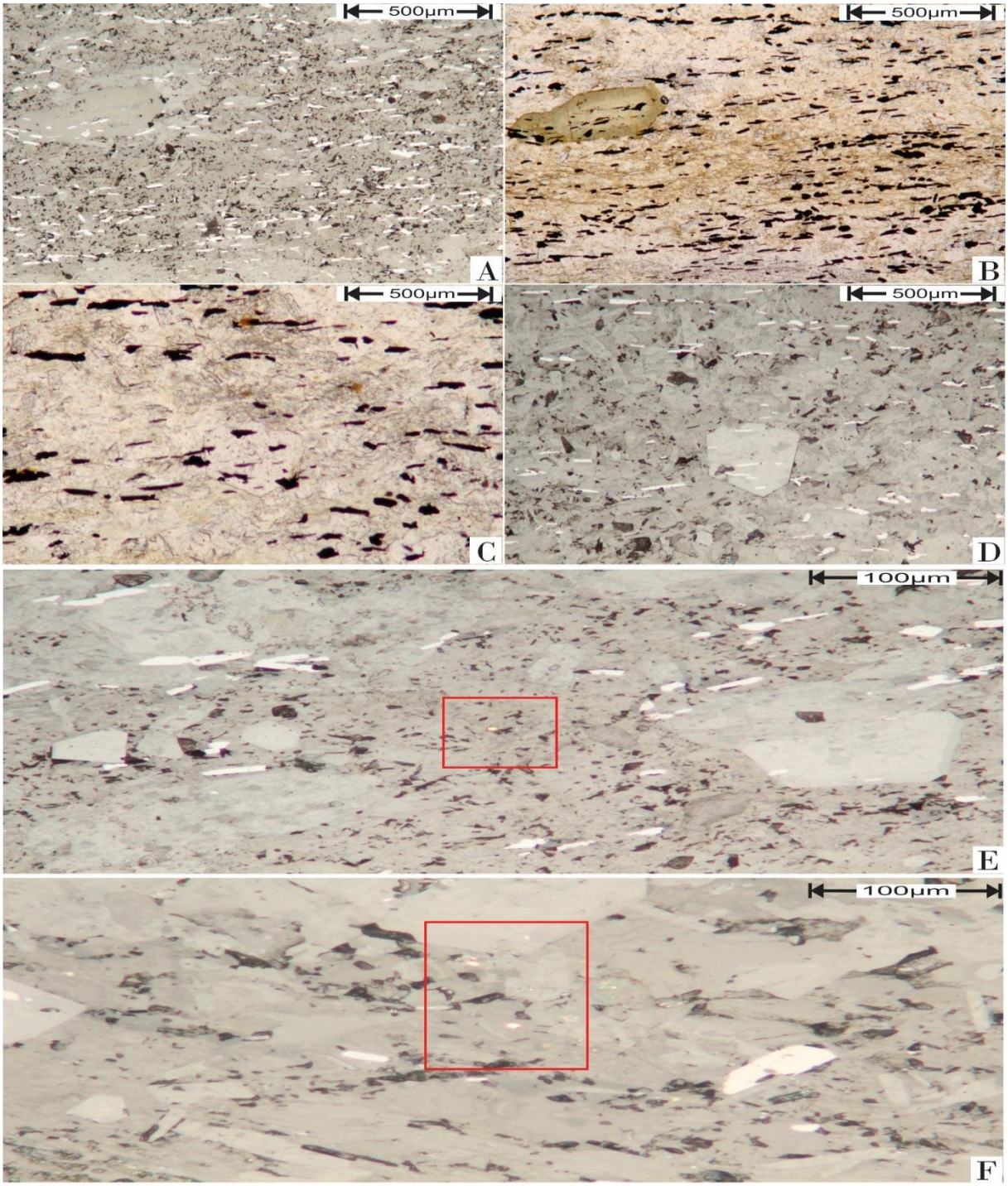

Figure 2.16: Mineralized wall rock (bleached foliated amphibolite) of a foliation parallel quartz vein. Photo B and C are taken in plane polarized light. A, D, E, and F, are taken in reflected light. All originate from sample HE-P36. A) Foliation parallel acicular grains of arsenopyrite (white) B) Same motive as picture A, note the tourmaline(light green) in the mineral matrix. C) Arsenopyrite (black) is truncating all other minerals. D) Hexagonal shape of tourmaline (light grey). E and F) Native gold grains (indicated by a red square) in the mineral matrix, always observed in the vicinity of arenopyrite.

3. Geochemistry

3.1. Introduction

The sampled material presented in this chapter originate from the dominating Skogsfjordvatn Group, where samples of foliated amphibolite are referred to as the *mafic rocks* and samples of the quartz-mica rich unit are referred to as the *felsic rocks*. Finally, the main purpose of the presentation of geochemical data is to determine the magmatic series, protoliths and relationships of the sampled material, in order to suggest a tectonic setting for the Ringvassøya Greenstone Belt. The total array of geochemical data is presented in Appendix B.

Since the localization of precious elements and estimation of ore-potential are among the objectives of this thesis, the concentrations of common ore-metals (Au, Ag, Cu and Ni) in the mineralizations of the study area(see section 2.5) are presented in section 3.3. This is done in order to get an overall impression of how ore-elements are distributed in the various mineralizations, and to further be able to favor a type of mineralization in terms of ore-potential(i.e. stratiform, structurally controlled and vein related).

3.1.1. Methodology

All the collected samples were prepared, packaged and sent to ALS geochemical lab in Piteå, Sweden. The total of 45 samples, each weighing approximately 300 g, were subjected to AU-ICP21 and ME-MS61 analyzing packages, to provide information concerning trace elements and gold content.

Au-ICP21

This analysis is provided by ALS Minerals, and is used for detecting Au at trace levels ranging from 0.001 to 10 ppm. The method was fit for the wide range of samples submitted, as the samples were not expected to contain ore-concentrations of gold. As the method provided ultra low detection limits, it made comparisons of samples possible even if they did not fit within the range of ore-grade. The samples were prepared by mechanical crushing and pulverizing to make 85% or more of the total mass pass through a sieve of 75 microns. The remaining material was then subjected to the following procedure described by ALS Minerals: “A prepared sample is fused with a mixture of lead oxide, sodium carbonate, borax, silica and other reagents as required, inquarted with 6 mg of gold-free silver and

then coupelled to yield a precious metal bead. The bead is digested in 0.5 mL dilute nitric acid in the microwave oven. 0.5 mL concentrated hydrochloric acid is then added and the bead is further digested in the microwave at a lower power setting. The digested solution is cooled, diluted to a total volume of 4 mL with de-mineralized water, and analyzed by inductively coupled plasma atomic emission spectrometry against matrix-matched standards."(Alsglobal.com) The total duration of this process is estimated to 3 weeks.

ME-MS61

The ME-MS61 analysis was chosen due to its ability to measure ultra-trace levels of various "pathfinder" elements related to exploration geology. The process dissolves most sulfide, oxide and carbonate minerals quantitatively, and leaves the silicates and resistive oxides untouched. This particular method also uses fusion in order to dissolute the material even further. The fusion dissolution technique allows for obtaining values of refractory minerals such as tin, tungsten, barite etc. Some of these minerals are usually associated with gold, and are therefore preferably included. Native minerals such as Au and Ag are representatively characterized due to the small sample size (0.25g) analyzed, and a combination with the Au-ICP method is therefore preferred. ALS describes this highly advanced technique on their web-pages: "A prepared sample (0.25 g) is digested with perchloric, nitric, hydrofluoric and hydrochloric acids. The residue is topped up with dilute hydrochloric acid and analyzed by inductively coupled plasma- atomic emission spectrometry. Following this analysis, the results are reviewed for high concentrations of bismuth, mercury, molybdenum, silver and tungsten and diluted accordingly. Samples meeting this criterion are then analyzed by inductively coupled plasma-mass spectrometry. Results are corrected for spectral interelement interferences" (Alsglobal.com). This method is widely used by prospecting companies all around the world, and the results are known to be trustworthy. In that case, it should be noted, as ALS minerals also describes at their web-page, the "four acid digestions are able to dissolve most minerals; however, although the term "near- total " is used, depending on the sample matrix, not all elements are quantitatively extracted." (Alsglobal.com)

3.1.2. Systematic errors

There are several factors to take into consideration when interpreting the results, since these will cause systematic errors in the representation of the data. First off, the sampled material from the Ringvassøya greenstone belt has undergone extensive metamorphism and alteration (see section 2.2), thus some elements (see below) will not be suitable as primary diagnostic elements due to their mobility under the given conditions. Such problems will arise in diagrams emphasizing Ba, Sr, Cr and Ni, whereas Ba and Sr are particularly mobile during weathering and metamorphism, and Cr and Ni are sensitive to the fractionation of olivine and pyroxenes (Pearce & Cann, 1973). Because of this, these elements are unsuitable for determination of protoliths, however, they are important indicators of the tectonic setting. For instance, Ba and Sr contents are generally higher in volcanic-arc basalts compared to ocean-floor basalts (Pearce & Cann, 1973), whereas the opposite is the case for Cr and Ni. On the other hand, a high content of Cr, Ni and MgO is indicative of olivine phenocrysts in unaltered varieties of rock. The presence of such phenocrysts will further reduce the contents of Zr, Y, Nb, Ti and Sr contents in the ground mass, essentially diluting the trace element values in the sampled rock(Pearce & Cann, 1973). Further, the clear juxtaposition of two units (i.e quartz-mica rich unit and foliated amphiblote) is an important aspect to consider (Figure 2.2 and 2.3). This could have caused the margins of the mafic and felsic units to mix to some extent, either as two ductile units, or as country-rock assimilation as one unit intruded/extruded after the other had consolidated. Finally, porphyroclastic samples and iron dissemination, this is especially the case for the felsic samples, where some of the samples originate from the contact with the foliated amphibolite, these porphyroclasts of hornblende in the matrix (see sub-section 2.2.3) which will result in irregularities in the plotted felsic rocks.

3.1.3. Calculations

In plots based on weight percentage (wt%) of oxides, the following calculation has been conducted: wt% (**ppm/10000**) of element multiplied by conversion factor of element = equivalent expressed as **oxide**

e.g., 2000ppm Ti to TiO_2 → 0.2 wt% (2000ppm/10000) Ti x 1.6681 = 0.334 wt% TiO_2

Conversion factors are presented in Appendix C.

3.2. Petrogenetic discrimination

3.2.1. Discrimination plots

The following characterization of the mafic samples is performed in accordance to Pearce and Cann's (1973) classification method for mafic rocks. The first step of this method involves plotting Y/Nb ratios against standardized values (based on known mafic rocks throughout the world), in order to determine the magma series of the given samples (Figure 3.1). With the diagram being based on mafic rocks in known volcano-tectonic environments, a further impression of this is also given concerning the tectonic setting.

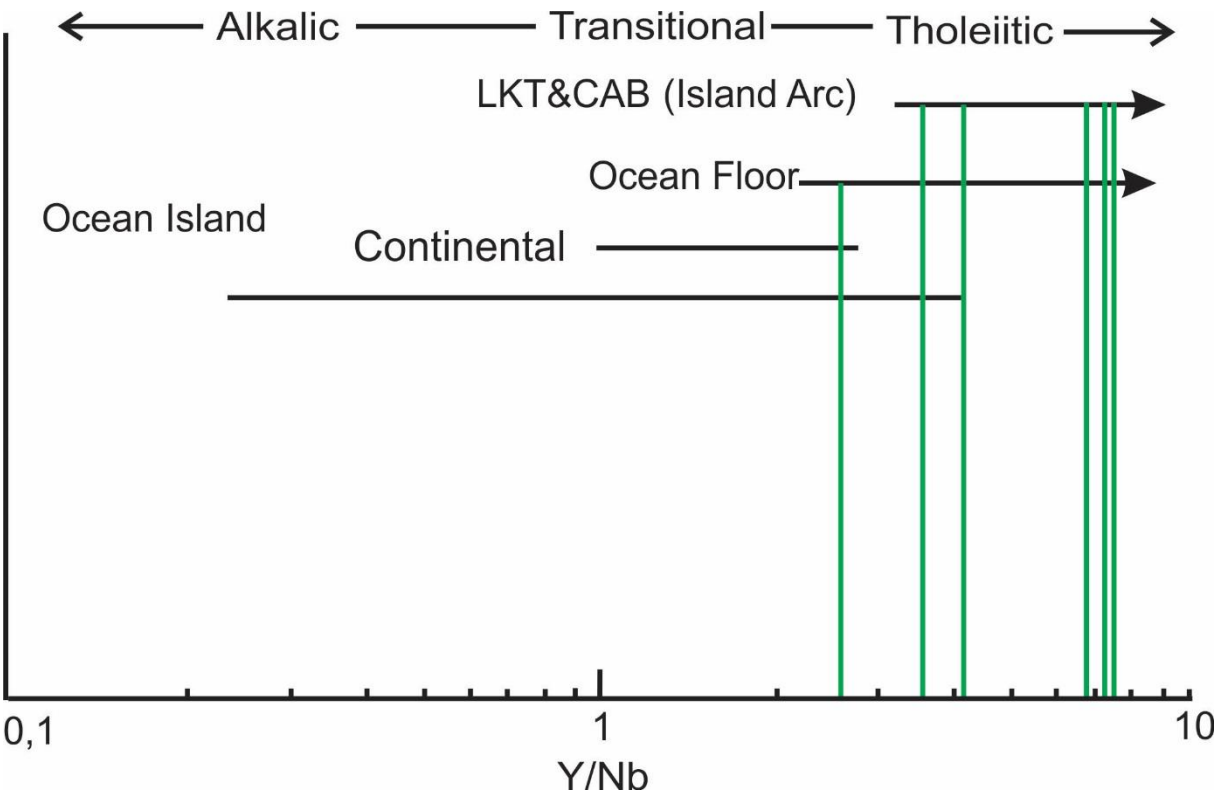

Figure 3.1: Determination diagram for petrographic character, modified and standardized from Pearce & Cann (1973). The green lines indicate samples of mafic rock in the study area, all plotted on the horizontal axis with logarithmic distribution. Y/Nb ratio for alkalic basalts is less than <1 for 'within-plate' basalts and less than <2 for ocean-floor basalts. For tholeiitic rocks, Y/Nb is >2 for 'within plate' basalts and >3 for ocean-floor basalts. LKT & CAB: low-K tholeiites and calc-alkaline basalts. Note the mafic samples displaying clear affinity to the tholeiitic magma series.

According to the discrimination method of Pearce and Cann (1973), the next step is to produce a ternary plot (Figure 3.2) of Ti, Zr and Y, in order to make a more accurately proposal of a tectonic setting. This step is based on a distinction between ocean-island basalts, continental basalts, ocean-floor basalts, and island-arc basalts, emphasizing the difference between 'within-plate' basalts and island-arc/sea-floor basalts.

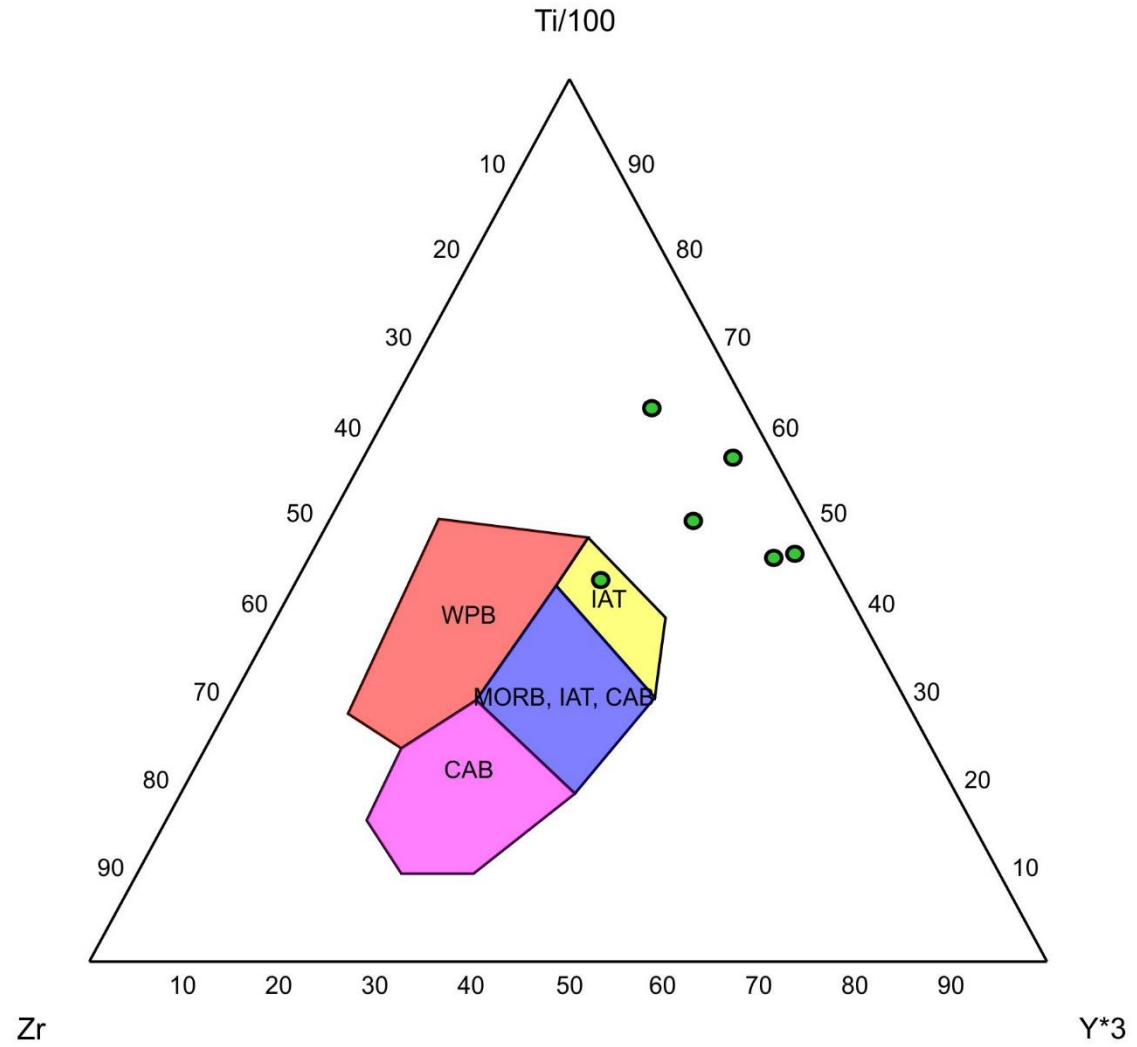

Figure 3.2: *Ternary plot of Ti, Zr and Y, modified from Pearce and Cann (1973) to differentiate between 'within-plate' basalts and island-arc/sea-floor basalts. WPB(Within plate basalts), IAT(Island arc tholeiites), CAB(Calc-alkaline basalt) and MORB(mid ocean ridge basalts). Green dots with black rims represent the mafic rocks of the study area. Note the high values of Y and Ti compared to Zr in all samples, causing the majority of mafic rocks to plot outside the characteristic fields. The mafic rocks plots closest to Island arc tholeiites, overall corroborating the previous plot of the method.*

The last step in Pearce and Cann's (1973) classification method is to emphasize elements with low mobility, in order to present more accurate results for further interpretation. Since the mineral content(see sub-section 2.2.1) observed in the mafic group suggest the samples have been subjected to metamorphism and weathering, a Ti/Zr diagram is preferred over a Ti–Zr–Sr ternary plot, as Sr is proven to be mobile during metamorphism(Pearce & Cann, 1973). Although a Ti–Zr–Sr ternary plot will offer greater representation of the geochemical data, a Ti/Zr diagram provides a good petrogenetic indication.

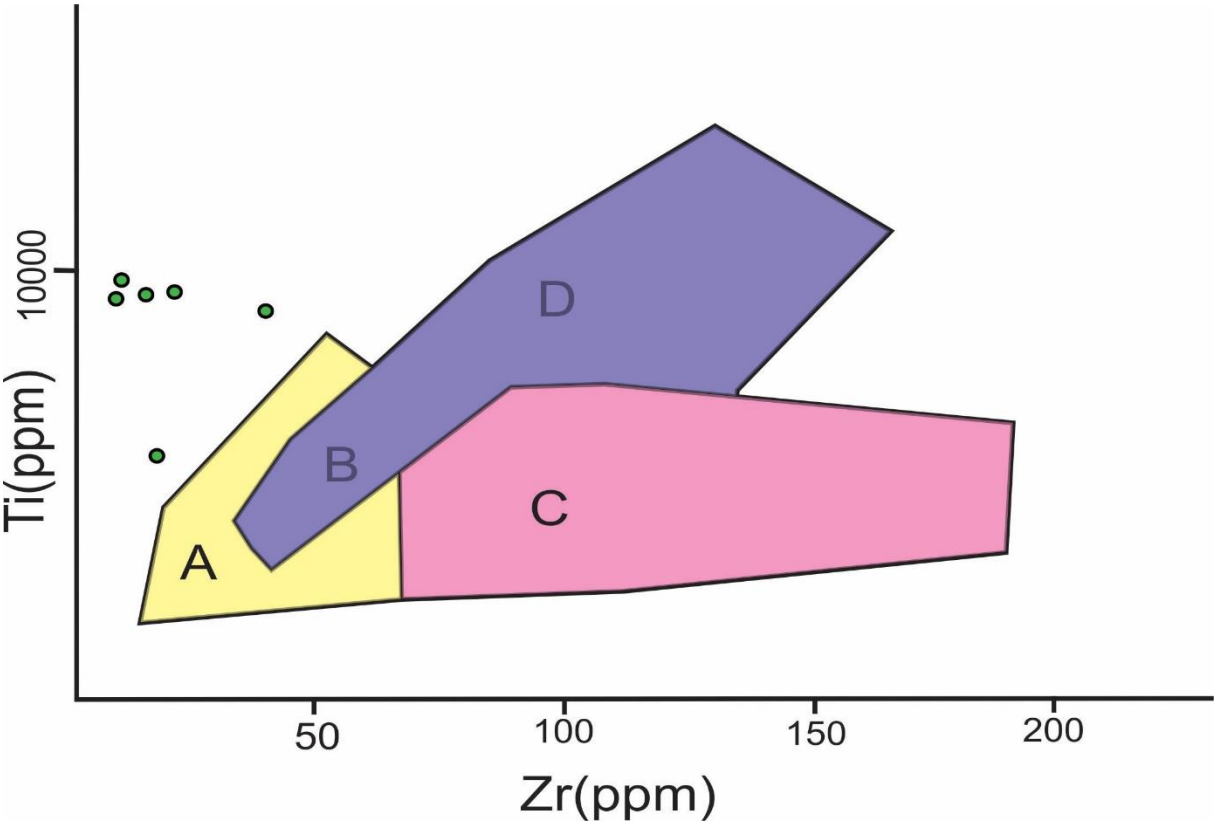

Figure 3.3: *Ti/Zr discrimination diagram, modified from Pearce and Cann (1973). This particular diagram is chosen due to it being less influenced by element mobility under various metamorphic facies, compared to a ternary plot of Zr, Sr and Ti as suggested by Pearce and Cann (1973). Fields A and B represent low-K arc tholeiites, C and B represent calc-alkaline basalts, and D and B represent ocean-floor basalts. Note the plotted mafic rocks(green dot with black rim) display the same trends as observed in the figures above; i.e., relation to low-K arc tholeiites and ocean-floor basalts (due to high Ti). The low Zr compared to Ti cause the samples to plot outside any of the given fields, similt to the ternary plot of Ti, Zr and Y.*

After subjecting the mafic group to Pearce and Cann's (1973) discrimination method, the samples state their relation to the tholeiitic magma series (Figure 3.1). The differentiation between tholeiitic and calc-alkaline magma series is often presented in an AFM diagram (Figure 3.4), displayed as a ternary plot of $Na_2O + K_2O$, MgO and FeO with total FeO is here used to account for the relatively large amount of sulfide disseminations in the felsic group of samples. It should however be noted that the effects of metamorphism, alteration and Fe-dissemination will cause the diagram to inherit flaws, advising the reader to interpret it with caution. The main reason for its application is to give a rough indication of magmatic character for the sampled material, and corroborate previous plots in Pearce & Cann's (1973) method.

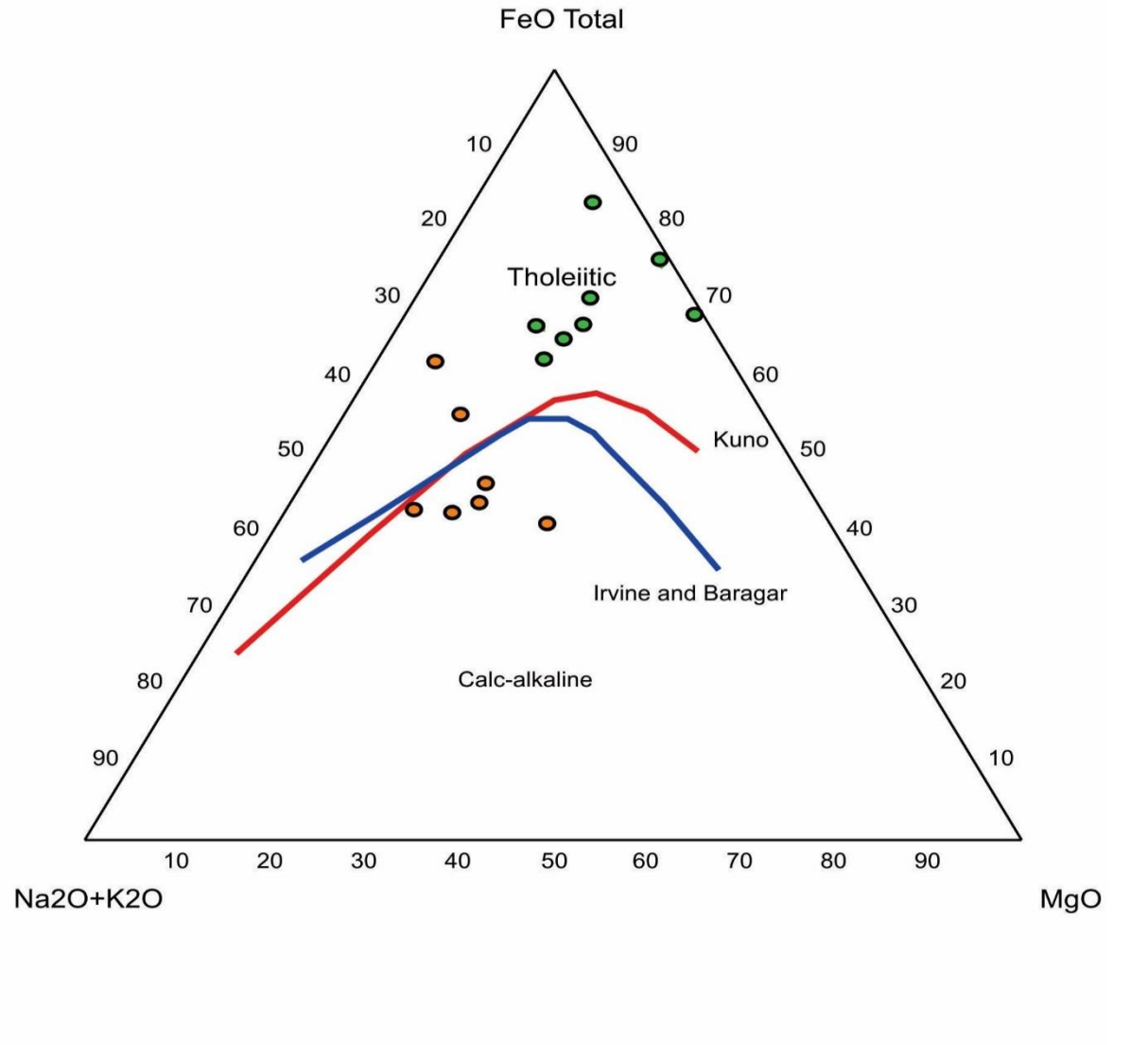

Figure 3.4: *The AFM diagram is presenting the tholeiitic or calc-alkaline trends in the sampled lithologies. The separation of the magmatic series is modified from Kuno (1968) and Irvine & Baragar (1971). A tholeiitic rock is reduced, whereas a calc-alkaline rock is oxidized (Blatt et al. 2006). Samples form the Skogsfjordvatn Group are represented by orange dots with black rim (felsic rocks) and green dots with black rim(mafic rocks). The tholeiitic trend of the mafic samples confirm previous plots, whilst the felsic samples present affinity to the calc-alkaline series. Note the two samples from the felsic rocks plotting in the tholeiitic magma series, this is probably due to pyrite dissemination in the mineral matrix (as proven in section 2.5).*

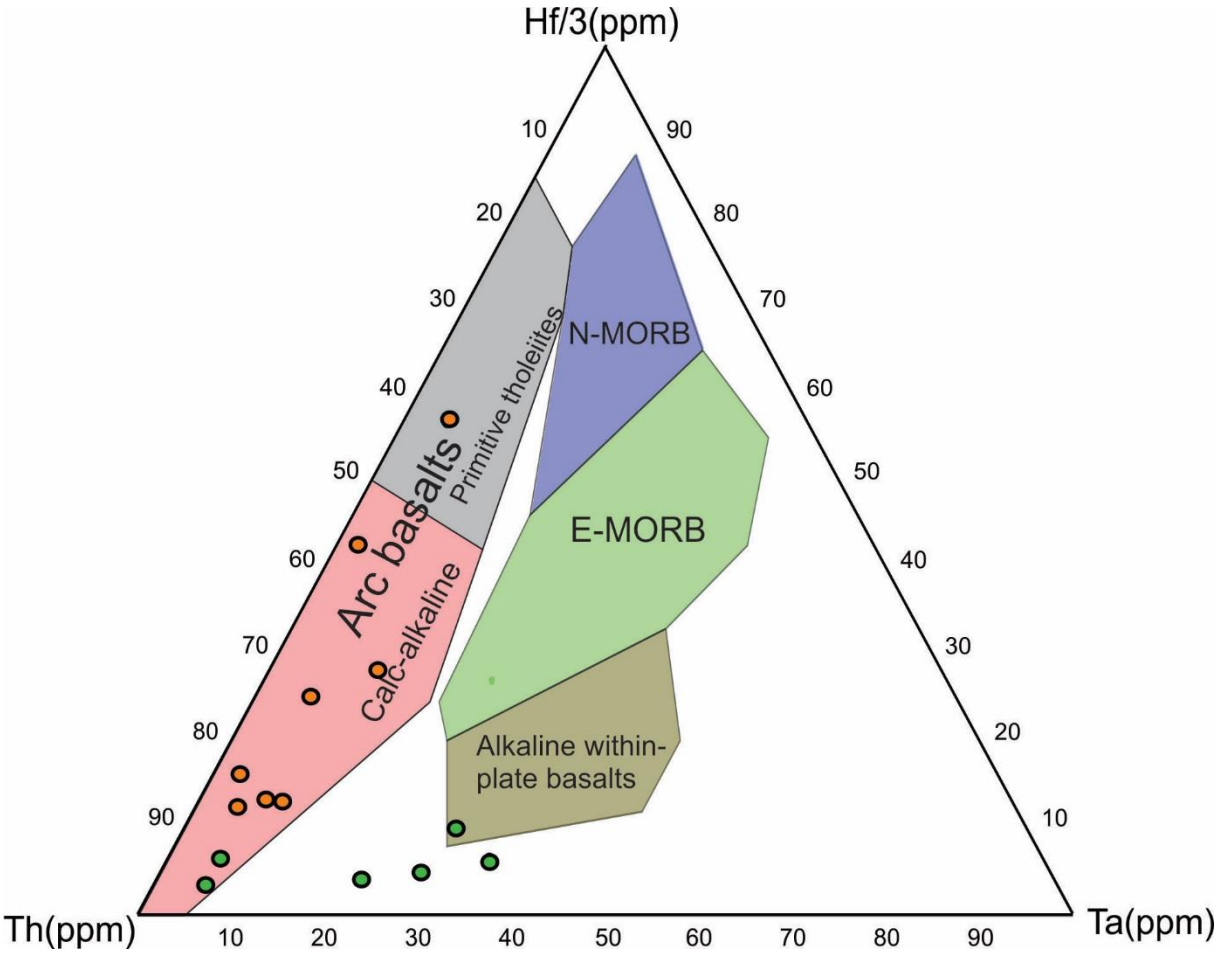

Figure 3.5: *Discrimination diagram modified from Wood (1980). Note that this diagram is tailored for basaltic rocks(though felsic can be plotted), and utilizes elements(Th and Ta) which are mobile during metamorphism and alteration(Pearce, 2006). Most of the felsic samples (orange dot with black rim) plot in the calc-alkaline field, related to volcaninc arcs, whereas the mafic samples (green dot with black rim) plot more scattered.*

Wood (1980) has also proposed a group of discrimination diagrams for suggesting character and tectonic setting for igneous rocks. The chosen diagram (Figure 3.5) utilizes Hf, Th and Ta for discrimination, whereas Th and Ta are mobile during alteration and metamorphism, thus the plots should be interpreted with caution. Finally, Floyd and Winchester (1977) propose a discrimination diagram (Figure 3.6) for identification of ancient volcanic suites and their differentiation products. Their discrimination diagram combine the use of Ti, Zr, Y, Nb, which are proven to be immobile during secondary alteration processes, adding the advantage of plotting rocks of any composition, not strictly basaltic as in Pearce and Cann's(1974) diagrams (Figure 3.1-3.3). The chosen diagram is therefore suitable for extrusive and intrusive volcanic rocks that have undergone alteration and/or metamorphism; e.g., keratophyres, tuffs, greenstones, spilites, etc (Floyd & Winchester, 1977).

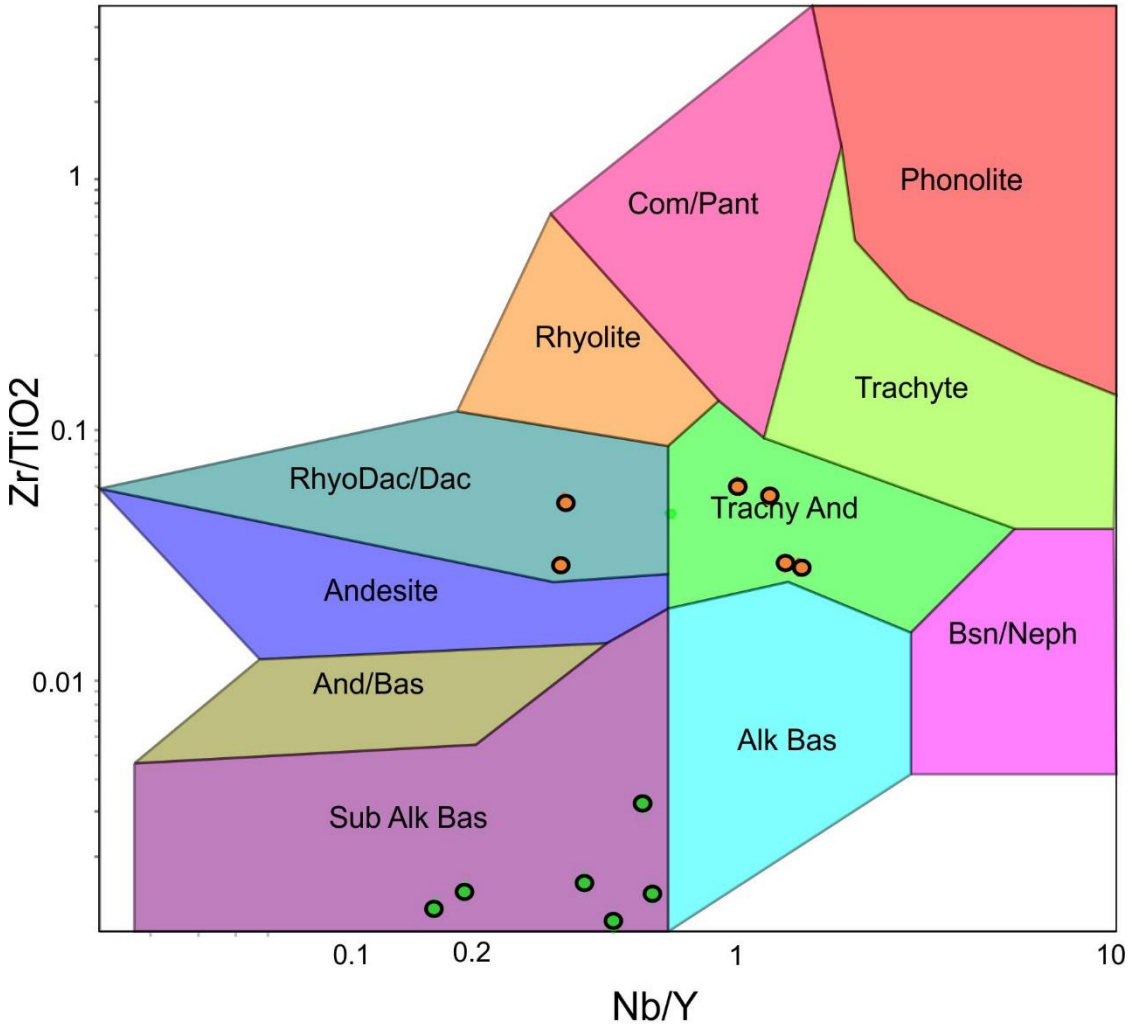

Figure 3.6: *Discrimination diagram using Zr/TiO_2 and Nb/Y, modified from Floyd and Winchester (1977) and based on worldwide metavolcanic suites. The diagram presents samples from mafic and felsic rocks in the study area, whereas the biggest outliners (most weathered) are excluded in order to make the plot more representative. The quartz-mica rich (felsic) unit is shown as orange dots, metabasalt samples are shown as green dots. Note that the mafic rocks plot in the tholeiitic/subalkaline basalt field, affirming the magma series suggested above. Yet again, notice how the peculiarly low Zr concentrations may be causing systematic errors in the discrimination. Samples from the quartz-mica rich unit plot as rhyodacite/dacite and trachyandesite, common intermediate to felsic volcanic rocks often found in island arc environments (Blatt et al., 2006)*

3.2.2. Multi-element diagrams

Multi-elements diagrams are applied to differentiate and define geochemical trends and characteristics in the groups of rocks form the Skogsfjordvatn Group (i.e felsic rocks and mafic rocks). The following diagrams are all based on MORB-normalizations, as mid ocean ridge basalt is a commonly used reference for geochemical classification of magmatic samples.

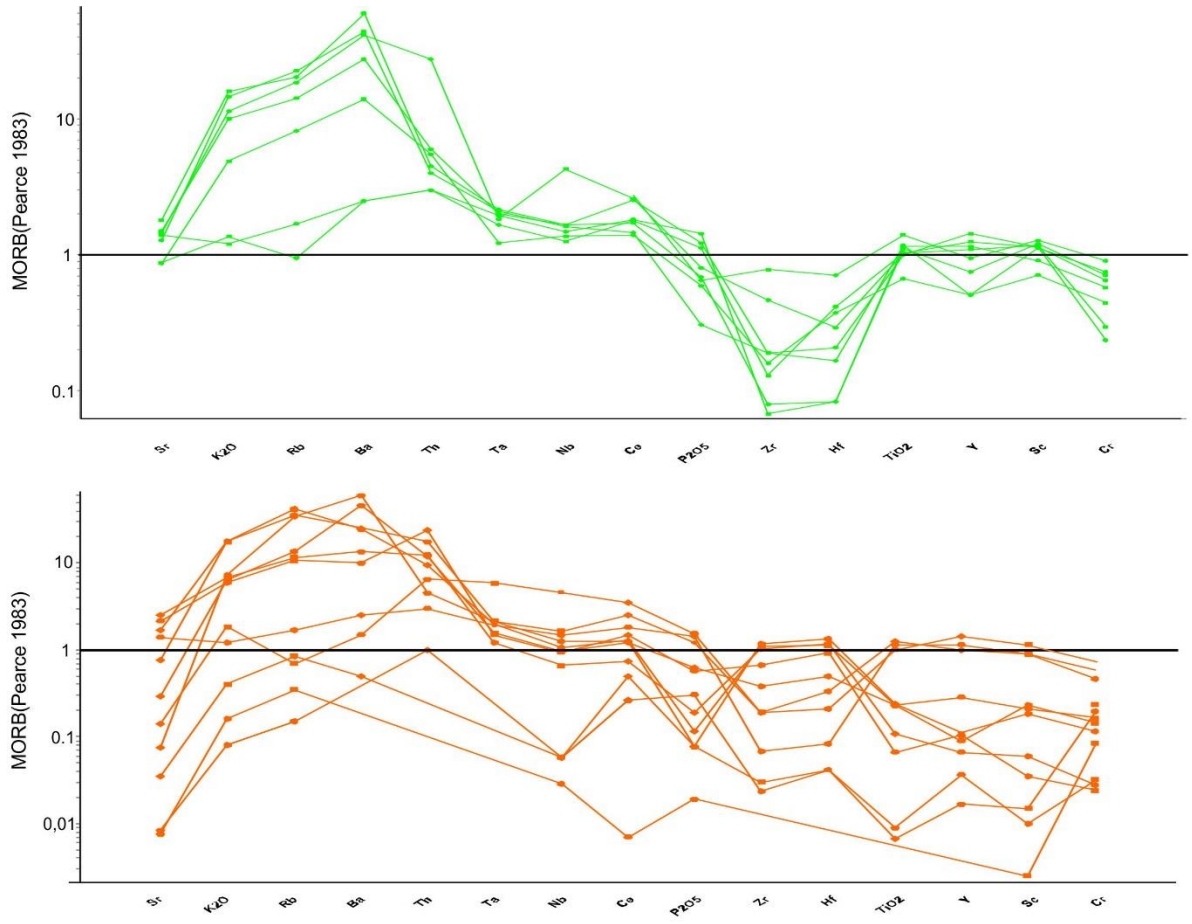

Figure 3.7: *Multi element diagrams in from of spider plots, based upon the MORB-normalization proposed by Pearce (1983). The uppermost plot diagram present the element associations in all mafic rocks(green lines), note the general trend of elevation of K_2O, Rb, Ba and Th versions the depletion of Zr and Hf. The lowermost diagram present the element associations in the sampled felsic rocks(orange lines). Note the broad array of element associations between the samples, this is due to the high degree of weathering and alteration in the sampled rocks. Further, the trend of depletion of Zr and Hf is not present in the felsic rocks, as in their mafic counterparts.*

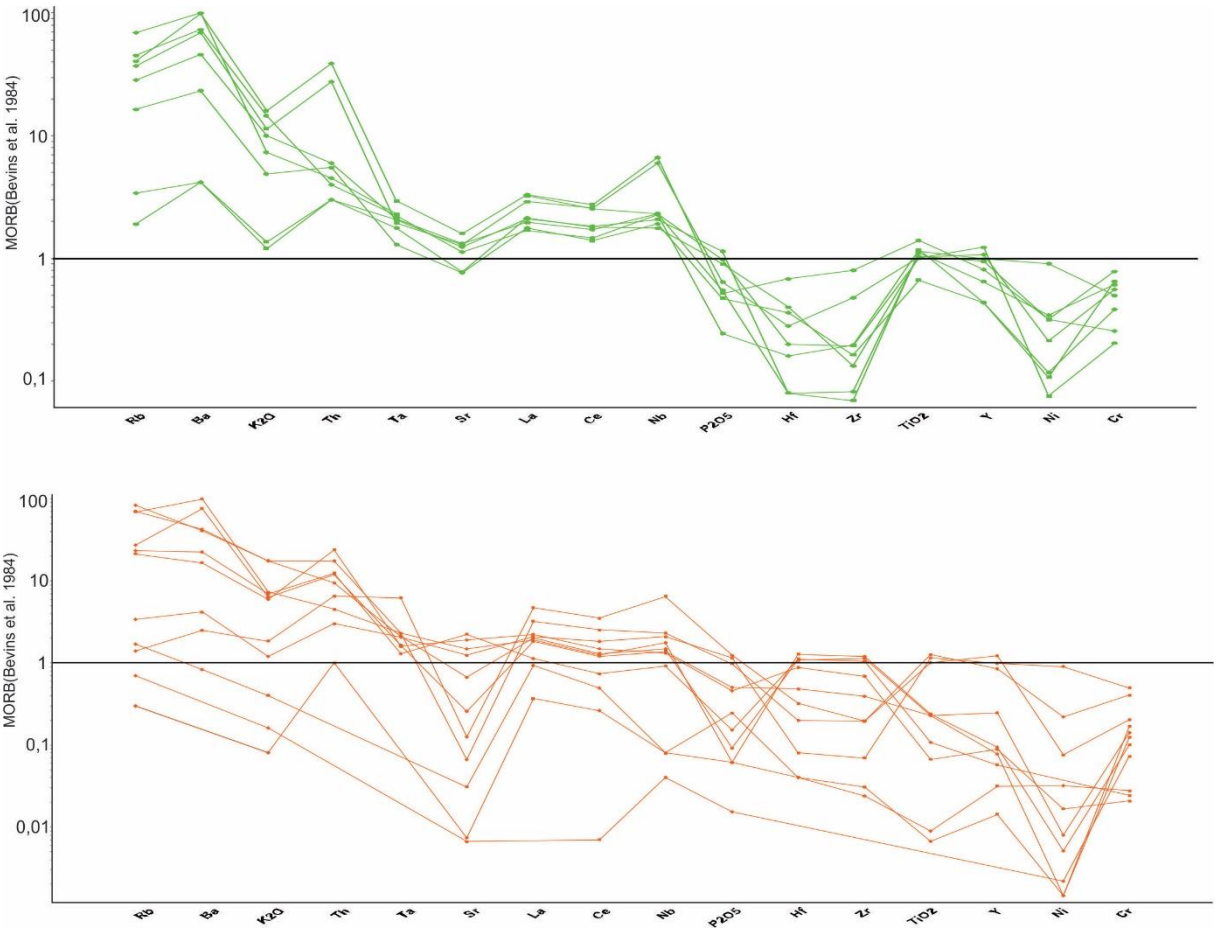

Figure 3.8: Multi-element spider diagram based on the MORB-normalization proposed by Bevins et al. (1984), presenting the element associations in the felsic(orange lines) and mafic(green lines) rocks. Overall presenting similar features as the diagram displayed above i.e. elevation of Rb and Ba versus depletion of Hf and Zr in the mafic rocks, and less signs of depletion of Hf and Zr in the felsic rocks. With this diagram based on Bevins' et al. (1984) suggested average values for MORB, the element ratios compared to the MORB-baseline is different from the plot (Figure 3.7) presented above.

3.3. Mineralization

The multi-element diagrams below present the values of common ore-metals (Ni, Cu, Au and Ag) in the sampled mineralizations (i.e foliation parallel, structurally controlled and vein related), in order to display how the metals are distributed in the different types of mineralization. These diagrams compare the concentrations of ore-metals to the primitive mantle normalization of Taylor & McLennan (1985). Since primitive mantle cannot be sampled, the normalization based on Taylor & McLennan's(1985) modeling and estimations. Thus, the normalized primitive mantle diagrams does not refer to a known composition like the MORB-normalized diagrams in sub-section 3.2.2.

3.3.1. Foliation parallel mineralization

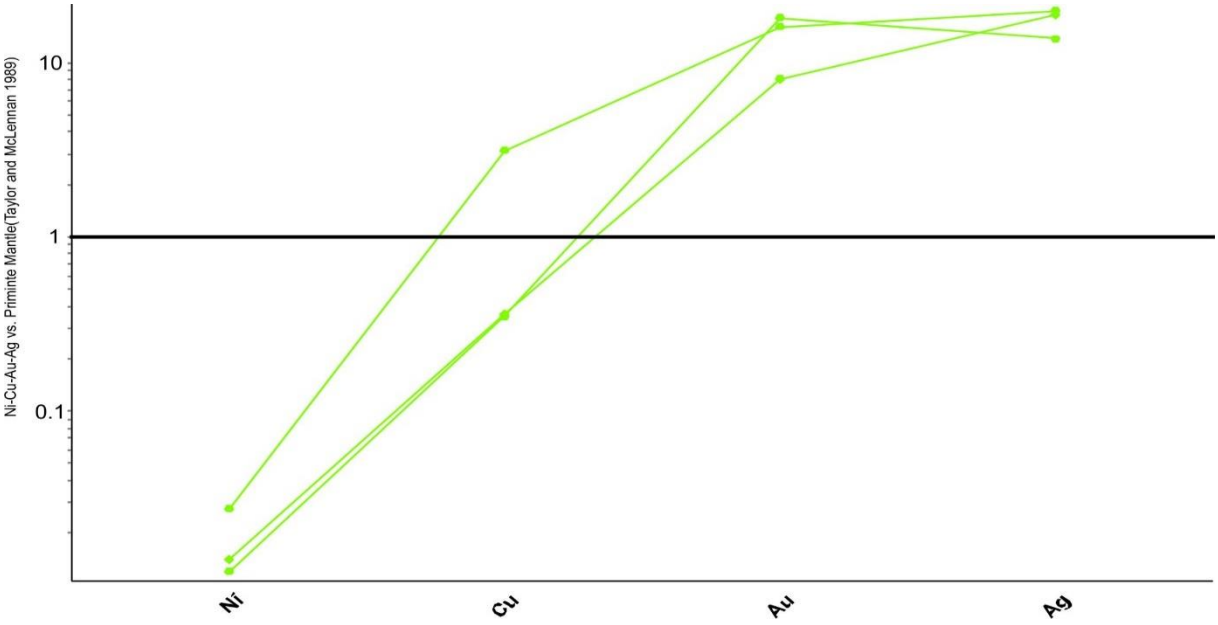

Figure 3.9: Multi-element diagram presenting the values of Ni, Cu, Au and Ag in the foliation parallel mineralization (Appendix B). The highest presented value of gold is 0,018 ppm, roughly 10 times the estimated values in the primitive mantle.

3.3.2. Mineralization related to structures (folds and faults)

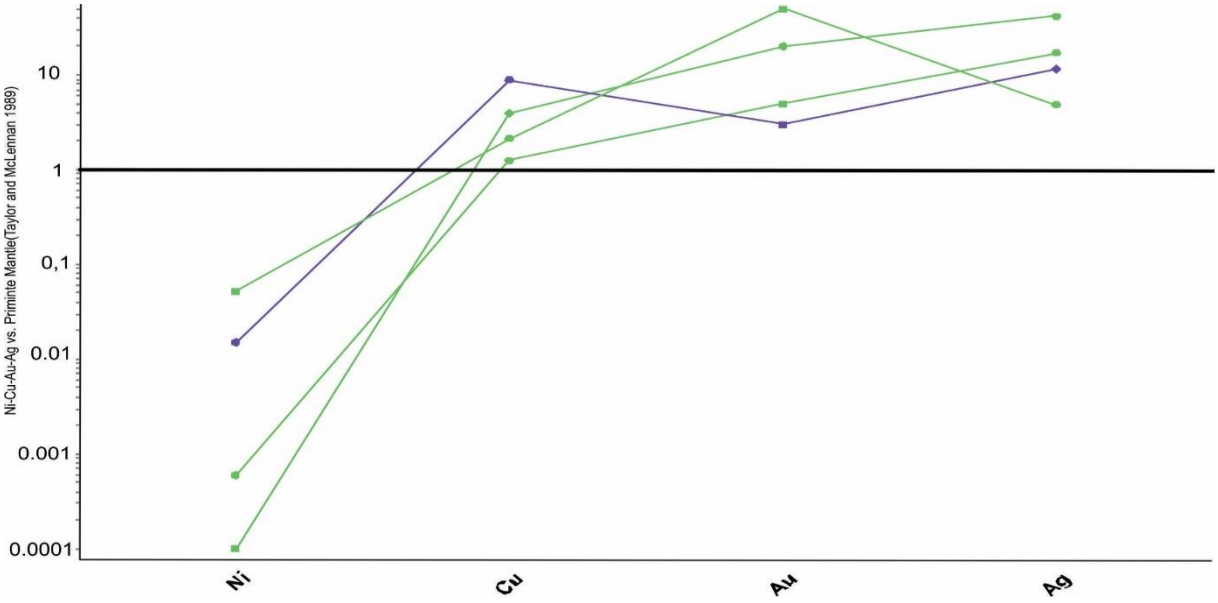

Figure 3.10: *Multi-element diagram presenting the values of Ni, Cu, Au and Ag in the structurally controlled mineralizations. The blue line represent the fold related mineralization and the green lines represent the fault related mineralization (see sub-section 2.5.2). The highest value of gold is 0,05ppm, roughly 50 times the estimated value in primitive mantle.*

3.3.3. Vein-related mineralization

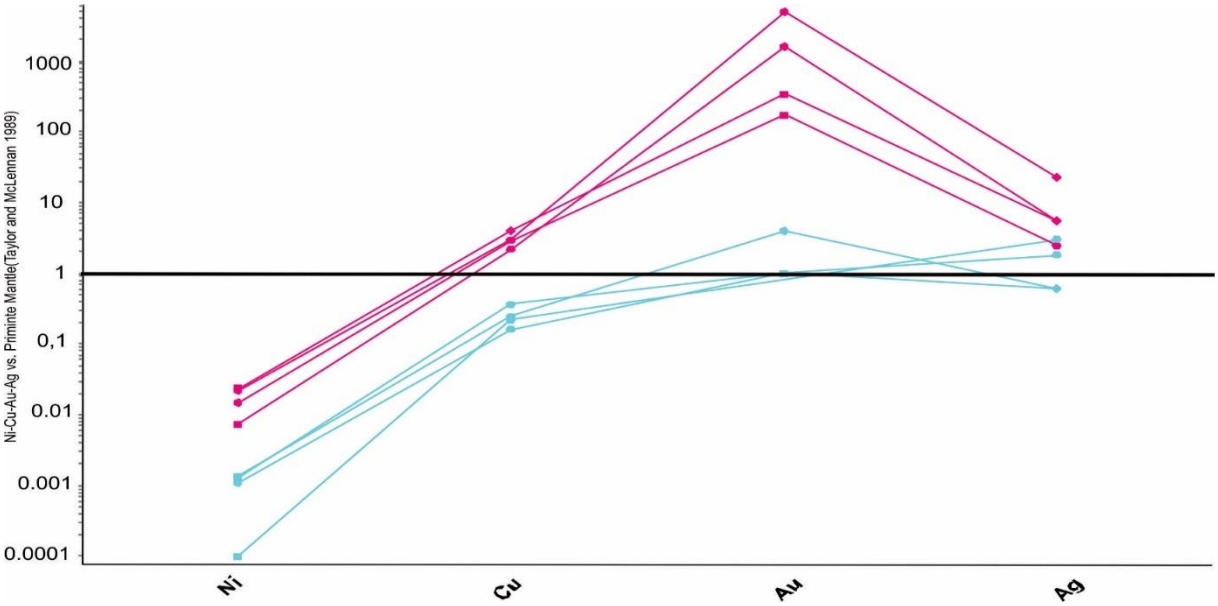

Figure 3.11: *Multi-element diagram presenting the values of Ni, Cu, Au and Ag in the vein related mineralization (see sub-section 2.5.3). The blue lines represent the quartz veins and the purple lines represent the wall rocks (bleached foliated amphibolite). Note how the quartz vein is barren in terms of gold, whereas the wall rock display values up to 50000 times the estimated amount in primitive mantle. The top values of gold in the host rock are 4,98 ppm, 1,61 ppm, 0,339 and 0,173, respectively (Appendix B).*

4. Discussion

Several key properties of the study area will be examined in this chapter. First, the origin of the dominant amphibolites and the mineralized quartz-mica rich unit (sedimentary versus igneous) will be discussed based on tectono-stratigraphic succession, contact relations and petrography of the RGB rocks in the study area, followed by a discussion of processes of formation of the various structural elements and their relation to the investigated lithologies and mineralizations. Further, focus is put on the geochemistry of the amphibolites and the quartz-mica rich unit in order to classify and discuss implications for tectonic setting. The final section addresses the origin and relationship of the various mineralizations, in view of ore genetic processes and ore potential of the study area.

4.1.Tectonostratigraphy and contact relations

The studied part of the Skogsfjordvatn Group is made up of a foliated succession of mostly various amphibolites, and a specific quartz-mica rich unit (see sub-section 2.2.3). The lithological boundary between the amphibolite and the quartz-mica rich unit on either side is thought to represent a conformable contact, supported by consistent parallelity of the main foliation on both sides of the contact, with no abrupt internal change in attitude (Figure 2.2 and 2.3). In the vicinity of this lithological boundary, petrographic investigation shows an increasing amount of leucocratic minerals in the foliated amphibolite and hornblende porphyroclasts in the quartz-mica rich unit (see sub-section 2.2.3; 2.2.4; Figure 4.1). These mineralogical changes, and no internal variations in attitude of the foliation, give further impression of a depositional origin, displayed as a gradual contact with strong features of alteration. The investigation of the lithological contact between the garnet-hornblende schist of Skogsfjord group and the underlying foliated amphibolites of Skogsfjordvatn group shows that this contact is tectonic, defined as a low angle ductile thrust-fault with SE-ward oblique dextral sense of shear (see sub-section 2.2.4; 2.4.2).

In the mapped area on Lassefjellet, no evidence was found to support the tectonostratigraphy established by Zwaan (1989), where the domains north of the quartz-mica rich unit are considered part of the Skogsfjord group. This thesis shows that the foliated amphibolites in the southern parts of Lassefjellet are petrographically similar to those farther north, with no major changes in mineralogical composition. To further support this suggestion, the mineral assemblage does not indicate a higher

metamorphic grade in the contact zone or within the amphibolites. The lack of a low angle ductile thrust fault (S2) is also viewed as an argument against Zwaan's(1989) definition, thus it is to be mentioned that Zwaan (1989) described the contact on the eastern side of the Skogsfjordvatn lake as gradual, rather than a thrust fault. Overall, as all the encountered rocks in the domain north of the quartz-mica rich unit on Lassefjellet display the same texture and structure as the foliated amphibolites of the Skogsfjordvatn group, the author chooses to define the domain as foliated amphibolite belonging to the Skogsfjordvatn group. This differs from the conclusions of previous studies, where the domains north of Lassefjellet have been interpreted as high-grade metamorphic rocks of the Skogsfjord group.

With the separation of the lithotectonic units in this thesis (i.e Skogsfjordvatn group and Skogsfjord group) being based upon the proposed tectonostatigraphy of Zwaan (1989), the extent of these two groups is disputed. Further, Zwaan's (1989) differentiation is partly based on a change in metamorphic grade between the two main groups, with the uppermost Skogsfjord group suggested to be related to a higher metamorphic facies (Zwaan, 1989). Petrographic studies of the two groups on each side of the contact indicate a regional gap in metamorphic grade, whereas the mineral content (see sub-section 2.3.1) of the overlying Skogsfjord group suggests higher metamorphic grades, and these are observations that support Zwaan's (1989) interpretation. It should be taken into consideration that the presumed higher metamorphic grade of the Skogsfjord group may only be local, occurring in the vicinity of the tectonic contact, as proposed by Bergh and Armitage (1998). The tectonic contact between the two groups is proposed to resemble a continuation of the previously mapped S2-shear zone (Bergh & Armitage, 1998; Zwaan, 1989) to the west of the study area, based on similarities in sense of shear. The suggestion that the lithological boundary between the foliated amphibolite and the quartz-mica rich unit is conformable (Figure 4.1) is overall supported by the previous investigations (Bergh & Armitage, 1998; Zwaan, 1989).

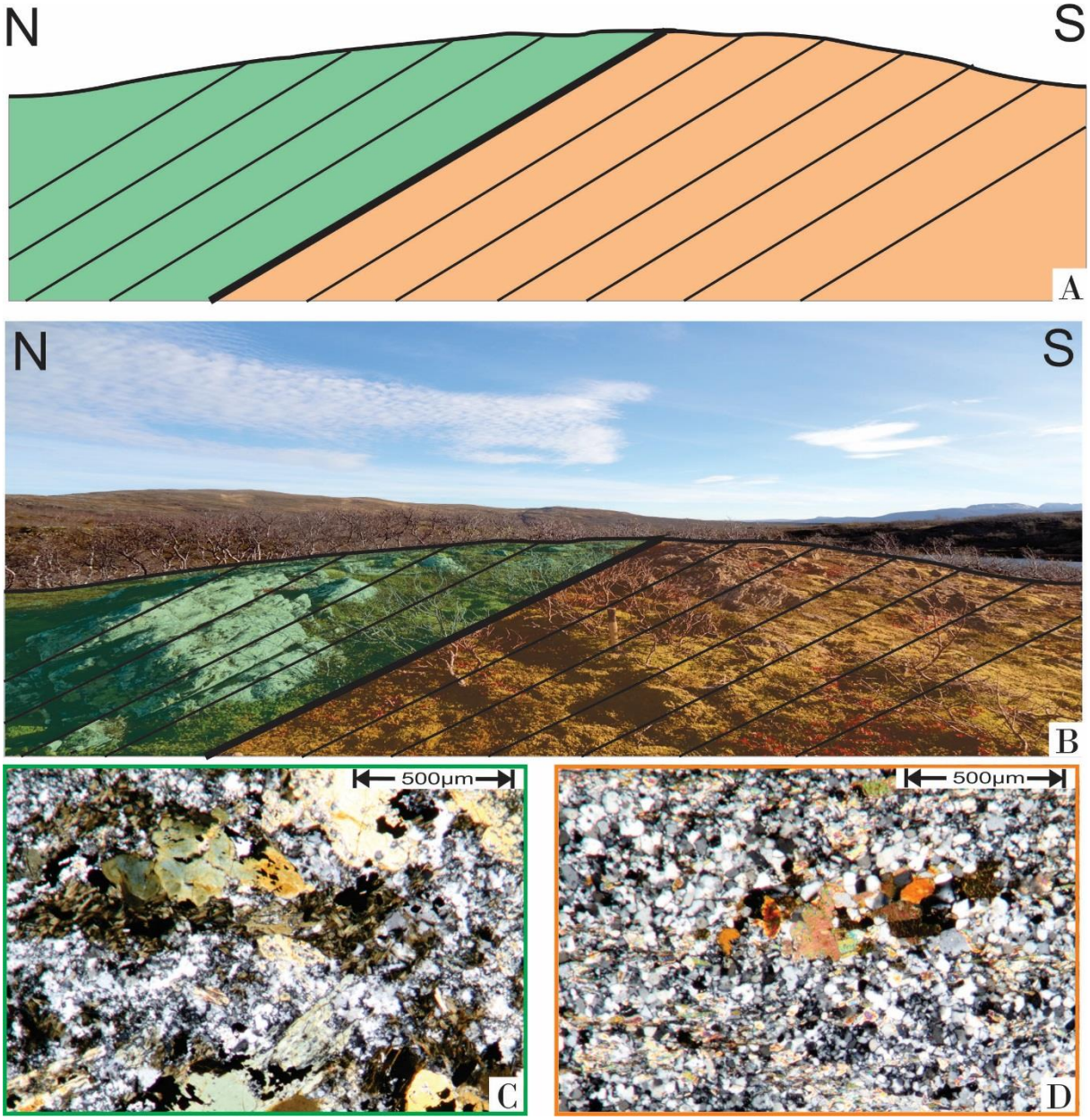

Figure 4.1: *Overview of the lithological border between the foliated amphibolite and the quartz-mica rich unit on top of Lassefjellet (Figure 2.3). A) Idealized model of the contact relationship and orientation of the foliation in the two units. B) Picture of the outcropped lithological border (looking east) with interpretation of the foliation and contact relationship. C) Photo of the bleached foliated amphibolite in thin section. Note the intense sericitization(white) in between the deformed hornblende grains(green/yellow). Picture originates from sample HE-P14 (see appendix A for location). D) Photo show remnants of a highly deformed hornblende porphyroclast (orange) in fine grained quartz (white and black)-sercite (light interference colors) matrix. Picture originates from sample HE-P15 (see appendix A for location), taken from the south side of the lithological border in the quartz-mica rich unit. Photo C and D are viewed in cross-polarized light.*

4.2. Origin of the country rock (foliated amphibolite)

The foliated amphibolite of the Skogsfjordvatn group is by far the most common rock type, making up the majority of the study area. This lithology is displayed as conformable units on either side of the mineralized quartz-mica rich unit, and thus both may be part of a meta-volcanic/sedimentary sequence. However, a magmatic origin for the amphibolites and an intrusive (felsic intrusive/sill) origin for the quartz-mica schist can also be possible. Therefore, the descriptive term "country rock" is used for the amphibolites to address only the position of the lithology in relation to the quartz-mica rich unit. The term "wall-rock" may also be descriptive in this context, again emphasizing it as a term of location in relation the quartz-mica rich unit, rather than an implication of the origin.

While amphibolite in general is a descriptive term for a weakly foliated medium-grade (i.e. amphibolite facies) mafic metamorphic rock dominated by hornblende-rich amphiboles, the mineral content alone cannot directly be used to infer the protolith or the origin of the rock. Since an amphibolite can be of both sedimentary and igneous origin (i.e para- and ortho-amphibolite), additional geochemical and mineral chemical data are needed to verify the origin. However, amphibolites are most commonly metamorphosed igneous rocks (ortho-amphibolites). Interpretations of the petrographical data and observations described in sub-section 2.2.1 suggest the investigated amphibolites are of magmatic origin, displaying a main composition of poikilitic hornblende with an aphanitic texture (Figure 2.4a,b). The observed foliation-parallel occurrences of the porphyritic type of amphibolite supports this further, especially if the feldspar porphyroclasts are interpreted as amygdales formed due to cavities in an extrusive lava flow. Overall, these structures suggest a relatively high cooling rate, possibly due to crystallization near/on the surface. With no primary sedimentary and/or volcanic structures observed in the foliated amphibolite, the gradational contact relations, lack of internal rhythmic banding, and few lithological facies variations further support the suggestion of a magmatic origin. This suggestion is supported by previous interpretations of a magmatic origin of the amphibolites in the Neoarchaean and Palaeoproterozoic West Troms Basement Complex, including the Ringvassøya Greenstone Belt (e.g Bergh & Armitage, 1998; Motuza, 2000; Zwaan, 1989).

As the amphibolites are displaying relatively consistent equilibrium mineral assemblages of hornblende and plagioclase, and lesser contents of low-grade metamorphic minerals (e.g chlorite and primary quartz), the lithology has presumably undergone regional medium-grade metamorphism. Therefore, a volcano-sedimentary origin cannot be excluded, since primary structures are usually masked or removed during medium-grade metamorphism. The geochemical data (see chapter 3) will be used to argue for a magmatic – possibly volcanic – origin (see below), and suggest the tectonic environment for the amphibolites

4.3. Origin of the quartz-mica rich unit

In the field, the quartz-mica rich unit is characterized as a light-colored foliated rock with a dark brown weathered, oxidized surface, similar to iron-oxide rich sedimentary ferricrete (Collinson, 2006). Hand specimens of this aphanitic rock display a banded texture, including zonal layers of quartz separated by a fine-grained muscovite (sericite) dominated matrix. The observations of sericite being interbedded with layers of quartz suggest that these rocks may have formed from original, layered quartz-sandstone and mudstone. However, quartz and phyllosilicate minerals can also form by metamorphism of felsic intrusives and volcanic host rocks, as well as during hydrothermal alteration of both volcanic and sedimentary rocks. In thin-section, the different varieties (weathered and un-weathered) of the unit present a broader range of minerals. Here feldspar (defined as plagioclase due to twinning) is observed in the fine grained muscovite matrix, all with sericite alteration halos suggesting the high sericite content may originate from altered feldspar. The impression of hydrothermal alteration is further supported by the continuous wriggly parallel cleavage domains, defined by spaced zonal alignment of anhedral quartz and pyrite grains in a textural equilibrium (Figure 2.6c) overall suggesting formation due to Fe-Si-saturated fluid-flow along the primary bedding planes. Whilst pyrite is well known in both sedimentary and igneous rocks, the more massive beds of iron sulfides observed along the foliation planes (see sub-section 2.5.1) may be remnants of a volcanogenic massive sulfide deposit (Galley et al., 2007; see sub-section 4.6.1), favoring a volcano-sedimentary origin of the unit. The volcano-sedimentary affinity is further supported by the observations of meta-sedimentary lenses within the unit, though their interbedded foliation parallel appearance combined with the aphanitic texture of the unit also give rise to the possibility of an extrusional origin. Traces of femic minerals (mostly chloritizised biotite and hornblende porphyroblast) are observed in the quartz-mica rich unit (especially towards the lithological borders). Even though the presence of these minerals alone cannot confirm an igneous affinity, they may indicate a close relation to the country rock. Overall, from the field appearance and petrography-mineralogy alone it is not possible to propose a reliable origin of the quartz-mica rich unit, mainly due to extensive alteration of the primary minerals. Thus, only a slight indication of a volcano-sedimentary affinity is presented here.

The studied quartz-mica rich unit has been investigated in previous studies of the Ringvassøya Greenstone Belt (e.g. Sandstad & Nilsson, 1998; Motuza, 2000; Bergh & Armitage, 1998; Zwaan, 1989), but its origin still remains enigmatic. In Zwaan's (1989) report on the unit, the author brings up the term keratophyre (first proposed by Fareth & Lindahl, 1981), a descriptive term rather than a specific

protolith, defined by Schermerhorn (1973) as a leucocratic sodic intermediate albite-pyric volcanic rock. Keratophyre is a term given to a large variety of rocks containing albite, thus a proper definition of keratophyre is hard to delimit. However, the petrographic investigation of this rock unit discloses traces of plagioclase in the sericite matrix; this plagioclase may very well be close to the albite endmember due to clear signs of twinning. Therefore, by suggesting the high content of sericite originated from altered plagioclase (albite), the term keratophyre might not be totally displaced in this context. Due to the moderate quartz contents presented in the samples (see sub-section 2.2.3) the term quartz keratophyre may be an even better fit, defined as leucocratic sodic felsic quartz-albite-phyric or albite-phyric volcanic rock (Schermerhorn, 1973), with an aphanitic groundmass of largely albite (in this case strongly sericitized) and quartz. Note that this is merely a suggestion from the author's side, all in attempt to verify the use of previous nomenclature.

In an unpublished report by Bergh & Armitage (1998), the authors suggest a sedimentary affinity. This tentative interpretation is purely based on field observations, as no thin sections or geochemical analyses were made. In Motuza's report (2000), a range of geochemical and petrographical results corroborates the igneous origin. Whilst this leads to an inconclusive impression of the origin based on literature, it opens up for unbiased view on the further interpreted trace element geochemistry, where values and distributional patterns are presenting important features regarding the origin, protolith and tectonic environment for the unit.

4.4. Discussion of structures influencing the map-pattern

Bergh & Armitage (1998) proposed a multiphase tectonic model (Figure 2.1) to explain the various deformation structures in the Ringvassøya Greenstone Belt (see sub-section 2.2.4). Their model (Figure 2.1) has been used as a framework for the observed structures and structural interpretations in the study area, and it provides valuable input to the discussion of ore potential (stratiform versus structurally controlled).

The dominant planar fabric of the studied rocks is the main S1 foliation, which is present both in the quartz-mica rich unit and the foliated amphibolites, striking on average WNW-ESE with a gentle to moderate dip the NNE (Figure 2.8). In the amphibolitic domains, sheared quartz veins related to arsenopyrite-gold mineralizations are observed striking parallel to the main S1 foliation. Stretching lineations (L1) have been observed on many foliation surfaces, and when present, they trend mostly E-W in foliated amphibolites at Innerelvdalen. In addition, gently NW-plunging intrafolial folds (F1) occur in foliation-parallel mineralization exposed in pits on Lassefjellet. These presumed D1-structures

(Bergh & Armitage, 1998), including the strong continuous foliation, the presence of intrafolial isoclinal folds, and the stretching lineations, all are consistent with formation by shortening and shearing almost perpendicular (or slightly oblique) to the strike of the foliation, i.e. due to ENE-WSW-directed shortening and likely thrusting and shearing along the foliation (cf. Bergh & Armitage, 1998; Bergh et al., 2010).

Large-scale variations in the orientation of the S1 foliation, e.g. gently NE dipping S1-foliation in the top of Innerelvdalen and gentle NW dip at the top of Lassefjellet, may represent the two flanks of a megascale F2-synform (Figure 2.8) with a gently NNE-plunging macrofold β-axis. Mesoscale upright to gently WNW plunging F2-folds are identified and mapped in all the dominant lithologies (e.g. in the quartz-mica rich unit and the foliated amphibolite). In the quartz-mica rich unit, these represent folded mineralization beds with slight signs of sulfide accumulation on the hinge zones (see sub-section 2.5.2). The mapped F2-folds display somewhat variable trends, ranging from WSW-ENE to NNW-SSE and mostly subvertical axial surfaces (see sub-section 2.2.4; Figure 2.8). Locally, asymmetric F2 folds occur in the footwall of closely related, gently NW-dipping axial-planar ductile shear zones (see sub-section 2.2.4). The S2-shear zones display mafic intrusions with phyllonitic chlorite-epidote rich surfaces (S2), likely formed at greenschist facies conditions. These surfaces present sets of kink-folds in the pyllonitic S1-fabric displaying a top to the SE movement, interpreted to represent the movement direction of the obliquely truncating S2-shear zone. The high variance in orientation of the mesoscale F2 folds does not entirely fit the tentative model, thus the change in orientation might have been caused by later reworking during the third stage of deformation. The low angle oblique ductile shear zone (described above) fit the model of Bergh & Armitage (1998) perfectly, suggesting SE-directed dextral strike slip motion and out of the syncline faulting, thus reactivation of the macrofold limbs may be a response to crustal shortening and oblique shearing. The northward plunge of the macrofold β-axis in the study area (Figure 2.8) is slightly different from the NW-trend of the macrofold mapped by Bergh & Armitage (1998), thus the location of the study area in the hinge area of the interpreted macrofold may have caused local variations.

N-NNE striking steep to vertical sinistral shear-zones are strongly affecting the map pattern, crosscutting and offsetting the main lithologies by up to 100 meters (Figure 2.2). In the quartz-mica rich unit, epigenic tabular bodies of iron sulfides are observed the traces of the N-NNE striking S3-shear zones, suggesting that replacement and accumulation of sulfides occurred syn-D3. In the outcrop scale, the main S1-foliation is folded by N-S and NNE-SSW trending drag-related folds with a steeply plunging β-axis (Figure 2.8) and the shear zones are axial-planar to these folds, supporting sinistral down-to-the S-SW movement in the shear-zones. Mapped lateral offset of the litholgies in Innerelva (Figure 2.2) and the orientation of the closely related, moderately plunging drag folds (F3) all favor sinistral down-

to-the S-SW movement-direction. All these N-S and NNE-SSW striking shear-zones and moderately plunging drag-related folds crosscut all other structures and lithologies, suggesting they represent the youngest set of ductile structures in the study area (cf. Bergh & Armitage, 1998). Accordingly, they are interpreted as the third phase of deformation (D3) caused by oblique shortening relative to D1 and D2.

4.5. Geochemistry and tectonic setting of the studied rocks

The mineralogical and contact relations discussed in section 4.1-4.3 suggest the two main lithologies (i.e. the quartz-mica rich unit and the foliated amphibolite) formed in relation to a volcano-sedimentary environment. The following geochemical discussion will therefore be based on the presumption that the sampled rocks are igneous-volcanic, rather than sedimentary.

4.5.1. Geochemical character and tectonic setting

All methods and discriminations plots used to describe to geochemical character and tectonic setting of the presumed igneous rocks in the studied part of the RGB are presented in chapter 3, and these plots are referred to throughout the discussion in this sub-section. The appendixes (Appendix A & B) include a complete list of geochemical data from all samples taken in the study area.

Mafic rocks

The first method (Figure 3.1-3.3) for classification of basaltic samples, defined by Pierce and Cann (1973), emplaces the foliated amphibolites in the tholeiitic magma series. This trend is also evident in the AFM-diagram (Figure 3.4), and is suggested to be caused by the fractional removal of olivine during crystallization, resulting in an increase of iron compared to magnesium. Further, the samples plot relatively clustered in the discrimination diagrams (Figure 3.1 to 3.3) of the method, with a slight relation to the ocean floor basalts and island-arc basalts presented, although no samples plot within any of the given domains. This systematic error is caused by very low zircon values in all the mafic samples (see Appendix B), most likely related to the fractional removal of olivine phenocrysts suggested above, essentially diluting the zircon content in the remaining melt. However, with the impression of relation to ocean floor basalt and island-arc basalts, it should be noted that the method has been proven to fail at distinguishing between the two given sub-groups, especially when dealing with back-arc basin basalts (BABB) which are intermediate between the two end members (Pearce &

Stern, 2006). Even so, the Nb/Y versus Zr/TiO2 discrimination diagram (Figure 3.6) defined by Floyd and Winchester (1977) affirm the magma series and affinity of the mafic rocks presented in Pierce and Cann's (1973) method, by plotting the samples firmly in the field of sub-alkaline basalt, also referred to as tholeiitic basalt. Tholeiitic basalt is the most common type of mafic volcanic rock, usually derived from spreading ridges in a back arc basin and/or in a mid ocean ridge (Blatt et al. 2006). Overall, the discrimination of the analyzed mafic rocks clearly indicate their tholeiitic magma series and relation to the sea floor, either formed in a back arc basin or a mid ocean ridge. However, since this discrimination plots are only based on a few elements, one should interpret these results with caution.

To get a better impression of a tectonic environment for the sampled mafic rocks of the study area, the multi-element diagrams (Figure 3.7 and 3.8) normalized for mid-ocean ridge basalt open up for a broad range of elements to be interpreted. The overall geochemical pattern of the mafic samples is viewed as a general enrichment of the subduction-mobile elements (Ba, Rb, K, Th, Sr), and depletion of the subduction-immobile elements (Zr, Hf, Ti, Ta and Nb)(Pearce & Stern, 2006). Variations of the subduction-mobile elements and Ta between the sampled rocks are explained by the former elements' greater mobility during alteration and metamorphism. According to Pearce and Stern (2006), a general depletion of subduction-immobile elements and enrichment of subduction-mobile elements can be seen as a key characteristic for back-arc basin basalts. Thereby, the results presented in the MORB-normalized multi-element diagrams strengthen the relation to a back arc basin (BABB). Overall, by interpreting all the geochemical results from both multi-element and discrimination diagrams, the most probable presumption based on the given geochemical data characterizes the mafic rocks as tholeiitic ocean-floor basalts with affinity to a back-arc (basin) tectonic environment.

Felsic rocks

In an attempt to suggest a magmatic series for the felsic rocks, all variations of the rocks are plotted in the AFM-diagram (Figure 3.4). The majority of samples display a calc-alkaline trend in this plot, whereas two samples plot in the tholeiitic domain, most likely due to iron-sulfides dissemination in the matrix. Wood's (1980) ternary plot (Figure 3.5) corroborates the suggested magmatic series, though with this diagram partly based on mobile elements, the plot should be interpreted with caution. In a further attempt to propose a general protolithic composition for the felsic rocks of the quartz-mica rich unit, the samples were plotted in Floyd and Winchesters (1977) discrimination diagram (Figure 3.6) utilizing Zr/TiO_2 and Nb/Y, and here the samples plot in the fields of rhyodacite, dacite and trachyandesites, with no relation to their tholeiitic basaltic counterparts. The proposed protholiths are generally related to volcanic arc environments (Blatt et al., 2006); this is confirmed by the firmly plotted

felsic samples in the arc-related fields in the ternary plot modified from Wood (1980). Furthermore, by closer examination of the MORB-normalized multi-element plots, the sampled felsic rocks do not present strong features of subduction zone related magmatism (e.g. depletion of high field strength elements; Karsten, 1996), compared to the pattern observed in the mafic rocks(see above). This suggests that the felsic rocks formed as rhyodacite/dacite and trachyandesite in a volcanic-arc environment, but from a different source than their mafic counterparts, possibly slab related and derived from higher levels of felsic (continental) crust.

In summary, the comparatively uniform and characteristic geochemical features discussed in this sub-section argue for an igneous-volcanic, but not sedimentary origin (especially when excluding highly weathered samples). Furthermore, by considering all the interpreted geochemical data from chapter 3, the author would suggest a strong relation to a volcanic arc tectonic environment, including continental-oceanic subduction and formation of a back arc basin. With all the protoliths being interpreted as extrusive igneous rocks, the presumption of a volcanic origin is additionally supported. The foliated amphibolites of the study area display relation to the tholeiitic magma series, and may have formed from primary melting of an accreting/subducting oceanic plate, and later been erupted as basalts in a back arc basin. The rocks of the calc-alkaline series (i.e. the quartz-mica rich unit) may then have formed at later stages of accretion/subduction, originating from a source of magma derived from a higher level in the crust (Figure 4.2). The protolithic composition of the calc-alkaline rocks suggests they originated from partly melted continental crust, and were brought to the surface due to slab-related volcanism, either erupted in a back arc basin or an arc volcano (Figure 4.2). The observed interbedding of rocks of different geochemical characteristics imply bimodal (i.e felsic and mafic) volcanism, both in time and space. Finally, the fact that the studied mafic and felsic rocks have undergone extensive metamorphism and possibly also hydrothermal alteration makes this interpretation somewhat ambiguous, and hence this classification and interpretation should be reviewed with caution.

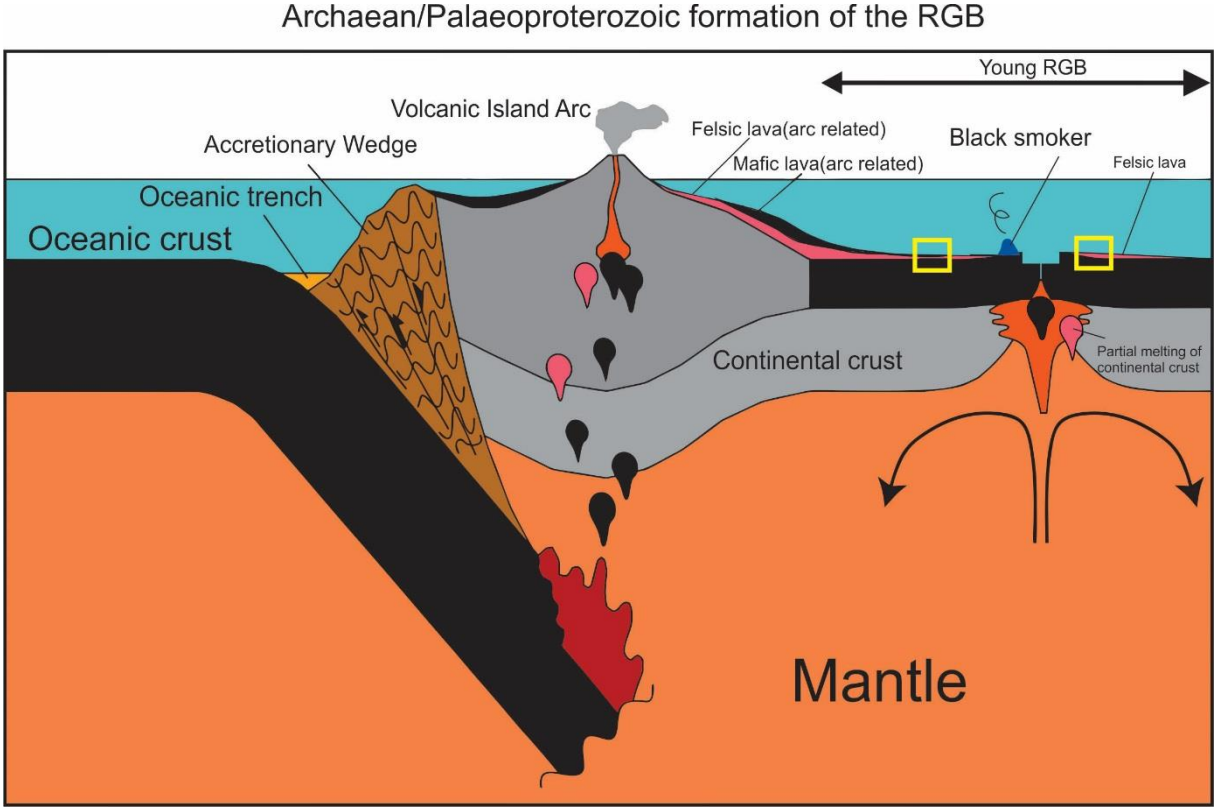

Figure 4.2: *Suggested formational environment for the Ringvassøya Greenstone Belt. The pink layers represent the felsic volcanic rocks and the black the basalts. The yellow squares indicate a potential position of the study area, though this merely a suggestion to show how the felsic and mafic rocks are interbedded in the study area, and how the iron sulfides may have formed from a black smoker complex (see sub-section 4.6.1). Felsic rocks (pink) are suggested to have formed from partial melting of the continental crust (TTG-gneisses) and brought to the surface by slab-related volcanism in a back arc basin and/or in a volcanic arc. As this tectonic setting includes the formation of volcanic and shallow-water sedimentary rocks, the proven occurrence of sedimentary units in the study area is justified. The model inferred above is however not conclusive, as geochemical discrimination plots only provide limited information about the origin and tectonic environment of mafic and felsic igneous rocks.*

It might be worth mentioning that Motuza (2000) did get zircons from the RGB dated 2848.5 +/- 3.9 and 2835 +/- 14 Ma, placing to formation of the Ringvassøya Greenstone Belt in the Archaean. As the theory of Archaean subduction is highly debated, the suggested back arc basin may represent an intracratonic ocean in between crustal fragments composed of TTG gneisses, eliminating the subducting plate from the model. Further, the author would like to point out that the formational age presented by Motuza (2000) is highly similar to the 2841.6 +/- 2.8 Ma age (Zwaan & Tucker 1996) of the TTG-gneisses in the southwestern parts of Ringvassøya. Overall, if the dated zircons originated from the TTG-gneisses and were brought to the RGB by partial melting of the continental crust (TTG) as this model (Figure 4.2) implies, the formational age of the RGB is suggesting to be post 2841.6 +/- 2.8 Ma, closer to the Palaeoproterozoic.

4.6. Mineralizations

This part of the discussion will emphasize the origin, relationship and ore-potential of the following types of mineralization: *foliation-parallel*, *structurally controlled* and *vein-related* mineralization.

4.6.1. Foliation-parallel mineralization (D1)

The stratiform massive sulfide mineralizations of the quartz-mica rich unit is by far the most common type of mineralization in the study area, with exposures in all prospecting pits (Figure 2.7d) from the top of Lassefjellet to Innerelvdalen (Figure 2.2 and 2.3). The disseminated sulfide beds present a folded structure, with a mineral assemblage of pyrite, muscovite and quartz. The observed muscovite is coarser-grained than the fine-grained muscovite (sericite) in the host rock (quartz-mica rich unit), suggesting the muscovite and quartz are remnants of sediments deposited along the primary bedding. This is further supported by the observed lenses of meta-sedimentary rocks (see sub-section 2.2.5) parallel to the main foliation, stating relation to a sedimentary environment. The main mineral, pyrite, is represented by rounded to semi-rounded sulfide grains, and this shape is suggested to be related to pre- or syn-formational transportation. The author therefore suggests that the sulfide mineralization formed roughly synchronous with the host rock, possibly caused by a flow of hydrothermal fluids inserting the sulfides in layers of sediment deposited on top of the host rock (Figure 4.3). Due to this insertion of sulfides in deposited sediment, the mineralization is seemingly replacing the host rock rocks partly or completely. The stratiform sulfides are therefore classified as syngenetic, though not crystallizing within the host rock in the form of mineral segregation (cf. Evans 1987), but formed as a result of submarine hydrothermal discharge.

Such hydrothermal discharge is related to what we today call “black smokers”. A black smoker is a hydrothermal “volcano” on the ocean floor, ventilating heated brine into the sea water. The “erupting” acidic and saline hydrothermal fluids are rich in metals dissolved from the underlying seabed, and when these interact with the cold ocean water they precipitate on top of/in sediments on the seabed (Robb, 2005). Most of these deposit types present a twofold ore distribution, one stratabound massive sulfide formation on the seafloor, and another multi-element disseminated mineralization in form of a stockwork, related to the feeder tubes underneath the black smoker complex (Ohmoto, 1996)(Figure 4.3a). The foliation-parallel sulfide mineralization of the study area is suggested to relate to the former, based on the stratabound occurrence and relation to sediments. With back-arc basins being among the most typical formational environments of black smokers, the former interpretations given in the geochemical discussion are supported.

As observed from the multi-element plot of ore-elements (Figure 3.9) in chapter 3, the stratiform mineralization does not present anomalous levels of any ore-metal. Zwaan (1989) suggest that there might be a relation between the keratophyre (quartz-mica rich unit) and gold, but such a spatial link is not observed in thin sections nor in the geochemical analysis (Appendix B). The author will therefore argue that the stratiform sulfide mineralization does not have any economic value, and no relation to gold occurrences. Fareth & Lindahl (1981) investigated the so-called *vasskis* (pyrite-pyrrhotite) mineralizations in the central parts of the Ringvassøya Greenstone Belt, and their work stated the same conclusion as given above.

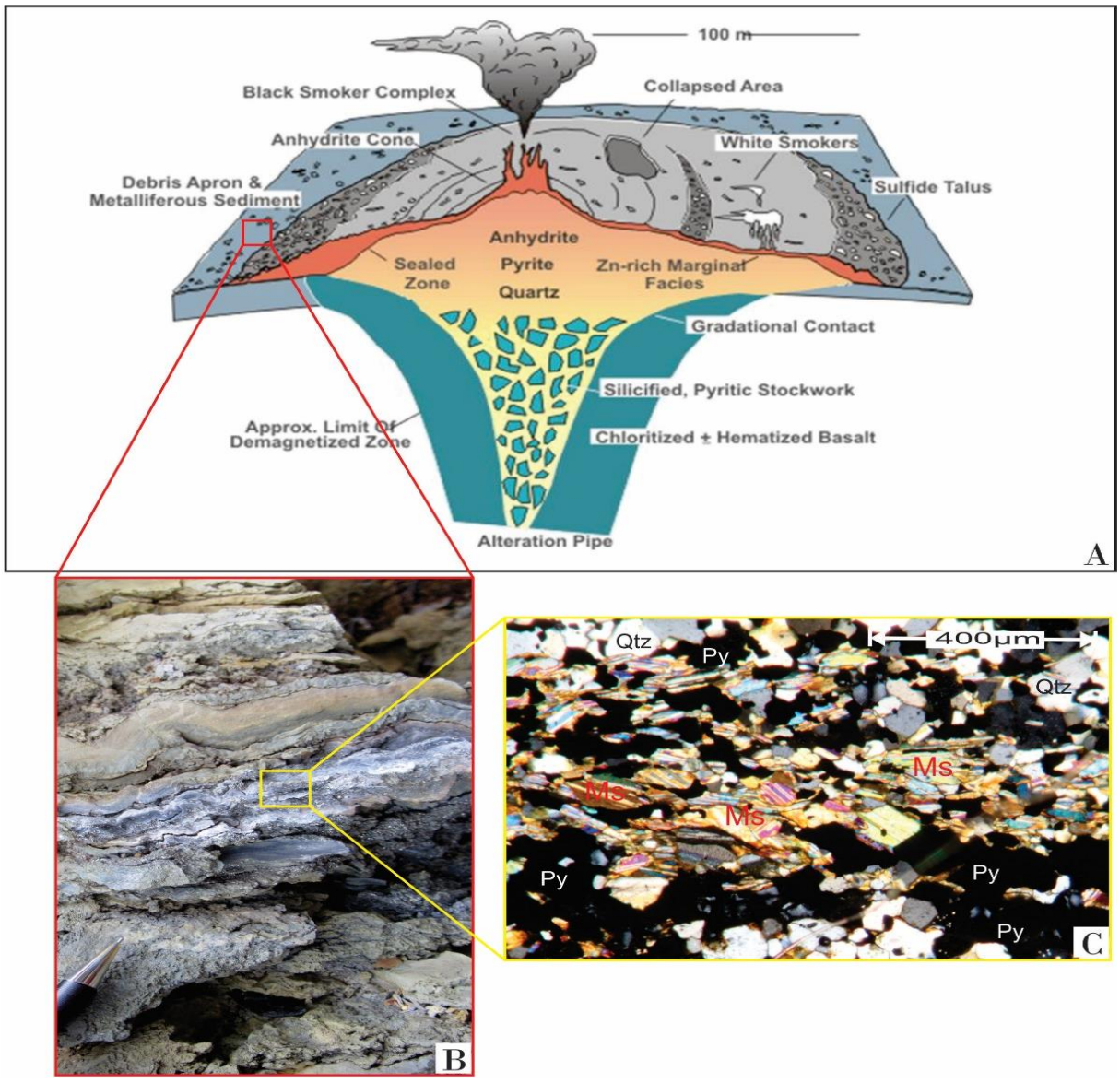

Figure 4.3: Suggested formational environment of the foliation-parallel sulfide mineralization. A) Cross section of an idealized black smoker complex modified from Galley et al. (2007). The hydrothermal discharge pumped up from the complex is suggested to have precipitated the observed iron sulfides. B) Picture of folded layers of disseminated iron-sulfides, interpreted to have formed in the vicinity of a black smoker complex. C) Thin section of disseminated iron-sulfides in picture B. Note how the muscovite grains are situated in between the grains of pyrite, presumably related to insertion of sulfides in sediment. Picture originates from sample HE-P28(See Appendix A for location).

4.6.2. Structurally controlled mineralization (D2-D3)

The only prominent example of fold-related mineralization in the study area is presented in an open antiform-structure (F2) in the lowermost prospecting pits on Lassefjellet (see sub-section 2.5.2). This mineralization presents similar texture and mineral assemblage as the stratiform mineralization, suggesting it represents folded layers of stratiform mineralization, rather than a new type of mineralization. The minor tabular sulfide mineralizations observed in the S3-shear zones are also highly similar to the stratiform ones, both in terms of texture and mineral assemblage. The appearance as tabular bodies in the S3-shear zones suggests the fault-related sulfide mineralization is epigenic, and remobilized into the shear-zone during younger defomational events (D3). The ore-element distribution (Figure 3.10) in the fold- and fault- related sulfide mineralization display no anomalous levels, further supporting their stated relation to the stratiform type. Overall, all structurally controlled mineralizations are suggested to represent remobilized stratiform massive sulfide mineralization, most likely precipitated from Fe-saturated fluids fluctuating in the structures syn- or post-deformation. The origin and ore-potential for all encountered sulfide mineralization (both structurally controlled and stratiform) is therefore interpreted to be the same (see above). Motuza (2000) suggested the sulfide mineralization in faults and folds was related to gold mineralization, but no such associations have been detected during this study.

4.6.3. Vein-related mineralization

The most prominent precious element occurrence (Figure 3.11) is encountered in a small outcrop in the amphibolitic domain north of Lassefjellet (Figure 2.3). The outcrop features a 40-cm thick quartz vein striking parallel to the S1 foliation, with a 50 cm-thick bleached selvage zone on both sides. The arsenopyrite–gold mineralization here is situated in the bleached foliated amphibolite, and the quartz vein is completely barren (Figure 3.11). Petrographic examination of this mineralization reveals features not observed anywhere else in the study area (see sub-section 2.5.3): grains of arsenopyrite oriented parallel to the S1 foliation; tourmaline and carbonate scattered throughout the matrix; and small grains (1-5 microns) of native gold in the vicinity of the arsenopyrite (Figure 2.16e,f). These observations are corroborated by the geochemical data (see sub-section 3.3.3; Appendix B) high arsenic contents in all gold-anomalous samples; elevated tungsten values in all samples; and highly anomalous levels of gold in the range 0.17- 4.98 ppm.

There is evidence to indicate that the arsenopyrite–gold mineralization formed syn-D1: (1) the quartz veins display a foliation-parallel orientation and show signs of shearing (strong undulatory extinction as a result of dislocation glide: see sub-section 2.4.3) in the veins, suggesting they formed pre- or syn-D1; (2) the presence of arsenopyrite in the bleached selvage zone around the quartz veins suggests arsenopyrite crystallized coevally with the quartz veins; and (3) gold occurs in proximity to the arsenopyrite grains (Figure 2.16e,f), a spatial association that suggests a genetic relationship. Considering all these relations, the gold is suggested to be related to the first (D1) deformational event.

The occurrence of tourmaline and carbonate in the bleached amphibolite indicates a different style of alteration to that observed adjacent to the quartz-mica rich unit (see sub-section 2.2.1), and identifies the mineralization in the bleached selvage zones as a new type that is unrelated to the previously investigated sulfides. Since arsenopyrite is known to be accompanied by gold in various orogenic gold deposits in Fennoscandia (Sundblad, 2003), an orogenic origin for the gold seems most likely. Previous studies of the Ringvassøya Greenstone Belt have also proposed as similar origin, and further proven quartz veins to be related with gold occurrence in the southern domains (cf. Sandstand & Nilsson 1998).

4.7. Implications for further prospecting

In order to suggest a model for further prospecting in the central part of the Ringvassøya Greenstone Belt, the author proposes the use of alteration trends as a tool for exploration. This suggestion is based on the petrographic investigation and field observation of the encountered types of mineralization (massive sulfide and aresenopyrite-gold) in the study area, where all investigated mineralization is related to alteration. Further, if one is able to distinguish an alteration process that relates to precious element occurrences, prospecting can be narrowed down and made more efficient.

In order to distinguish the different alteration trends in the sampled material, Large et al. (2001) propose the alteration box plot (Figure 4.4). This plot utilizes AI (Alteration Index) versus CCPI (Chlorite-Carbonate-Pyrite Index), and the use of “least altered boxes”, with the latter as a tool to determine if the sampled material is extensively altered or relatively fresh. The least-altered boxes are based on Large et al.’s (2001) previous work with variously altered rocks.

The alteration index (AI) is calculated from the following equation:

$$\underline{100\ (K_2O + MgO)}$$

$$(K_2O + MgO + Na_2O + CaO)$$

The chlorite-carbonate-pyrite index (CCPI) is calculated from the following equation:

$$\underline{100\ (MgO + FeO)}$$

$$(MgO + FeO + Na_2O + K_2O)$$

The diagonal separates the alteration trends associated with hydrothermal alteration (top right) from the ones associated with digenetic alteration trends (bottom left), whereas the former is associated with ore-potential.

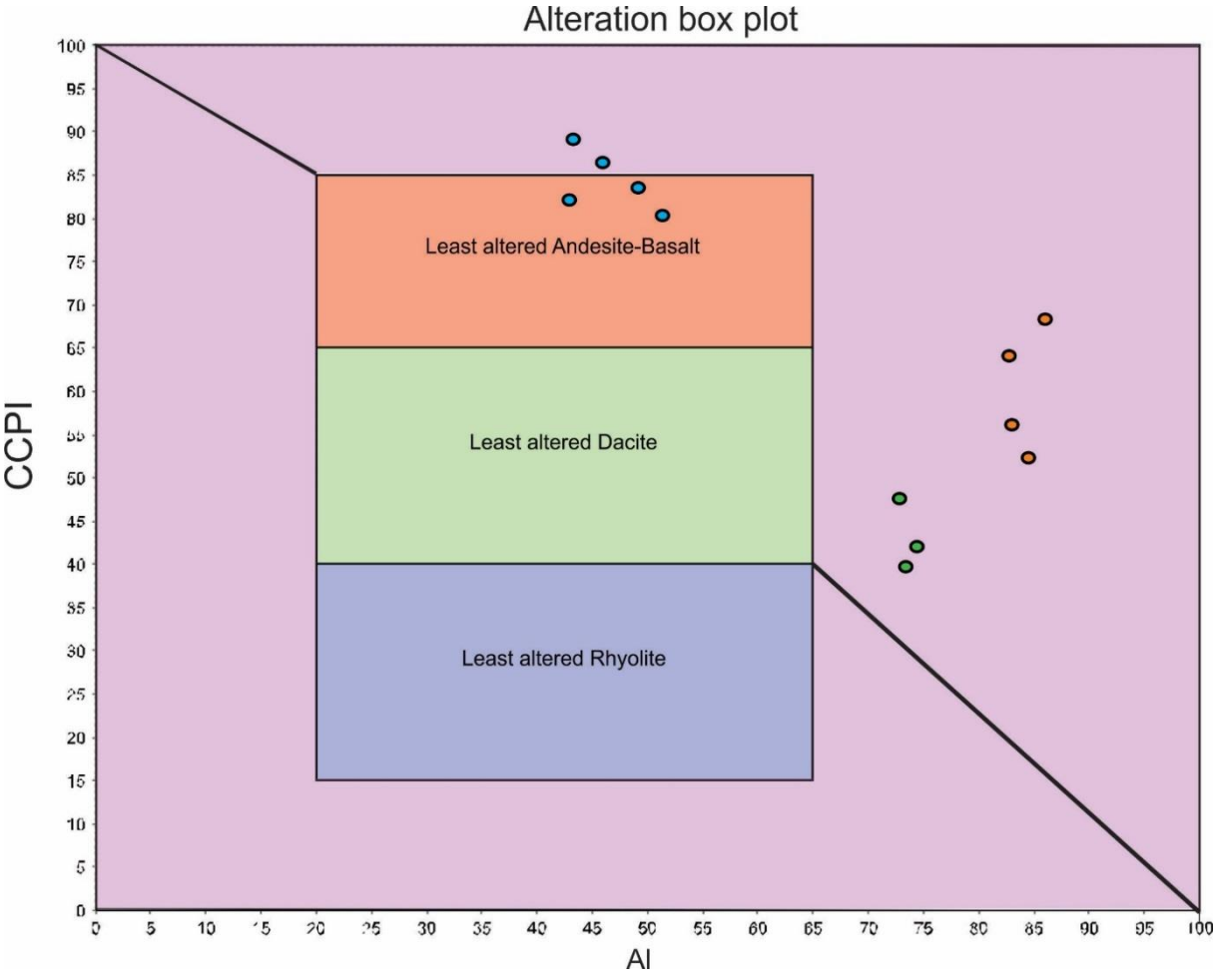

Figure 4.4: *Plot of AI versus CCPI presenting the alteration trends, including least altered boxes, and black diagonal line distinguishing the diagenetic (below) and hydrothermal (above) alteration trends. (Modified from Large et al., 2001.) The green dots represent the altered foliated amphibolite in the vicinity of the quartz-mica rich unit. The orange dots represent the quartz-mica rich unit. The blue dots with a black outline represent the bleached foliated gold-bearing amphibolite. Note how the bleached gold-bearing foliated amphibolite plot far away from the two other groups.*

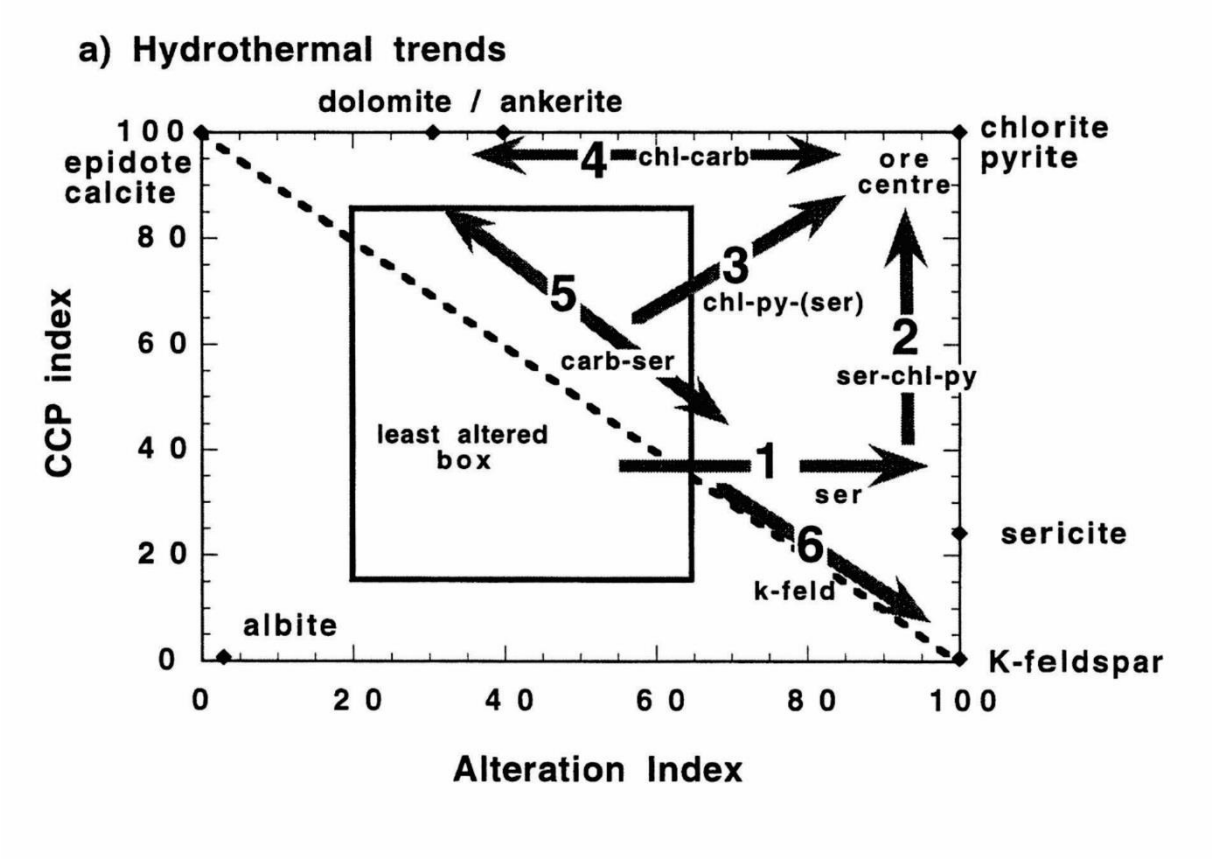

Figure 4.5: Diagram displaying the hydrothermal alteration trends in Figure 4.4. 1: Weak sericite alteration 2: Intense sericite-chlorite-pyrite alteration 3: Chlorite-sericite-pyrite alteration 4: Chlorite-carbonate alteration 5: Carbonate-sericite alteration 6: K-feldspar-sericite alteration. Figure from Large et al., 2001.

Examining the trends in Figure 4.4, a clear connection between the altered quartz-mica rich unit and the bordering bleached foliated amphiblote (see sub-section 2.2.1) presents itself, suggesting that similar types of alteration occurred in the two units. Figure 4.4 defines the alteration as weak sericite alteration in the bleached amphibolite and intense sericite-chlorite+-pyrite alteration in the quartz-mica rich unit, corresponding well with the petrographic observations (see sub-section 2.2.1; 2.2.3). The alteration trend in the bleached foliated gold-bearing amphibolite is defined as carbonate-sericite alteration, and this is also evident in the petrographic observations (see sub-section 2.5.3). The most important feature presented in Figure 4.4 is the clear differentiation in hydrothermal alteration trends of plotted samples, where no relation between the gold bearing rocks and the other plotted samples is displayed. This suggest that no relationship exists between the occurrence of gold and the hydrothermal alteration of the quartz-mica rich unit, thus eliminating any suggested link between the two (cf. Zwaan, 1989). Further, gold occurrences in this part of the Ringvassøya Greenstone Belt are suggested to be associated with carbonate-sericite alteration.

In summary, this study has proven several new valuable tools to make greenfield exploration in the central part of the Ringvassøya Greenstone Belt more efficient:

-Focus on foliation parallel quartz veins and wall rock, and thereby eliminating prospecting in the abundant iron-sulfides, in order to narrow down the number of potential targets.

-Apply the presented alteration box plot as a template to distinguish between alteration trends, and further determine a vector towards a gold occurrence by favoring the carbonate-sericite alteration.

-Recognize the presented mineral correlations of sub-section 4.6.3, and thereby utilize the occurrence of tungsten and arsenopyrite as pathfinder minerals for further gold exploration.

5. Conclusion

The studied quartz-mica rich unit in the central Ringvassøya Greenstone Belt appears interbedded, with a conformable lithological contact to the surrounding foliated amphibolite. All lithologies in the study area are highly influenced by three main deformational events (D1-D3), resulting in the formation of: (1) The main foliation S1 as a result of ENE-WSW-directed shortening, (2) upright to gently plunging F2-folds and low angle oblique thrusting S2-shear zones, as a response to crustal shortening and oblique shearing, and (3) steep to vertical S3-shear zones and related drag-folded (F3) main S1-foliation, caused by oblique shortening relative to D1 and D2 (cf. Bergh & Armitage, 1998).

Petrographical and geochemical data suggest the studied lithologies formed in a volcano-sedimentary environment, possibly in relation to the formation of a back-arc basin. The quartz-mica rich unit formed as felsic extrusive volcanic rock, related to the calc-alkaline magmatic series and possibly derived from partial melting of the continental crust. The foliated amphibolite formed as basalt of the tholeiitc magma series, possibly in association with a subducting oceanic plate. The mapped interbedding of the two different lithologies imply bi-modal (felsic-mafic) volcanism, both in time and space.

Two distinct types of mineralizations are encountered in the study area. One stratiform pyrite mineralization, forming disseminated to massive layers impregnated in sediments within the felsic volcanic quartz-mica rich unit. This mineralization has later been remobilized into F2-fold hinges and S3-shear zones during D2 and D3 deformational events. Another, newly discovered gold-arsenopyrite mineralization is related to the wall rock of S1-folation parallel quartz vein in the foliated amphibolite. No relationship is recorded between the two types, and only the latter is suggested to have ore-potential.

Finally, in order to narrow down the targets for greenfield prospecting for gold in the central part of Ringvassøya Greenstone Belt, the author would like to suggest a focus on S1-foliation parallel quartz-veins and wall rocks. By emphasizing the provided alteration-trend model as a prospecting tool, one should be able to distinguish alteration processes proven favorable for the occurrence of gold, and thus make prospecting more efficient.

References

Agnicoeagle.com: http://www.agnicoeagle.com/en/operations/northern-operations/kittila/pages/default.aspx (Accessed May 26st 2015)

ALSglobal.com: http://www.alsglobal.com/en/Our-Services/Minerals/Geochemistry/Downloads (Accessed May 26st 2015)

Armitage, P. E., & Bergh, S. G. (2005). Structural development of the Mjelde-Skorelvvatn Zone on Kvaløya, Troms: a metasupracrustal shear belt in the Precambrian West Troms Basement Complex, North Norway. *Norwegian Journal of Geology/Norsk Geologisk Forening*, *85*.

Bergh, S. G., & Torske, T. (1988). Palaeovolcanology and tectonic setting of a Proterozoic metatholeiitic sequence near the Baltic Shield margin, northern Norway. *Precambrian research*, *39*(4), 227-246.

Bergh, S. G., & Armitage, P. E. B. (1998). Structural reconnaissance field work on western Ringvassøy. *University of Tromsø Report, 32 pp*.

Bergh, S.G., Kullerud, K., Corfu, F., Armitage, P.E.B., Davidsen, B., Johansen, H.W., Pettersen, T. & Knudsen, S. (2007). Low-grade sedimentary rocks on Vanna, North Norway: a new occurrence of a Palaeoproterozoic (2.4-2.2 Ga) cover succession in northern Fennoscandia. *Norwegian Journal of Geology 87, 301-318.*

Bergh, S.G., Kullerud, K., Armitage, P.E.B., Zwaan, K.B., Corfu, F., Ravna, E.J.K. & Myhre, P.I. (2010). Neoarchaean to Svecofennian tectono-magmatic evolution of the West Troms Basement Complex, North Norway. *Norwegian Journal of Geology, 90*: 21-48.

Bergh, S.G., Corfu, F., Myhre, P.I., Kullerud, K., Armitage, P.E.B., Zwaan, C.B., Ravna, E.J.K., Holdsworth, R.H. & Chattopadhya, A. (2012). Was the Precambrian basement of western Troms and Lofoten-Vesterålen in northern Norway linked to the Lewisian of Scotland? A comparison of crustal components, tectonic evolution and amalgamation history. *Tectonics. In Tech*, Chapter 11, 283-330,

Bergh, S. G., Kullerud, K., Myhre, P. I., Corfu, F., Armitage, P. E. B., Zwaan, K. B., & Ravna, E. J. K. (2014). Archaean Elements of the Basement Outliers West of the Scandinavian Caledonides in Northern Norway: Architecture, Evolution and Possible Correlation with Fennoscandia. In *Evolution of Archean Crust and Early Life* (pp. 103-126). Springer Netherlands.

Berthelsen, A., & Marker, M. (1986). 1.9-1.8 Ga old strike-slip megashears in the Baltic Shield, and their plate tectonic implications. *Tectonophysics*, *128*(3), 163-181.

Bevins, R. E., Kokelaar, B. P., & Dunkley, P. N. (1984). Petrology and geochemistry of lower to middle Ordovician igneous rocks in Wales: a volcanic arc to marginal basin transition. *Proceedings of the Geologists' Association*,*95*(4), 337-347.

Bingen, B., Nordgulen, O., & Viola, G. (2008). A four-phase model for the Sveconorwegian orogeny, SW Scandinavia. *Norsk Geologisk Tidsskrift*, *88*(1), 43.

Binns, R. E., (1983): Rapport om berggrunnsgeologiske undersøkelser på Kvaløy og Ringvassøy, Troms, sommeren 1983. *Norsk Geologiske Undersøkelse Rapport 046/83.016D, 24 pp*

Blatt, H., Tracy, R. J., & Owens, B. (2006). *Petrology: igneous, sedimentary, and metamorphic*. Macmillan.

Bratrein, H. D. (1989). Karlsøy og Helgøy bygdebok: folkeliv, næringsliv, samfunnsliv. Karlsøy kommunale bibliotek.

Braathen, A., & Davidsen, B. (2000). Structure and stratigraphy of the Palaeoproterozoic Karasjok Greenstone Belt, north Norway-regional implications. *Norsk Geologisk Tidsskrift*, *80*(1), 33-50.

Cassidy, K. F., & Wyche, S. (2012). Thematic Issue: Archean Evolution—Yilgarn Craton. *Australian Journal of Earth Sciences*, *59*(5), 599-601.

Collinson, J. D. (2006). Sedimentary structures.

Corfu, F., & Noble, S. R. (1992). Genesis of the southern Abitibi greenstone belt, Superior Province, Canada: evidence from zircon Hf isotope analyses using a single filament technique. *Geochimica et Cosmochimica Acta*, *56*(5), 2081-2097.

Corfu, F., Armitage, P. E., Kullerud, K., & Bergh, S. G. (2003). Preliminary U-Pb geochronology in the West Troms Basement Complex, North Norway: Archaean and Palaeoproterozoic events and younger overprints. Geological Survey of Norway Bulletin, 441, 61-72.

Corfu, F. (2004). U-Pb age, setting, and tectonic significance of the anorthosite-mangerite-charnockite-granite-suite, Lofoten-Vesterålen, Norway. *Journal of Petrology, 45*, 1799-1819.

Corfu, F., Gasser, D., & Chew, D. M. (Eds.). (2014). New Perspectives on the Caledonides of Scandinavia and Related Areas. Geological Society of London.

Daly, J. S., Balagansky, V. V., Timmerman, M. J., & Whitehouse, M. J. (2006). The Lapland-Kola orogen: Palaeoproterozoic collision and accretion of the northern Fennoscandian lithosphere. *Geological Society, London, Memoirs*,*32*(1), 579-598.

De Wit, M. J., & Ashwal, L. D. (1997). *Greenstone belts*. Oxford University Press, USA.

Evans, A. M. (1987). Introduction to ore geology.

Fareth, E., & Lindahl, I. (1981). Oversikt over berggrunn og vurdering av mineraliseringer på Ringvassøya, Karlsøy og Tromsø, Troms. *Norges geologiske undersøkelse Report, 1750/14D*.

Floyd, P. A., & Winchester, J. A. (1977). Geochemical discrimination of different magma series and their differentiation products using immobile elements. *Chemical geology*, *20*, 325-343.

Galley, A. G., Hannington, M. D., & Jonasson, I. R. (2007). Volcanogenic massive sulphide deposits. *Mineral deposits of Canada: A synthesis of major deposit-types, district metallogeny, the evolution of geological provinces, and exploration methods: Geological Association of Canada, Mineral Deposits Division, Special Publication*, *5*, 141-161.

Gaál, G., & Gorbatschev, R. (1987). An outline of the Precambrian evolution of the Baltic Shield. *Precambrian Research*, *35*, 15-52.

Gaál, G., & Sundblad, K. (1990). Metallogeny of gold in the Fennoscandian Shield. *Mineralium Deposita*, *25*(1), S104-S114.

Glascock, M. D. (1988). Tables for neutron activation analysis.

Gorbatschev, R., & Bogdanova, S. (1993). Frontiers in the Baltic shield.*Precambrian Research*, *64*(1), 3-21.

GTK.fi: http://en.gtk.fi/ExplorationFinland/Moreinfo/suurikuusikko.html (Accessed May 26st 2015)

Hanski, E. J., Huhma, H., Lehtonen, M. I., & Rastas, P. (1997). Isotopic (Sm-Nd, U-Pb) and geochemical evidence for an oceanic crust to molasses evolution of the Paleoproterozoic Kittilä greenstone complex, northern Finland. COPENA conference at NGU, August 18–22, 1997. *Abstracts and Proceedings, NGU Report*, *97*, 131.

Hölttä, P., Balagansky, V., Garde, A., Mertanen, S., Peltonen, P., Slabunov, A., Sorjonen-Ward, P. & Whitehouse, M.(2008). Archaean of Greenland and Fennoscandia*. Episodes, 31,* 13-19.

Ihlen, P. M. and Furuhaug, L. (2000). Gold resources on Ringvassøy, Troms-III: Geochemistry of heavy-mineral consentrates from stream sediments and potential gold sources. *Norges Geologiske Undersøkelse report*, 2000(059).

Indrevær, K., Bergh, S. G., Koehl, J. B., Hansen, J. A., Schermer, E. R., & Ingebrigtsen, A. (2013). Post-Caledonian brittle fault zones on the hyperextended SW Barents Sea margin: New insights into onshore and offshore margin architecture. *Norwegian Journal of Geology/Norsk Geologisk Forening*, *93*.

Irvine, T., & Baragar, W. (1971). A guide to the chemical classification of the common volcanic rocks. *Canadian journal of earth sciences*, *8*(5), 523-548.

Karsten, J. L., Klein, E. M., & Sherman, S. B. (1996). Subduction zone geochemical characteristics in ocean ridge basalts from the southern Chile Ridge: Implications of modern ridge subduction systems for the Archean.*Lithos*, *37*(2), 143-161.

Kretz, R. (1983). Symbols for rock-forming minerals. *American mineralogist*,*68*(1-2), 277-279.

Kullerud K, Skjerlie KP, Corfu F, De La Rosa J. (2006). The 2.40 Ga Ringvassøy mafic dykes, West Troms Basement Complex, Norway: The concluding act of Early Paleozoic continental breakup. *Precambrian Research 150*, 183-200

Kuno, H. (1968). Differentiation of basalt magmas. *Basalts*, *2*(3), 623-688.

Laajoki, K. (2005). Karelian supracrustal rocks. *Developments in Precambrian Geology*, *14*, 279-341.

Lahtinen, R., Garde, A., Melezhik, V.A. (2008). Palaeoproterozoic evolution of Fennoscandia and Greenland*. Episodes, 31*, 20-28.

Lahtinen, R. (2012). Evolution of the Bedrock of Finland: An Overview. In *From the Earth's Core to Outer Space* (pp. 47-59). Springer Berlin Heidelberg.

Large, R. R., Gemmell, J. B., Paulick, H., & Huston, D. L. (2001). The alteration box plot: A simple approach to understanding the relationship between alteration mineralogy and lithogeochemistry associated with volcanic-hosted massive sulfide deposits. *Economic Geology*, *96*(5), 957-971.

Larson, S. Å., & Berglund, J. (1992). A chronological subdivision of the Transscandinavian Igneous Belt—three magmatic episodes?.

Lieungh, B. (1985). Gull-prospekteringen på Ringvassøy. En samlet oversikt over utførte arbeider og resultater. ASPRO Rapport nr 1620, 23p *Bergvesenets rapport nr. BV 678.*

Lme.com: https://www.lme.com/en-gb/pricing-and-data/pricing/official-price/ (Accessed May 21st 2015)

Mints, M. V., Berzin, R.G., Suleimanov, A.K., Zamozhnyaya, N.G., Stupak,V.M., Konilov, A. N., Zlobin, V.L. and Kaulina, T.V., (2004). The deep structureof the Early Precambrian crust of the Karelian Craton, SoutheasternFennoscandian Shield: Results of the investigation along CMP profile 4B: *Geotectonics,* v. 38, pp. 10–29.

Minsaas, O. (1980). Detaljkartlegging i Hessfjordområdet, Ringvassøy. NGU rapport 1800/14E, 14pp.

Motuza, G. (2000) .Descriptions to the geological map of the central parts of the Ringvassøya greenstone belt, Troms county, northern Norway. pp26 + amendments.

Myhre, P.I., Corfu, F., Bergh, S. (2011): Palaeoproterozoic (2.0–1.95 Ga) pre-orogenic supracrustal sequences in the West Troms Basement Complex, North Norway. *Precambrian Research, 186,* 89-100.

Myhre, P.I., Corfu, F., Bergh S.G. & Kullerud, K. (2013). U-Pb geochronology along an Archaean geotransect in the West Troms Basement Complex, North Norway. Norwegian Journal of Geology, 93, 1–24.

Ngu.no: http://www.ngu.no/prosjekter/minn (Accessed May 21st 2015)

Ohmoto, H. (1996). Formation of volcanogenic massive sulfide deposits: the Kuroko perspective. *Ore geology reviews*, *10*(3), 135-177.

Ojala, V. J. (Ed.). (2007). *Metallogeny and tectonic evolution of the Northern Fennoscandian Shield: field trip guidebook* (Vol. 54). *Geological survey of Finland.*

Olesen, O., & Sandstad, J. S. (1993). Interpretation of the Proterozoic Kautokeino Greenstone Belt, Finnmark, Norway from combined geophysical and geological data. *Nor. Geol. Unders. Bull*, *425*, 41-62.

Olesen, O., Torsvik, T. H., Tveten, E., Zwaan, K. B., Loseth, H., & Henningsen, T., (1997). Basement structure of the continental margin in the Lofoten Lopphavet area, northern Norway: Constraints from potential field data, on-land structural mapping and palaeomagnetic data. *Norsk geologisk tidsskrift*, *77*(1), 15-30.

Passchier, C. W., & Trouw, R. A. (2005). Microtectonics, 2nd edition.

Patison, N. L. (2007). Structural controls on gold mineralisation in the Central Lapland Greenstone Belt. *Geol. Surv. Finland, Special Paper*, *44*, 107-124.

Pearce, J. A., & Cann, J. R. (1973). Tectonic setting of basic volcanic rocks determined using trace element analyses. *Earth and planetary science letters*,*19*(2), 290-300.

Pearce, J. A. (1983). Role of the subcontinental lithosphere in magma genesis at active continental margins.

Pearce, J. A., & Stern, R. J. (2006). Origin of back-arc basin magmas: Trace element and isotope perspectives. *Back-Arc Spreading Systems: Geological, Biological, Chemical, and Physical Interactions*, 63-86.

Poutiainen, M., & Partamies, S. (2003). Fluid inclusion characteristics of auriferous quartz veins in Archean and Paleoproterozoic greenstone belts of eastern and southern Finland. *Economic Geology*, *98*(7), 1355-1369.

Ramberg, I. B. (Ed.). (2008). The making of a land: geology of Norway. Geological Society of London.

Ramsay, D. M., Sturt, B. A., Zwaan, K. B., & Roberts, D. (1985). Caledonides of northern Norway. *The Caledonian Orogen: Scandinavia and related areas. Edited by DG Gee and BA Sturt. Wiley, Chichester, UK*, 163-184.

Regjeringens mineralstrategi: https://www.regjeringen.no/nb/aktuelt/offensiv-mineralstrategi/id717090/ (Accessed May 21st 2015)

Rindstad, B.I. (1977). En malmgeologisk undersøkelse av forekomstene i Nonsdal-Skognes området på Ringvassøy. Unpublished diplomoppgave, NTH, Trondheim, 59p.

Robb, L. J. (2005). Introduction to ore-forming processes.

Roberts, D. (2003). The Scandinavian Caledonides: event chronology, palaeogeographic settings and likely modern analogues. *Tectonophysics*,*365*(1), 283-299.

Sandstad, J. S., & Nilsson, L. P. (1998). Gullundersøkelser på Ringvassøya; sammenstilling av tidligere prospektering og feltbefaring i 1997. *Norges geologiske undersøkelse Report*, *98*(07).

Schermerhorn, L. J. G. (1973). What is keratophyre?. *Lithos*, *6*(1), 1-11.

Svinndal, S. (1974). Oversiktsrapport over Ringvassøy kisforekomster. USB-arkiv, 42p.

Sundblad, K. (2003). Metallogeny of gold in the Precambrian of northern Europe. *Economic geology*, *98*(7), 1271-1290.

Taylor, S. R., & McLennan, S. M. (1985). The continental crust: its composition and evolution.

Torske, T., & Bergh, S. G. (2004). The Caravarri Formation of the Alta-Kautokeino greenstone belt, Finnmark, North Norway; a Palaeoproterozoic foreland basin sequence. *Norges geologiske undersøkelse Bulletin*, *442*, 5-22.

Vuollo, J., & Huhma, H. (2005). Paleoproterozoic mafic dikes in NE Finland.*Developments in Precambrian Geology*, *14*, 195-236.

Wood, D. A. (1980). The application of a Th Hf Ta diagram to problems of tectonomagmatic classification and to establishing the nature of crustal contamination of basaltic lavas of the British Tertiary Volcanic Province. *Earth and planetary science letters*, *50*(1), 11-30.

Xie, Q., Kerrich, R., & Fan, J. (1993). HFSE/REE fractionations recorded in three komatiite-basalt sequences, Archean Abitibi greenstone belt: Implications for multiple plume sources and depths. *Geochimica et Cosmochimica Acta*,*57*(16), 4111-4118.

Zwaan, K. B. (1989). Berggrunnsgeologisk kartlegging av det prekambriske grønnsteinsbelte på Ringvassøy, Troms. Norges Geologiske Undersøkelse Report 89.101.

Zwaan, K. B. (1995). Geology of the Precambrian West Troms Basement Complex, northern Norway, with special emphasis on the Senja Shear Belt: a preliminary account. *Norges Geologiske Undersøkelse Bulletin 427, 33-36.*

Zwaan, K. B., & Tucker, R. D. (1996). Absolute and relative age relationships in the Precambrian West Troms Basement Complex, northern Norway. In *22nd Nordic Geological Winter Meeting, Åbo, Finland* (p. 237).

Zwaan, K. B., Fareth, E. & Grogan, P. W. (1998). Geologisk kart over Norge, berggrunnskart TROMSØ, M 1:250.000. *Norges geologiske undersøkelse*.

Åhäll, K. I., & Connelly, J. N. (2008). Long-term convergence along SW Fennoscandia: 330m. y. of Proterozoic crustal growth [Precam Res 161 (2008) 452–472]. *Precambrian Research*, *163*(3), 402-421.

Appendix A

Samples

SampleID	Description	Lithology
HE-P1	n/a	Outside study area
HE-P2	n/a	Outside study area
HE-P3	S3 tabular mineralization	Mineralization
HE-P4	Mineralization in F2-fold	Mineralization
HE-P5	S1 stratiform mineralization	Mineralization
HE-P6	Weathered quartz-mica rich unit	Quartz-mica rich unit
HE-P7	S1-truncating quartz vein	Quartz-mica rich unit
HE-P8	S1-truncating quartz vein	Quartz-mica rich unit
HE-P9	Weathered quartz-mica rich unit	Quartz-mica rich unit
HE-P10	Mafic intrusion in S2-shear zone	Dyke
HE-P11	Mafic intrusion in S2-shear zone	Dyke
HE-P12	Boudinaged S1-parallel mineralization	Mineralization
HE-P13	Phyllonite rim on mafic dyke (S2)	Dyke
HE-P14	Bleached foliated amphibolite	Foliated amphibolite
HE-P15	Quartz-mica rich unit close to P14.	Quartz-mica rich unit
HE-P16	Altered foliated amphibolite	Foliated amphibolite
HE-P17	Weathered quartz-mica rich unit	Quartz-mica rich unit
HE-P18	Meta-sedimentary appearance	Quartz-mica rich unit
HE-P19	Weathered quartz-mica rich unit	Quartz-mica rich unit
HE-P20	S3 tabular mineralization	Mineralization
HE-P21	S3 tabular mineralization	Mineralization
HE-P22	Mafic intrusion in S3-shear zone	Dyke
HE-P23	Weathered quartz-mica rich unit	Quartz-mica rich unit
HE-P24	Weathered quartz-mica rich unit	Quartz-mica rich unit
HE-P25	Weathered quartz-mica rich unit	Quartz-mica rich unit
HE-P26	S1-foliation parallel quartz	Quartz vein
HE-P27	Massive S1-parallel mineralization	Mineralization
HE-P28	Disseminated S1-parallel mineralization	Mineralization
HE-P29	Weathered quartz-mica rich unit	Quartz-mica rich unit
HE-P30	Foliated amphibolite	Foliated amphibolite
HE-P31	Bleached foliated amphibolite	Foliated amphibolite
HE-P32	Un-weathered quartz-mica rich unit	Quartz-mica rich unit
HE-P33	Bleached foliated amphibolite	Foliated amphibolite
HE-P34	Foliated amphibolite	Foliated amphibolite
HE-P35	Foliated amphibolite	Foliated amphibolite
HE-P36	Bleached foliated amphibolite	Foliated amphibolite
HE-P37	Bleached foliated amphibolite	Foliated amphibolite
HE-P38	S1-foliation parallel quartz vein	Quartz vein
HE-P39	S1-foliation parallel quartz vein	Quartz vein
HE-P40	S1-foliation parallel quartz vein	Quartz vein
HE-P41	Bleached foliated amphibolite	Foliated amphibolite
HE-P42	Bleached foliated amphibolite	Foliated amphibolite

HE-P43	Mafic intrusion	Dyke
HE-P44	Meta-sedimentary appearance	Quartz-mica rich unit
HE-P45	Weathered quartz-mica rich unit	Quartz-mica rich unit

Location of samples gathered in the study area.

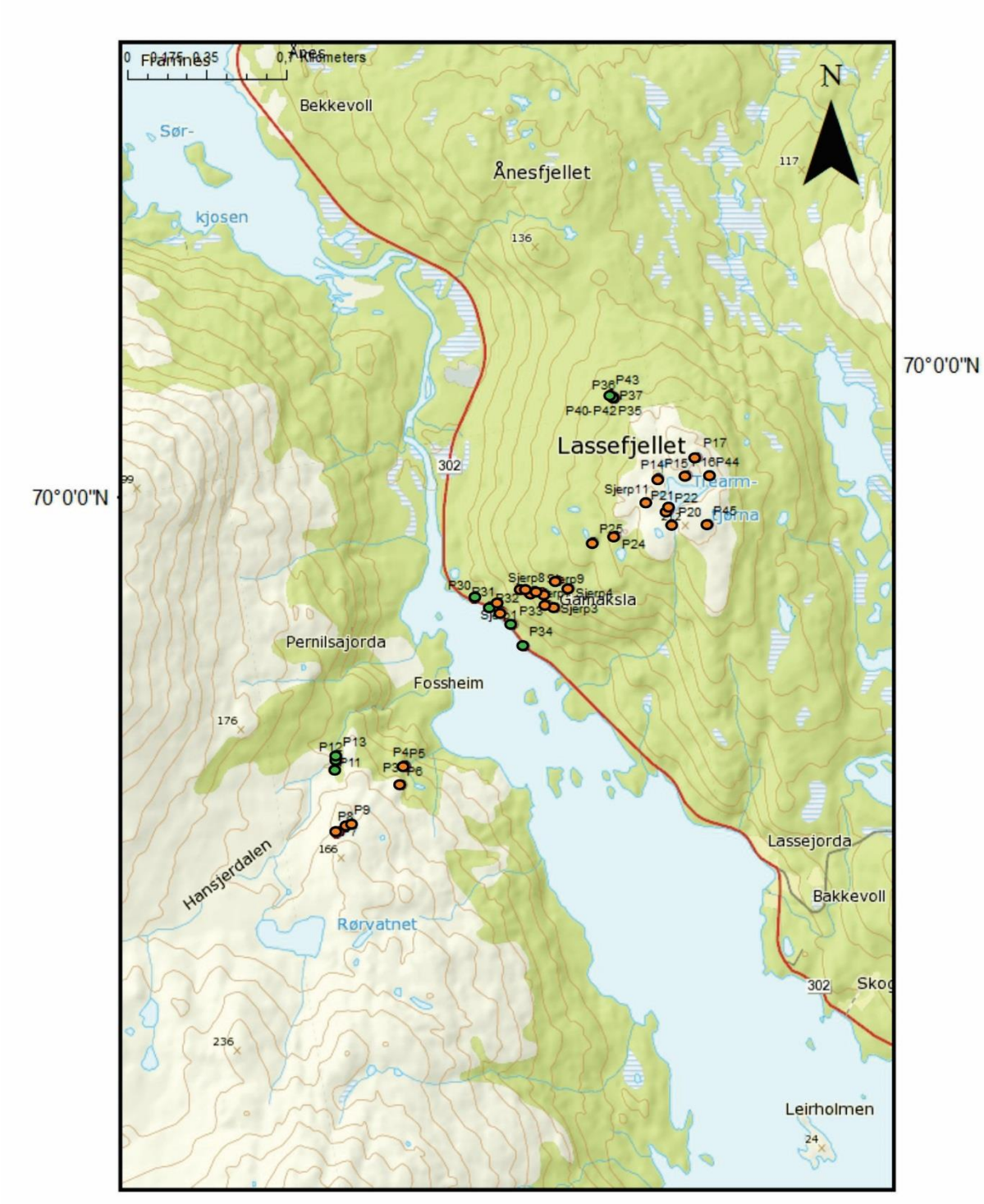

Color indicates the general lithology surrounding the sampled material. Orange: Quartz-mica rich unit Green: Foliated amphibolite

Appendix B

Whole-Rock Analysis

Sample ID	Au	Ag	Al	As	Ba	Be	Bi	Ca	Cd	Ce	Co	Cr	Cs
	ppm	ppm	%	ppm	ppm	ppm	ppm	%	ppm	ppm	ppm	ppm	ppm
HE-P1	<0.001	0,01	6,3	1,1	70	1,8	0,01	0,83	0,02	3,54	0,4	7	0,11
HE-P2	0,026	0,54	5,68	1,6	130	0,83	2,08	3,94	0,15	52,8	72,6	17	0,35
HE-P3	0,02	0,68	4,1	59,4	290	0,53	1,01	0,34	<0.02	3,61	0,6	64	1,06
HE-P4	0,005	0,28	7,15	23,1	480	1,14	0,54	1,19	0,03	6,21	1,5	97	1,37
HE-P5	0,008	0,3	3,92	244	140	0,55	0,49	0,88	0,04	9,97	38,4	30	0,56
HE-P6	0,002	0,15	2,46	11	100	0,28	0,38	0,17	0,02	5,11	1	21	0,32
HE-P7	<0.001	0,01	2,01	3,2	70	0,39	0,03	0,09	0,02	0,94	0,2	26	0,32
HE-P8	<0.001	0,02	0,06	3,4	<10	<0.05	0,02	0,01	<0.02	0,07	0,2	21	<0.05
HE-P9	<0.001	0,11	7,09	2,1	200	1,55	0,07	1,96	0,02	14,9	0,2	6	0,67
HE-P10	<0.001	0,13	8,26	1,9	510	1,36	0,11	1,35	0,02	12,55	0,3	29	1,55
HE-P11	0,045	0,37	3,35	22,9	400	3,23	0,1	7,81	0,46	124	73,6	478	4,44
HE-P12	0,023	0,63	4,45	2,5	20	0,29	0,63	3,7	0,25	16,35	69,4	42	0,08
HE-P13	0,001	0,02	5,32	<0.2	90	0,52	0,04	8,03	0,2	102,5	46,8	562	2,14
HE-P14	0,006	0,13	0,19	16,6	<10	0,21	0,13	0,18	0,1	2,66	4,3	24	<0.05
HE-P15	<0.001	0,01	7,76	4,4	620	1,32	0,02	0,73	0,02	72,1	0,8	5	0,54
HE-P16	0,018	0,03	7,78	189	620	1,16	0,26	0,62	0,03	48	0,4	5	0,51
HE-P17	0,001	0,1	8,46	1,3	750	1,05	0,27	0,71	<0.02	14,6	0,2	15	1,52
HE-P18	0,006	0,21	0,19	122	<10	0,06	0,06	0,06	0,03	2,62	0,4	8	<0.05
HE-P19	0,018	0,28	4,55	44	920	1,5	0,39	1,12	0,36	12,1	1,4	41	1,11
HE-P20	0,003	0,19	6,21	1,7	30	1,52	0,13	4,73	0,14	35,1	18	117	0,1
HE-P21	0,05	0,08	6,29	162	<10	0,07	0,23	0,67	<0.02	132,5	31,3	569	0,25
HE-P22	0,014	0,06	7,51	5,2	10	0,88	0,07	6,5	0,19	42,8	44,6	170	<0.05
HE-P23	0,008	0,24	5,15	53	460	0,32	0,22	0,34	<0.02	5,27	0,3	53	0,98
HE-P24	0,001	0,06	7,04	34,7	270	0,93	0,13	1,61	<0.02	7,35	0,3	7	0,52
HE-P25	0,013	0,24	6,25	39,1	490	0,53	0,22	0,98	<0.02	13,05	1,3	36	1,16
HE-P26	<0.001	0,05	0,2	2,2	10	<0.05	0,02	0,06	0,02	4,93	0,2	49	0,08
HE-P27	0,016	0,32	2,4	109	90	0,33	0,76	0,54	0,3	11,6	198,5	36	0,34
HE-P28	0,018	0,22	0,55	105,5	10	0,11	0,29	0,14	<0.02	1,35	65,8	34	<0.05

Sample ID	Au	Ag	Al	As	Ba	Be	Bi	Ca	Cd	Ce	Co	Cr	Cs
	ppm	ppm	%	ppm	ppm	ppm	ppm	%	ppm	ppm	ppm	ppm	ppm
HE-P30	0,019	0,05	6,67	3,6	1200	0,35	0,05	3,59	0,25	25,3	19,1	59	6,15
HE-P31	<0.001	0,02	7,49	10,3	650	1,43	0,04	0,61	0,05	60,4	1,1	5	0,85
HE-P32	0,002	0,06	8,4	1035	920	1,18	0,09	0,77	0,03	52,9	31,5	80	1
HE-P33	0,002	0,08	8,6	22,1	50	0,42	0,04	2,81	0,08	18,25	65,8	144	0,57
HE-P34	0,001	0,05	6,93	2,2	50	0,55	0,06	6,39	0,12	17,9	45,5	74	<0.05
HE-P35	0,038	0,04	4,98	1305	280	1,14	0,08	1,83	0,1	13,95	19,1	111	0,42
HE-P36	4,98	0,37	10,25	>10000	1190	3,21	0,31	3,75	0,17	27,6	84,8	227	1,01
HE-P37	1,61	0,09	8,97	69,9	880	1,61	0,1	2,83	0,11	14,65	8,1	188	0,86
HE-P38	0,004	0,01	0,26	79,7	10	0,07	0,04	0,1	0,04	5,38	1,8	14	<0.05
HE-P39	0,001	0,01	0,12	24,2	10	0,05	0,02	0,04	0,04	2,36	1,1	23	<0.05
HE-P40	0,001	0,03	0,12	11,5	10	<0.05	0,02	0,06	0,04	2,98	0,8	20	<0.05
HE-P41	0,173	0,04	8,73	3220	830	2,51	0,14	2,98	0,07	25,9	56,4	162	0,71
HE-P42	0,339	0,09	8,61	1215	550	1,87	0,18	3,09	0,14	17,2	38,8	177	0,67
HE-P43	0,016	0,17	6,13	5	40	0,57	0,04	4,79	0,19	18,15	46,6	74	0,05
HE-P44	0,073	0,34	7,69	7,9	570	0,89	0,37	1	0,03	10,35	0,4	72	1,22
HE-P45	0,017	0,37	0,5	44	10	0,05	0,27	0,09	0,05	2,38	1,8	15	<0.05

Sample ID	Cu	Fe	Ga	Ge	Hf	In	K	La	Li	Mg	Mn	Mo	Na
	ppm	%	ppm	ppm	ppm	ppm	%	ppm	ppm	%	ppm	ppm	%
HE-P1	5,1	0,36	19	0,24	3,1	0,014	0,2	1,3	1,1	0,03	70	0,59	4,6
HE-P2	542	7,89	16,4	0,28	1,1	0,114	0,16	19,2	4,2	0,56	863	2,89	1,92
HE-P3	111	11,8	13,9	0,16	1,4	0,106	1,34	1,6	7,4	0,44	147	3,72	0,6
HE-P4	35,5	1,94	22,4	0,17	2,6	0,086	2	2,8	12,2	0,74	168	4,24	1,69
HE-P5	10,1	20,8	9,17	0,19	1,4	0,029	0,68	4,3	5,8	0,42	118	2,3	1,11
HE-P6	49,6	4,71	9,41	0,11	0,8	0,043	0,4	2,6	10,9	1,4	273	1,44	0,58
HE-P7	5	0,48	4,97	0,11	<0.1	0,012	0,52	0,6	3,1	0,04	32	2,07	0,33
HE-P8	9,6	0,51	0,28	0,11	<0.1	<0.005	0,02	<0.5	0,5	<0.01	26	1,58	0,02
HE-P9	14,2	1,18	17,85	0,2	2,2	0,029	0,74	6,7	8	0,21	153	1,38	2,93
HE-P10	27,6	0,86	27,2	0,2	3,2	0,032	2,19	5,7	16,8	0,73	221	1,68	1,75
HE-P11	238	11,6	14,85	0,32	3,7	0,114	0,83	58,6	18,3	7,27	1840	1,01	0,49
HE-P12	1330	27,7	11	1,55	1,8	0,062	0,05	7	5,8	2,46	13300	0,9	0,17
HE-P13	4,6	7,53	13,9	0,37	0,6	0,064	0,26	41,5	36,1	5,89	1600	0,49	0,01
HE-P14	33,9	12,25	0,65	0,11	<0.1	0,026	0,01	1,1	2,3	1,44	3530	0,6	0,02
HE-P15	5,8	1,01	20	0,19	2,2	0,031	2,08	27,3	12	0,21	288	0,44	2,78
HE-P16	9,9	0,96	20,9	0,18	2,2	0,03	1,83	22	8,5	0,22	247	0,75	3,08
HE-P17	14,9	2,88	25,1	0,19	1,3	0,059	3,11	7,1	18,5	0,68	154	0,4	1,18
HE-P18	27,9	4,43	0,8	0,11	0,1	0,012	0,01	1,1	0,6	0,2	253	1	0,01
HE-P19	77,9	8,54	14,95	0,15	1,2	0,152	0,79	5,5	12,2	0,85	2770	1,83	0,29
HE-P20	252	15,35	18,05	0,95	0,8	0,158	0,23	14,1	16,2	3,03	2040	0,48	0,75
HE-P21	60,3	9,61	24,1	0,71	0,7	0,11	0,03	58,6	34,5	5,84	1080	2,49	0,02
HE-P22	110,5	10,7	19,6	0,39	0,6	0,085	0,18	16,6	21,3	3,82	1880	0,37	1,53
HE-P23	7,4	3,67	18,75	0,13	3,5	0,033	2,02	2,5	9,6	0,28	265	2,33	0,41
HE-P24	14,2	1,1	18	0,15	2,8	0,035	0,86	3,4	7,3	0,6	81	1,12	2,42
HE-P25	10,8	2,76	18,2	0,17	2,7	0,082	2,2	6	12,8	0,9	188	1,81	0,4
HE-P26	6,2	1,12	0,71	0,12	0,1	<0.005	0,05	2,8	0,7	0,05	85	1,48	0,02
HE-P27	88,1	34,1	6,61	0,14	0,8	0,03	0,36	5	5,5	0,27	199	1,49	0,61

Sample ID	Cu	Fe	Ga	Ge	Hf	In	K	La	Li	Mg	Mn	Mo	Na
	ppm	%	ppm	ppm	ppm	ppm	%	ppm	ppm	%	ppm	ppm	%
HE-P29	26,8	13,3	19,4	0,15	3,7	0,042	1,87	2,8	10,7	0,57	141	2,32	0,3
HE-P30	92,5	16,65	18,55	1,04	0,5	0,073	0,91	9,7	16,8	2,05	8540	0,9	0,42
HE-P31	11,3	1,14	18,55	0,16	2,4	0,018	1,64	27,3	8,2	0,2	528	0,51	3,55
HE-P32	50	3,15	28,5	0,2	3,1	0,085	2,76	24,6	15,1	1,13	240	1,53	1,13
HE-P33	157,5	10,9	22,7	0,33	0,2	0,078	0,15	6,3	17,4	3,88	1230	0,46	2,5
HE-P34	124	10,9	22	0,3	1	0,096	0,17	6,4	14,4	2,72	1700	0,93	1,92
HE-P35	52,6	3,59	14,5	0,16	0,9	0,048	0,61	5,3	8,1	0,74	822	1,3	0,96
HE-P36	83,6	7,35	35,7	0,31	1,7	0,142	1,99	9,9	19,9	1,62	1760	1,68	1,51
HE-P37	62	5,43	28,4	0,17	0,4	0,113	1,81	5,1	16	1,22	1350	0,71	1,57
HE-P38	6,9	0,46	0,64	0,1	<0.1	0,006	0,02	2,2	1,3	0,07	175	1,3	0,07
HE-P39	10,2	0,41	0,33	0,07	<0.1	0,006	0,01	1	0,7	0,03	111	1,99	0,04
HE-P40	4,6	0,35	0,34	0,08	<0.1	<0.005	0,02	1,2	0,8	0,03	81	2,1	0,03
HE-P41	82,5	4,86	25,6	0,2	0,7	0,109	1,42	8,7	12,3	0,86	985	1,45	1,9
HE-P42	114	5,8	25,9	0,21	0,2	0,093	1,25	5,9	16,5	1,33	1330	0,66	1,94
HE-P43	156,5	9,61	20,6	0,2	0,4	0,114	0,13	6,7	14	2,79	2080	0,42	1,33
HE-P44	3	0,59	26,1	0,12	3,5	0,116	2,63	4,5	12,2	0,62	111	2,66	1,48
HE-P45	66,8	14	2,38	0,07	0,2	0,029	0,02	1	0,9	0,26	910	0,44	0,01

Sample ID	Nb	Ni	P	Pb	Rb	Re	S	Sb	Sc	Se	Sn	Sr	Ta
	ppm	ppm	ppm	ppm	ppm	ppm	%	ppm	ppm	ppm	ppm	ppm	ppm
HE-P1	4,2	0,3	10	8,9	4,7	<0.002	0,01	0,15	1,8	<1	0,2	89,9	0,61
HE-P2	7,3	30,8	2400	5,9	6,6	0,01	2,68	0,75	16,9	8	1	123,5	0,73
HE-P3	3,2	0,2	330	6,1	56,8	<0.002	0,34	4,73	9,8	6	2,1	68,2	0,24
HE-P4	5,3	1,2	190	10,4	81	0,005	0,2	1,63	20,3	5	2,5	227	0,42
HE-P5	2,2	28,2	10	12,1	29,2	0,005	>10.0	1,68	4,2	7	1,2	145	0,18
HE-P6	1,4	1,9	570	5,6	18,5	<0.002	0,13	0,17	3,4	4	0,5	31	0,14
HE-P7	0,3	0,4	10	3	20,9	0,002	0,01	0,14	0,9	<1	0,3	50	<0.05
HE-P8	0,1	0,3	10	1,2	0,7	<0.002	0,01	0,15	0,1	<1	<0.2	0,9	<0.05
HE-P9	3,3	2,3	300	18,6	21,4	<0.002	0,03	0,27	1,4	<1	0,5	259	0,27
HE-P10	4,4	0,7	40	8,8	71	<0.002	0,02	0,32	7,3	1	1,5	202	0,39
HE-P11	45,4	321	1770	3,9	46,3	<0.002	0,03	0,5	40,1	1	2,4	170	2,78
HE-P12	3,5	44,8	310	1,5	0,4	<0.002	5,3	0,45	7,9	4	0,8	4,6	0,28
HE-P13	2,8	357	1770	6,1	16,4	<0.002	0,03	1,73	23,8	<1	1	212	0,17
HE-P14	0,2	7,3	300	4,5	0,3	<0.002	0,08	0,21	5,2	1	0,2	1,6	<0.05
HE-P15	5,8	1,2	320	5,2	66	<0.002	0,03	0,17	1,7	<1	0,7	105	0,46
HE-P16	6	0,3	310	5	48,5	<0.002	0,01	0,27	1,5	<1	1	150,5	0,48
HE-P17	2,8	0,2	410	5,3	94,5	<0.002	0,06	0,81	7,2	1	1,4	149	0,23
HE-P18	0,2	4,4	160	4,9	0,3	<0.002	0,06	0,43	0,4	1	<0.2	1	<0.05
HE-P19	3,4	1,1	330	2,8	27,4	0,002	0,09	1,07	8,4	2	1,7	35	0,28
HE-P20	16,2	30,2	810	2	1,4	<0.002	0,53	1,68	35,5	3	1,8	17	1,06
HE-P21	10,8	104	1140	1,9	0,8	<0.002	0,52	0,51	22,9	1	0,5	51,4	0,43
HE-P22	17,3	100,5	940	3,9	1,3	<0.002	0,06	0,87	41,9	1	1,5	202	1,11
HE-P23	1,2	0,4	40	10,8	57,7	<0.002	0,19	2,75	14,9	3	2,2	63,9	0,1
HE-P24	2,3	<0.2	100	4,7	23,4	<0.002	0,02	0,41	2,4	1	0,6	304	0,22
HE-P25	3,7	0,2	60	17,2	83,4	0,002	0,35	2,15	9,3	2	1,7	90,9	0,36
HE-P26	0,2	0,2	40	3,7	1,7	<0.002	0,08	0,4	0,6	1	<0.2	4,2	<0.05
HE-P27	0,3	55,1	130	9,4	11,6	0,005	>10.0	2,55	3,4	3	0,4	72,2	<0.05
HE-P28	0,2	24	<10	4,8	1,6	0,002	>10.0	2,61	0,7	3	0,4	18,4	<0.05

Sample ID	Nb	Ni	P	Pb	Rb	Re	S	Sb	Sc	Se	Sn	Sr	Ta
	ppm	ppm	ppm	ppm	ppm	ppm	%	ppm	ppm	ppm	ppm	ppm	ppm
HE-P31	5,7	0,5	280	4,6	57,1	<0.002	0,07	0,27	1,6	1	0,6	203	0,46
HE-P32	2,1	72,5	490	4,3	83,2	<0.002	0,96	0,51	16,9	1	1,6	142	0,15
HE-P33	5,2	125	750	2,9	3,4	0,002	0,23	0,47	36,5	3	0,4	168,5	0,35
HE-P34	4,4	43,6	590	1,8	1,9	0,003	0,22	0,74	47,2	2	0,8	105	0,3
HE-P35	4,8	16,2	310	4,3	16,4	0,002	0,1	0,3	28,5	1	0,7	104	0,22
HE-P36	16,6	44	340	11	40,5	0,005	0,55	1,65	51	3	2,4	217	0,5
HE-P37	5,7	14,8	160	5,1	45,2	0,005	0,05	0,26	45,2	1	1,7	153,5	0,38
HE-P38	1	2,7	90	1,5	0,6	0,002	0,02	0,14	1,1	<1	<0.2	3,1	<0.05
HE-P39	0,8	2,6	20	2,4	0,4	<0.002	0,01	0,14	0,9	<1	<0.2	1,6	<0.05
HE-P40	0,8	2,2	20	5,3	0,4	0,002	0,01	0,15	0,6	<1	<0.2	1,8	<0.05
HE-P41	15	29,4	420	7,4	37,1	0,002	0,18	0,58	45,5	2	1,7	176	0,33
HE-P42	5,8	47,6	360	5,4	28,5	0,005	0,21	0,33	48,1	2	1,2	180	0,36
HE-P43	4,8	37,6	660	2,6	2	0,002	0,06	1,91	46,4	2	0,9	57,8	0,33
HE-P44	5,4	0,9	140	12,6	89,8	0,002	0,02	4,93	15,5	2	3,7	159	0,52
HE-P45	0,5	6,6	270	3,2	0,7	0,002	0,29	6,97	0,9	1	0,2	2	<0.05

Sample ID	Te	Th	Ti	Tl	U	V	W	Y	Zn	Zr
	ppm	ppm	%	ppm	ppm	ppm	ppm	ppm	ppm	ppm
HE-P1	<0.05	5,3	0,016	0,03	2,7	4	0,2	6,1	8	46,2
HE-P2	0,56	2,3	0,636	0,15	0,4	45	0,6	78,7	57	22,5
HE-P3	1,25	1,9	0,207	1,17	0,3	68	0,8	1	32	49,2
HE-P4	0,52	3,1	0,34	1,76	1	118	1,2	5,1	28	92,5
HE-P5	0,22	0,5	0,114	0,69	0,3	25	0,5	3,1	25	46,1
HE-P6	0,38	1,5	0,074	0,33	0,3	33	0,7	1,1	46	26,3
HE-P7	<0.05	0,2	0,01	0,21	<0.1	12	0,2	0,1	4	1,1
HE-P8	<0.05	<0.2	<0.005	<0.02	<0.1	1	0,1	<0.1	6	<0.5
HE-P9	0,09	4,8	0,06	0,44	1,1	5	0,5	3,1	39	60,6
HE-P10	0,11	3,5	0,215	1,19	0,9	50	1,6	3,3	21	106
HE-P11	0,15	8,2	1,84	0,46	1,5	311	1,8	26,1	200	127
HE-P12	1,2	2,7	0,124	0,02	0,6	25	0,3	22,9	160	64,6
HE-P13	<0.05	4,9	0,3	0,33	1,1	152	1,2	16,9	211	24,7
HE-P14	0,13	<0.2	0,007	<0.02	<0.1	11	0,4	6,2	139	1,6
HE-P15	<0.05	6,4	0,08	0,34	1,5	3	1,5	8,7	14	63,1
HE-P16	0,07	6,4	0,082	0,26	1,5	3	2	7,8	17	64,4
HE-P17	<0.05	2,6	0,264	0,81	0,6	56	1,2	2,6	22	36,8
HE-P18	0,16	0,2	0,008	<0.02	<0.1	3	0,9	1,1	39	2,1
HE-P19	0,39	2,4	0,206	0,24	0,6	44	1,6	8,6	163	34,4
HE-P20	0,13	1,3	1,135	0,05	0,2	267	0,7	29,7	213	17,3
HE-P21	0,4	5,9	0,166	0,03	1,2	149	0,4	10,9	288	22,6
HE-P22	0,05	1,3	1,25	0,04	0,2	298	0,4	28,8	193	18,7
HE-P23	0,45	0,8	0,144	1,13	0,6	91	0,5	3,2	6	130,5
HE-P24	0,09	2,5	0,097	0,31	0,7	17	0,4	2	16	92
HE-P25	0,26	1,9	0,205	0,9	0,8	58	0,9	2,7	19	100,5
HE-P26	0,12	<0.2	0,006	0,03	<0.1	6	0,1	0,5	5	2,7
HE-P27	0,48	1,1	0,029	0,26	0,3	21	0,2	2,9	83	27,1

Sample ID	Te	Th	Ti	Tl	U	V	W	Y	Zn	Zr
	ppm	ppm	%	ppm	ppm	ppm	ppm	ppm	ppm	ppm
HE-P29	0,33	1,6	0,108	0,88	0,5	74	0,6	2,6	12	128,5
HE-P30	<0.05	0,9	0,903	0,63	0,2	304	0,8	43	173	17,1
HE-P31	<0.05	6,1	0,085	0,37	1,3	3	1,2	8,3	38	65,7
HE-P32	0,3	5	0,173	0,43	1,5	96	1,7	14	48	104
HE-P33	<0.05	0,6	1,035	0,05	0,1	283	1,9	34,6	172	6,1
HE-P34	0,05	0,6	0,932	0,03	0,1	338	0,7	33	135	11,7
HE-P35	0,12	1,1	0,6	0,06	0,3	226	15,4	15,2	65	14,4
HE-P36	0,41	7,8	1,265	0,17	2,2	541	66,4	28,4	134	70,2
HE-P37	<0.05	0,8	1,055	0,16	0,3	429	46,8	15,3	103	17,2
HE-P38	<0.05	1	0,011	<0.02	0,2	7	1,1	6,4	9	3,4
HE-P39	<0.05	0,3	0,008	<0.02	0,1	3	1	2	5	2
HE-P40	<0.05	0,4	0,005	<0.02	0,1	2	0,7	2,8	6	2,3
HE-P41	0,1	5,5	0,924	0,12	1	354	46,7	37,6	75	42,1
HE-P42	0,1	1,2	0,999	0,13	0,4	377	44	22,6	108	7,2
HE-P43	0,05	0,7	0,89	0,02	0,1	331	0,6	32,7	149	6,3
HE-P44	0,28	0,9	0,294	1,07	1,1	101	7,9	9,7	15	136,5
HE-P45	0,17	0,3	0,027	<0.02	0,1	9	0,7	2,3	56	6,6

Appendix C

Mineral abbreviations, conversion factors and software

Table 1. Mineral Symbols

Acm	acmite	Elb	elbaite	Ntr	natrolite
Act	actinolite	En	enstatite (ortho)	Ne	nepheline
Agt	aegirine-augite	Ep	epidote	Nrb	norbergite
Ak	åkermanite	Fst	fassite	Nsn	nosean
Ab	albite	Fa	fayalite	Ol	olivine
Aln	allanite	Fac	ferroactinolite	Omp	omphacite
Alm	almandine	Fed	ferroedenite	Oam	orthoamphibole
Anl	analcite	Fs	ferrosilite (ortho)	Or	orthoclase
Ant	anatase	Fts	ferrotschermakite	Opx	orthopyroxene
And	andalusite	Fl	fluorite	Pg	paragonite
Adr	andradite	Fo	forsterite	Prg	pargasite
Anh	anhydrite	Gn	galena	Pct	pectolite
Ank	ankerite	Grt	garnet	Pn	pentlandite
Ann	annite	Ged	gedrite	Per	periclase
An	anorthite	Gh	gehlenite	Prv	perovskite
Atg	antigorite	Gbs	gibbsite	Phl	phlogopite
Ath	anthophyllite	Glt	glauconite	Pgt	pigeonite
Ap	apatite	Gln	glaucophane	Pl	plagioclase
Apo	apophyllite	Gt	geothite	Prh	prehnite
Arg	aragonite	Gr	graphite	Pen	protoenstatite
Arf	arfvedsonite	Grs	grossularite	Pmp	pumpellyite
Apy	arsenopyrite	Gru	grunerite	Py	pyrite
Aug	augite	Gp	gypsum	Prp	pyrope
Ax	axinite	Hl	halite	Prl	pyrophyllite
Brt	barite	Hs	hastingsite	Po	pyrrhotite
Brl	beryl	Hyn	haüyne	Qtz	quartz
Bt	biotite	Hd	hedenbergite	Rbk	riebeckite
Bhm	boehmite	Hem	hematite	Rds	rhodochrosite
Bn	bornite	Hc	hercynite	Rdn	rhodonite
Brk	brookite	Hul	heulandite	Rt	rutile
Brc	brucite	Hbl	hornblende	Sa	sanidine
Bst	bustamite	Hu	humite	Spr	sapphirine
Cam	Ca clinoamphibole	Ill	illite	Scp	scapolite
Cpx	Ca clinopyroxene	Ilm	ilmenite	Srl	schorl
Cal	calcite	Jd	jadeite	Srp	serpentine
Ccn	cancrinite	Jh	johannsenite	Sd	siderite
Crn	carnegieite	Krs	kaersutite	Sil	sillimanite
Cst	cassiterite	Kls	kalsilite	Sdl	sodalite
Cls	celestite	Kln	kaolinite	Sps	spessartine
Cbz	chabazite	Ktp	kataphorite	Sp	sphalerite
Cc	chalcocite	Kfs	K feldspar	Spn	sphene
Ccp	chalcopyrite	Krn	kornerupine	Spl	spinel
Chl	chlorite	Ky	kyanite	Spd	spodumene
Cld	chloritoid	Lmt	laumontite	St	staurolite
Chn	chondrodite	Lws	lawsonite	Stb	stilbite
Chr	chromite	Lpd	lepidolite	Stp	stilpnomelane
Ccl	chrysocolla	Lct	leucite	Str	strontianite
Ctl	chrysotile	Lm	limonite	Tlc	talc
Cen	clinoenstatite	Lz	lizardite	Tmp	thompsonite
Cfs	clinoferrosilite	Lo	loellingite	Ttn	titanite
Chu	clinohumite	Mgh	maghemite	Toz	topaz
Czo	clinozoisite	Mkt	magnesiokatophorite	Tur	tourmaline
Crd	cordierite	Mrb	magnesioriebeckite	Tr	tremolite
Crn	corundum	Mgs	magnesite	Trd	tridymite
Cv	covellite	Mag	magnetite	Tro	troilite
Crs	cristoballite	Mrg	margarite	Ts	tschermakite
Cum	cummingtonite	Mel	melilite	Usp	ulvöspinel
Dsp	diaspore	Mc	microcline	Vrm	vermiculite
Dg	diginite	Mo	molybdenite	Ves	vesuvianite
Di	diopside	Mnz	monazite	Wth	witherite
Dol	dolomite	Mtc	monticellite	Wo	wollastonite
Drv	dravite	Mnt	montmorillonite	Wus	wüstite
Eck	eckermannite	Mul	mullite	Zrn	zircon
Ed	edenite	Ms	muscovite	Zo	zoisite

Abbrivated mineral named(from Kretz, 1983)

Table 39. Multipliers for Element-to-Oxide and Oxide-to-Element Conversions

Element-to-Oxide			Multiplier	Oxide-to-Element			Multiplier
Al	--->	Al_2O_3	1.890	Al_2O_3	--->	Al	0.5291
B	--->	B_2O_3	3.215	B_2O_3	--->	B	0.3110
Ba	--->	BaO	1.116	BaO	--->	Ba	0.8961
Be	--->	BeO	2.778	BeO	--->	Be	0.3600
C	--->	CO_2	3.663	CO_2	--->	C	0.2730
Ca	--->	CaO	1.399	CaO	--->	Ca	0.7148
Cd	--->	CdO	1.143	CdO	--->	Cd	0.8749
Co	--->	CoO	1.272	CoO	--->	Co	0.7862
Cr	--->	Cr_2O_3	1.462	Cr_2O_3	--->	Cr	0.6840
Cs	--->	Cs_2O	1.060	Cs_2O	--->	Cs	0.9434
Cu	--->	CuO	1.252	CuO	--->	Cu	0.7987
Fe	--->	FeO	1.287	FeO	--->	Fe	0.7770
Fe	--->	Fe_2O_3	1.431	Fe_2O_3	--->	Fe	0.6988
FeO	--->	Fe_2O_3	1.112	Fe_2O_3	--->	FeO	0.8993
Ga	--->	Ga_2O_3	1.689	Ga_2O_3	--->	Ga	0.5921
K	--->	K_2O	1.205	K_2O	--->	K	0.8299
La	--->	La_2O_3	1.172	La_2O_3	--->	La	0.8532
Li	--->	Li_2O	2.150	Li_2O	--->	Li	0.4651
Mg	--->	MgO	1.658	MgO	--->	Mg	0.6031
Mn	--->	MnO	1.292	MnO	--->	Mn	0.7740
Mn	--->	Mn_2O_3	1.437	Mn_2O_3	--->	Mn	0.6959
Mn	--->	Mn_3O_4	1.389	Mn_3O_4	--->	Mn	0.7199
Mo	--->	MoO_3	1.499	MoO_3	--->	Mo	0.6671
Na	--->	Na_2O	1.348	Na_2O	--->	Na	0.7418
Nd	--->	Nd_2O_3	1.167	Nd_2O_3	--->	Nd	0.8569
Ni	--->	NiO	1.272	NiO	--->	Ni	0.7862
P	--->	P_2O_5	2.294	P_2O_5	--->	P	0.4359
Pb	--->	PbO	1.078	PbO	--->	Pb	0.9276
Rb	--->	Rb_2O	1.094	Rb_2O	--->	Rb	0.9141
Si	--->	SiO_2	2.141	SiO_2	--->	Si	0.4671
S	--->	SO_3	2.500	SO_3	--->	S	0.4000
Sc	--->	Sc_2O_3	1.534	Sc_2O_3	--->	Sc	0.6519
Sr	--->	SrO	1.182	SrO	--->	Sr	0.8460
Ti	--->	TiO_2	1.669	TiO_2	--->	Ti	0.5992
U	--->	U_3O_8	1.179	U_3O_8	--->	U	0.8482
V	--->	V_2O_5	1.786	V_2O_5	--->	V	0.5599
Y	--->	Y_2O_3	1.271	Y_2O_3	--->	Y	0.7868
Zn	--->	ZnO	1.245	ZnO	--->	Zn	0.8032
Zr	--->	ZrO_2	1.351	ZrO_2	--->	Zr	0.7402

Element-oxide-element conversion factors table. (from Glascock, 1988).

Application Software

All presented maps and photos are digitalized and edited with CorelDRAW Graphics Suite X5. Additional georeferencing and map production is executed in ArcMap 10.2 and ArcGIS software. Multi-element diagrams presented throughout the thesis are made with ioGAS-software, designed for analyzing geochemical data.